

Graduation project

Determining the suitability and application of CNT test specimens for failure assessment of welded high strength steels

Thomas Opraus

Technische Universiteit Delft

GRADUATION PROJECT

DETERMINING THE SUITABILITY AND APPLICATION OF CNT TEST SPECIMENS FOR FAILURE ASSESSMENT OF WELDED HIGH STRENGTH STEELS

by

Thomas Opraus

in partial fulfillment of the requirements for the degree of

Master of Science
in Mechanical Engineering

at the Delft University of Technology,
to be defended publicly on Tuesday June 27, 2017 at 13:00.

Student number:	4004841	
Project duration:	September 1, 2016 – June 27, 2017	
Supervisor:	Dr. ir. V. Popovich	TU Delft
Thesis committee:	Dr. M. Janssen,	TU Delft
	Dr. ir. A. C. Riemslag,	TU Delft
	Dr. ir. B. Hu,	Allseas Engineering
	Dr. ir. J. H. den Besten	TU Delft

An electronic version of this thesis is available at <http://repository.tudelft.nl/>.

Abstract

Research has shown the Circumferentially Notched Tensile (CNT) Specimen to potentially be a size-independent fracture toughness specimen. This research focusses on expanding the practical applicability of the CNT specimen as well as using it to perform fracture toughness tests on S690QT steel and simulated CGHAZ material in S690.

Based on literature research the research goals of the research were to investigate different pre-cracking methods with the focus of creating cracks with little or no eccentricity, improve the accuracy of CTOD measurements, determine the equivalency between CNT and conventional fracture toughness, determine the size of the plastic zone at the crack tip specimen and find alternative methods of microstructure simulation.

In order to improve pre-cracking rotational bending (RB) and standalone compression compression (C-C) fatigue were used, both lead to low eccentricity cracks, where the length of the crack could be influenced by changing the process parameters or specimen geometry. Room temperature CTOD measurements were performed on both, where RB specimen showed an average CTOD of 0.12 mm and C-C specimen of 0.18 mm. This difference is believed to be caused by the unique stress free situation at the crack tip of the C-C specimen.

By using digital image correlation (DIC) and optical microscopy, the most accurate approximation of the CTOD was determined by comparing extensometer data to optical measurements. Influence of the eccentricity of the ligament was on the fracture toughness was found to increase for brittle material. Equivalency between CNT and conventional specimen was determined by comparing both RB and C-C specimens CTOD at low temperature (-100 °C). C-C specimen were found to show comparable fracture toughness, while RB showed an increased value.

The size of the plastic zone was measured using EBSD, measurements on annealed S690 and low carbon steel failed to show distinctive plasticity, possibly caused by insufficient plastic strain.

Inductive heating was tested as a replacement for Gleeble heat treatment with promising results, however the Gleeble was used for producing all S690 CGHAZ samples. C-C was found to be the only viable pre-fatiguing method, creating average crack length extensions of 0.49mm and an eccentricity of 0.18 mm. CNT results showed a slightly lower room temperature CTOD compared to conventional specimen (0.12 mm vs 0.08 mm), low temperature results showed comparable CTOD values.

More research is recommended in further development of the new standalone C-C pre-fatiguing method, improving the inductive heating and cooling setup, expanding the DIC test setup, determining the plastic zone size by performing more EBSD measurements or by performing nanoindentation measurements and using CNT specimen on very brittle materials.[1]

Nomenclature

β	Notch angle [°]
Δa	Crack length extension [m]
Δ	Gauge Length [m]
δ_c	Critical CTOD [m]
δ_t	CTOD [m]
ϵ	Strain [m/m]
ρ	Notch tip radius [m]
σ	Stress [Mpa]
σ_{ys}	Yield stress [Mpa]
τ	Shear force [MPa]
a	Crack length [m]
B	Thickness [m]
D	Outer Diameter CNT [m]
d	Inner Diameter CNT [m]
E	Young's Modulus[Gpa]
$f(\frac{a}{W})$	Geometry specific solution for K
J	J -integral [J/m^2]
K_I	Stress Intensity Factor [$Mpa\sqrt{m}$]
K_{Ic}	Critical stress intensity [$Mpa\sqrt{m}$]
L	Length [m]
P	Axial Force [N]
r_y	Irwin Plastic Zone size [m]
W	Width [m]
AALT	Adapted AFSuM Low Temperature
BCC	Body Centered Cubic

CMOD Crack Mouth Opening Displacement [m]
COD Crack Opening Displacement [m]
CT Compact Tension Specimen
CTOD Crack Tip Opening Displacement [m]
DBTT Ductile-to-brittle transition temperature
EPFM Elastic-Plastic Fracture Mechanics
FEM Finite Element Modeling
HAZ Heat Affected Zone
HSS High-strength steel
LEFM Linear-Elastic Fracture Mechanics
SEM Scanning Electron Microscope
SENB Single Edge Notched Bending

Contents

Abstract	i
Nomenclature	ii
1 Introduction	1
2 Theory and background	3
2.1 Fracture mechanics	3
2.1.1 Fracture toughness	3
2.1.2 Failure mechanisms of a cracked body	4
2.1.3 LEFM	5
2.1.4 EPFM	6
2.1.5 Critical values	7
2.2 Parameters influencing fracture toughness	7
2.2.1 Stress states at the crack tip	7
2.2.2 Temperature dependence	10
2.3 Fracture toughness testing	11
2.3.1 Conventional samples	11
2.3.2 Non-conventional samples	12
2.4 Influence of welding on fracture toughness	13
2.4.1 Weld microstructures	13
2.4.2 Heat affected zone simulation	14
2.5 High-strength steel	15
2.5.1 Types	15
2.5.2 Challenges	15
3 Literature background on the CNT specimen	18
3.1 CNT	18
3.1.1 Theoretical advantages of CNT specimen	18
3.1.2 Geometry	19
3.1.3 Dimensioning	19
3.2 Solutions	22
3.2.1 K-solutions	22
3.2.2 CTOD	22
3.2.3 EBSD	24
3.3 Experimental considerations	26
3.3.1 Pre-fatiguing of CNT specimen	26
3.3.2 Equivalency to other test methods	29
3.4 Conclusions and recommendation	31
3.5 Research Scope	32
3.6 Research questions and test plan	33

4	Experimental methods	34
4.1	Material	34
4.2	Sample preparation	35
4.2.1	Machining	35
4.2.2	Pre-fatiguing	36
4.2.3	HAZ simulation	38
4.3	Fracture Toughness testing	40
4.3.1	Crack Opening Displacement Measurement	40
4.3.2	Unloading-compliance testing	41
4.3.3	Low-temperature testing	41
4.4	Post-processing	42
4.4.1	Fracture surfaces	42
4.4.2	Crack opening measurements	43
4.4.3	CTOD and compliance	44
4.5	Plastic zone measurements	46
4.6	Full test table	47
5	Results and discussion	48
5.1	Pre-fatiguing	48
5.1.1	Rotational bending	48
5.1.2	Compression - Compression	49
5.2	Fracture Toughness testing	51
5.2.1	Crack Opening Displacement measurements	51
5.2.2	Load-Displacement measurements	53
5.2.3	Optical microscopy	56
5.2.4	Digital Image Correlation	57
5.2.5	Temperature effect	58
5.3	Plastic zone size	61
5.4	Application of CNT specimen to CGHAZ material	64
5.4.1	Gleeble	64
5.4.2	UHF	66
5.4.3	Tensile tests	67
5.4.4	Fracture toughness testing	68
5.5	Summary of results	73
6	Conclusions	75
7	Recommendations	77
	Appendices	79
A	Compression - Compression fatigue	80
B	Stress intensity factor calculations	82
C	Full experimental data	83
C.1	Pre-fatigue	83
C.1.1	Rotational Bending	83
C.1.2	Compression - Compression	84
C.2	Fracture toughness tests	85
C.2.1	Rotational bending	85
C.2.2	Compression - Compression	85
C.2.3	Comparison between RB and C-C specimen	85

C.2.4	Optical microscopy measurements	86
C.2.5	DIC	87
C.3	CGHAZ material	89
C.3.1	Gleeble heat treatment	89
C.3.2	UHF heat treatment	90
C.3.3	Tensile curves	91
C.4	Fracture surfaces and Load-displacement curves	92
C.4.1	C1 - C25	92
C.4.2	RB1 - RB12	98
C.4.3	S7 - S9	102
C.4.4	LTRB1 - LTRB5	103
C.4.5	GRT1 - GRT 3	104
C.4.6	GLT 1 - GLT 3	105
References		108

Chapter 1

Introduction

In August 2016 'Pioneering Spirit', decommissioned the 16000 tonne Yme platform off the coast of Norway by removing it completely in a single lift, a feat which has never before been achieved. Pioneering Spirit is the world's largest ship and has been designed for the single-lift installation and removal of large oil and gas platforms and the installation of record-weight pipelines, having been built by the Allseas Group.

With this 'Pioneering Spirit' fits in a trend in the offshore industry to build ever larger and stronger structures. In order to achieve this more and more reliance has been placed on the use of high-strength steels, often constructions would even be unfeasible without the use of it.

Even though their strength makes the application of high-strength steels indispensable, a lack of knowledge about their response to service- and fabrication conditions remains. One of the main concerns focuses on the reliability and quality of welded connections, in particular on the effect of the accompanying heat affected zone.

Another problem faced by high-strength steels is the increased danger they face from imperfections in the material. These imperfections are impossible to prevent due to the scale of the constructions in which these materials are applied. Furthermore the higher strengths make these steels more vulnerable to imperfections than low strength steels. For this reason it is important to gain fundamental knowledge about the fracture toughness behaviour of high-strength steels, an example of which is S690QT, which has been used in the construction of 'Pioneering Spirit'. A consequence of the strength of these materials is that very large fracture toughness specimen are required to perform valid plane strain testing. This means a lot of material, time and money is involved, making such testing too expensive for most applications.

A possible solution for this problem is the use of the Circumferentially Notched Tensile (CNT) fracture toughness specimen. Research performed over the last 40 years has shown this specimen to be a potential candidate for determining the fracture toughness of different engineering materials, as the CNT specimen is considered to be in plane strain condition for all sizes. The CNT specimen is easily machined from a small amount of material. However, lack of understanding regarding the CNT specimens behavior results in its limited applicability

Research goal

This graduation thesis is focused on the application of the CNT specimen to fracture toughness measurements of high-strength S690QT steel. The focus is on applying the CNT specimen for fracture toughness testing on both base material and simulated coarse grained heat affected zone material (CGHAZ) of S690QT. Several factors will need to be investigated to achieve this goal, such as pre-cracking of the specimen, possibility of measuring the CTOD and plastic zone size, and alternative methods of microstructure simulation. Next to this also attention is given to determination of the constraint factor in CNT samples.

Contents of the report

Chapter 2 contains an introduction into the theoretical basics of fracture mechanics and fracture toughness testing. It also gives a general background surrounding the effects of welding on the fracture toughness and further information about high-strength steels.

Chapter 3 deals with previous literature concerning the CNT specimen, and concludes with the research questions and goals that were found from literature.

Chapter 4 deals with experimental methods employed during the research and discusses sample preparation, fracture toughness testing and post-processing of all data.

Chapter 5 deals with the results found and discusses these results.

Chapter 6 concludes the report by answering these research questions and giving recommendations for further research.

Chapter 7 gives recommendations for further research following the observations made during this project.

Finally the appendices give further information about various subjects that did not fully fit the scope of this report, as well as containing the complete results for the experiments done during this research.

Chapter 2

Theory and background

In this chapter the theoretical background of this graduation thesis will be given. It focuses on Fracture Mechanics and the theoretical and experimental application of this theory. This first section will give a short introduction into the most important aspects of fracture mechanics.

2.1 Fracture mechanics

Fracture mechanics is defined as the field of mechanics concerned with the study of propagation of cracks in materials. In modern materials science it is an important tool to study the mechanical performance of components. It applies the physics of stress and strain to the microscopic crystallographic defects, being cracks, found in real materials to predict the macroscopic mechanical failure of bodies. Also, fracture surfaces are studied in fracture mechanics to understand the causes of failure and to verify the theoretical failure predictions with the real life failure results.

2.1.1 Fracture toughness

In materials science, fracture toughness is the property which describes the ability of a material containing a crack to resist fracture, and is one of the most important design parameters for any engineering application. There are two common ways to describe the fracture toughness of a material. When little or no plasticity has occurred before fracture Linear-Elastic Fracture Mechanics (LEFM) is used and fracture toughness is expressed using the stress intensity concept. LEFM however is only valid when plasticity is confined to a small area around the tip of a crack, which only happens in fracture of high-strength metallic materials, intrinsically brittle materials and tougher materials with a crack in plane strain condition. There are many material classes which are too ductile to permit the use of LEFM. For those materials Elastic-Plastic Fracture Mechanics is used (EPFM). In EPFM two fracture toughness parameters are commonly used, the J-integral and the Crack Tip Opening Displacement (CTOD) .

In engineering it is desirable for materials to have a high fracture toughness, reducing the risk of failure caused by local stress concentrations and cracks in structures.

2.1.2 Failure mechanisms of a cracked body

In fracture mechanics three distinct modes of failure can be discerned, which are shown in figure 2.1. Mode I loading, where the principal load is applied normal to the crack plane, opens the crack. Mode II corresponds to in-plane shear loading and slides one crack face with respect to the other. Mode III refers to out-of-plane shear. A cracked body can be loaded in any one of these modes, or a combination of two or three modes. Mode I failure is the predominant mode in many cases, because it is most commonly present and because it has the lowest fracture toughness, and is therefore the focus of most research.

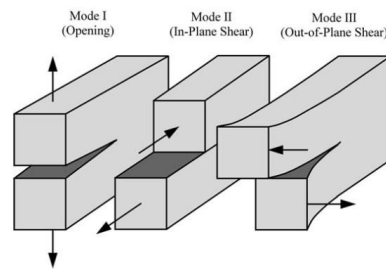


Figure 2.1: The three modes of crack surface displacements [Janssen, 2002][1]

Different materials show different ways of resisting failure, and therefore also show different ways of failing once failure occurs. The two most extreme cases are brittle and ductile fracture, however most fractures turn out to be a combination of these two.

Brittle fracture Brittle fracture, or cleavage, occurs by direct separation along crystallographic planes due to a breaking of the atomic bonds. In materials that fail in a brittle way little or none plasticity precedes failure, and because little energy is required to create a new surface brittle materials have a low fracture toughness. Brittle fracture is statistical in nature: the microstructure will contain a distribution of brittle phases of different types and grain sizes, and the location of the largest of these will be most important as the weakest link determines the incidence of cleavage fracture.

As can be seen in the SEM photograph in figure 2.2a, brittle fracture can be recognized from the relatively flat surface, caused by the perpendicular crack growth with little visual plastic deformation. So called 'river lines', which connect lower or higher lying parallel planes in the direction of local crack propagation, can also be recognized as well as grain-like or faceted textures, which are usually of the same size as the grains.

Ductile fracture In ductile failure a large amount of plasticity occurs before fracture. Because ductile fracture involves high amounts of plasticity, the fracture behaviour of a crack changes fundamentally from the brittle case. Energy is dissipated at the crack tip by plastic deformation before a crack will propagate.

For ductile failure under uniaxial loading necking will occur, followed by the formation of microvoids, which will propagate in the perpendicular direction of the loading. These microvoids are well recognizable as dimples when studying the surface of a ductile fracture and are an indicator of this kind of failure. The shape of these dimples depends on the type of loading that caused

the fracture growth, with a tensile load causing equiaxed dimples as can be seen in figure 2.2b. These dimples often contain inclusions. In steel the carbides present often act as the initiation sites in the middle of the voids.

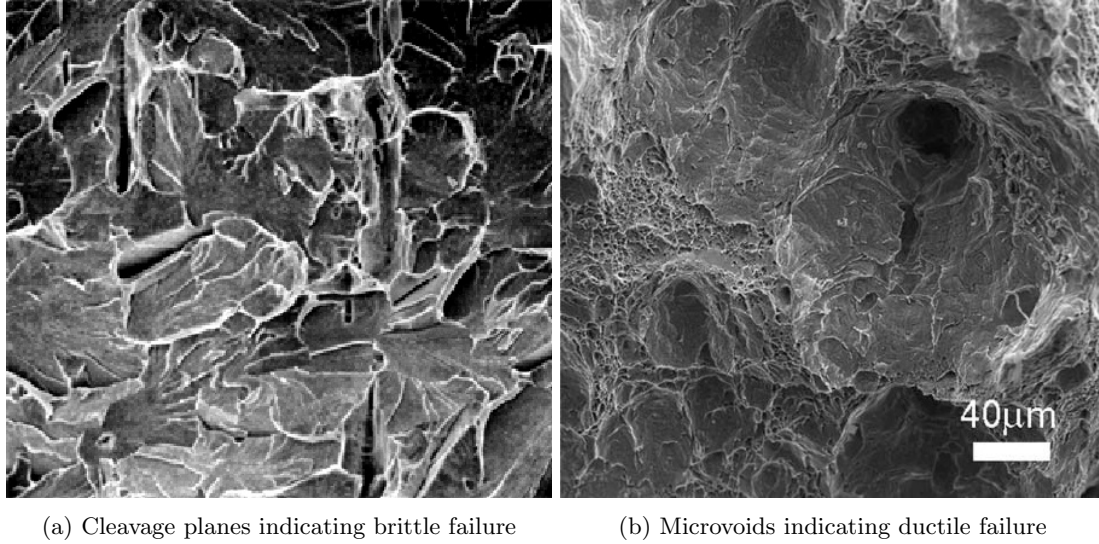


Figure 2.2

2.1.3 LEFM

Originally fracture mechanics were developed only for materials which obey Hooke's law without any plasticity occurring, meaning purely elastic behavior. Later a number of corrections for small scale yielding were applied which allowed fracture mechanics to be used for more ductile materials, however they remained restricted to materials which were essentially linear elastic. This is the class of Linear Elastic Fracture Mechanics.

Stress intensity concept

The most used fracture mechanical parameter for LEFM is the stress intensity factor K . This parameter characterizes the stress distribution near the tip of a crack in a linear-elastic body, and is a quantity that expresses the impact of a crack on a loaded structure. The stress intensity factor can be calculated as:

$$K_I = C\sigma\sqrt{\pi a} \cdot f\left(\frac{a}{W}\right) \quad (2.1)$$

with σ being the stress applied to the structure in MPa, a the length of the crack and the subscript I after K denoting the mode of loading, in this case mode I. For convenience K_I is usually expressed in the form $\text{MPa}\sqrt{\text{m}}$. This description has been derived for an infinitely large cracked plate, for finite dimension a correction factor is introduced into the equation. The $f(\frac{a}{W})$ and C are used as geometry specific solution which expand the applicability beyond infinitely large plates..

The exact requirements for a K-type test will be discussed later in this document, but one value is of importance, and that is the size of the plastic zone in front of the crack. This plastic

zone was described by Irwin as:

$$2r_y = \frac{1}{\pi} \left(\frac{K_{Ic}}{C\sigma_{ys}} \right)^2 \quad (2.2)$$

where σ_{ys} is the yield stress of the material, K_{Ic} is the critical plane strain stress intensity, and C is the plastic constrain factor, which will be further explained in chapter 2.2.1. In LEFM it is determined that only small-scale yielding is allowed to take place. This means the plastic zone must be a certain factor smaller than any of the other dimensions of the sample, this factor is usually taken as 8 [2]. This means that the plastic zone $2r_y$ must be 8 times smaller than any of the other lengths.

2.1.4 EPFM

If a material shows too much ductility during fracture LEFM can no longer be used. That is the point where Elastic-Plastic Fracture Mechanics need to be used. EPFM is divided into two commonly used fracture parameters, the J-integral and the CTOD.

J-integral

The J -integral[3] concept was introduced by Rice who, based on an energy approach, formulated J as a path-independent line integral with a value equal to the decrease in potential energy per increment of crack extension in linear or non-linear elastic material. It's path independence implies J can be seen as a measure of the intensity of stresses and strains at the tips of notches and cracks. For this reason J can be viewed as a stress intensity parameter, comparable to K .

There are two common approaches to the J -integral, the line integral approach and the energy approach. In the energy approach a path-independent contour integral is introduced for the analysis of cracks. This integral is equal to the energy release rate in a non-linear elastic body that contains a crack, which allows it to describe the loss of potential energy per increment of crack growth.

The other option is the line integral approach. In this approach finite element modeling is used to measure stress and strain distributions around the crack tip. These distributions are called the HRR singularity and allow the J -integral to completely describe the conditions within the plastic zone around the crack tip, thus allowing the use of J as a stress intensity parameter.

CTOD

The other EPFM parameter is the Crack Tip Opening Displacement (CTOD)[4], which is based on the notion that the stresses at the crack tip always reach an finite stress, thus making the plastic strain at the crack tip control fracture. What this means is that when examining cracked (ductile) specimens it can be observed that prior to fracture the previously infinitely sharp crack has been blunted by plastic deformation. The degree of this blunting at fracture, measured as the extent to which the tip of the crack has opened at fracture, is a suitable measure for the fracture toughness of the material. This crack opening parameter is known as the CTOD and is denoted with δ_t and is expressed in units of distance. Using the Irwin plastic zone analysis made it possible to find an analogous relation between the CTOD and the K value which follows:

$$\delta_t = \frac{4}{\pi} \frac{K_I^2}{EC\sigma_{ys}} \quad (2.3)$$

This relation is only valid for an infinite plate with a central crack, finding similar solutions for different geometries is very difficult.

Experimentally measuring the CTOD is a difficult procedure where the Crack Mouth Opening Displacement (CMOD), is measured by attaching a clip gauge extensometer to the crack mouth, which relates the displacement of the crack mouth to the applied force, thus allowing the CTOD to be related to the force.

2.1.5 Critical values

In the previous chapter the K_{1c} has already been mentioned, being the critical stress intensity that a material can sustain. K_{1c} however is not the only critical value available, there is also J_{1c} , the critical J value, and δ_c , the critical CTOD value. Important to realize about these values is that instead of being a stress state, they are the maximum loading a material can resist while not failing, thus making them a material parameter, instead of a measured value.

2.2 Parameters influencing fracture toughness

Many material parameters have an influence on the fracture toughness of a material, these parameters can be divided in macroscopic and microscopic parameters. These groups will be presented here, after which a number of parameters will be discussed further.

Macroscopic parameters The most important macroscopic parameters are: crack depth, specimen thickness, tension vs. bending stresses, stress state around the crack tip and the strain rate.

Microscopic parameters The most important microscopic parameters are: grain size, carbide size, shape and orientation, brittle inclusions and phases.

2.2.1 Stress states at the crack tip

In the early development of fracture mechanics two important two-dimensional stress state concepts were introduced, the plane stress condition and the plane strain condition. Even though these two concepts have been shown to be over simplistic they still play an important role in present day fracture mechanical theory and will therefore be introduced as a basic introduction into the concept of stress states.

Plane stress Plane stress is defined as a situation where $\sigma_z = \tau_{yz} = \tau_{zx} = 0$, with σ the principal normal stress and τ shear stress. This means that all stresses present, both normal and shear, are in a single plane, as seen in figure 2.3 a. The plane stress situation was said to be present in thin cracked sections, and meant the crack tip was not constrained in the transverse direction of the crack.

The plane stress condition is usually associated with poor constraint, due to the fact that the crack is only constrained in the plane, but not in the transverse direction. For this reason the plastic constraint factor (C) in the Irwin plastic zone size (equation 5.1) is 1. This low constraint therefore leads to a large plastic zone, meaning a large amount of energy is required for crack growth and fracture.

Because of the lack of constraint in plane stress so called shear lips will form at the free surfaces of a crack, because there is no material present to prevent the inward deformation of the material on the free surface.

Plane strain Plane strain is defined as $\epsilon_z = \epsilon_{yz} = \epsilon_{xz} = 0$ where ϵ is the strain, as seen in figure 2.3 b. The plane strain condition provides good constraint, due to the material being constrained in all directions and therefore leads to a smaller plastic zone than the plane stress state. The constraint factor in plane strain theoretically is 3, meaning that the plastic zone in plane strain would be a factor 9 smaller than in plane stress. This means that the well constrained plane strain state theoretically leads to a lower fracture toughness than the plane stress state. That is why in fracture mechanical testing the plane strain fracture toughness parameters must be determined, the consequences of this will be explained in the chapter on testing.

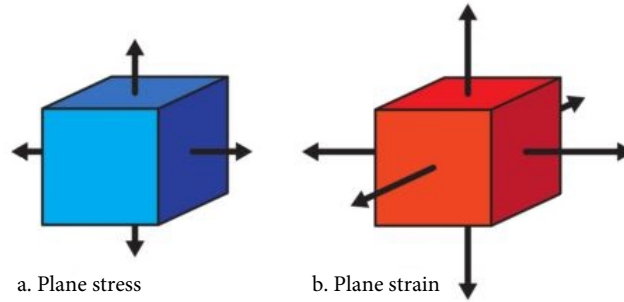


Figure 2.3: The plane stress and plane strain condition [Hengeveld 2014] [5]

Triaxiality

As said in the previous section the two-dimensional expressions for plane strain and plane stress are somewhat outdated. These expressions were developed in a period before adequate computational solutions were available for calculation three-dimensional solutions. This allowed for a better understanding of the stress state along the entire crack.

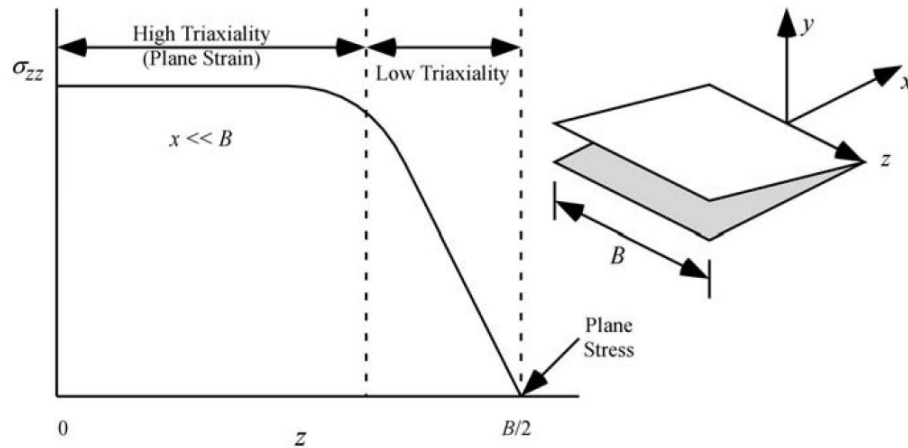


Figure 2.4: Stress states along a crack as a function of thickness [Anderson 2005]

What was shown was that a state of plane stress only exists on the actual free surface of the crack, and that the stress triaxiality increased towards the center of the crack, which is in plane strain, or fully triaxially loaded, if the sample is wide enough, as shown in figure 2.4.

Thickness dependence

As seen in the previous section the stress state of the crack tip depends on the width of the tested specimen and its plastic zone size. The traditional model therefore states that a tested specimen must have a minimum thickness, dependent on K_{Ic} and σ_{ys} to assure enough of the crack front is in plane strain conditions. This plane strain fracture toughness, K_{Ic} is then seen as a 'specimen-size-independent' material property, shown in figure 2.5.

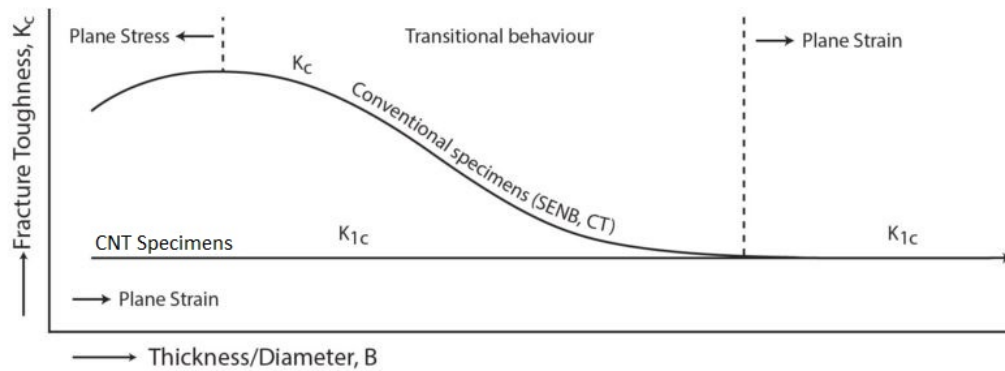


Figure 2.5: A minimum width is needed for plane strain conditions [Hengeveld 2014]

However later research has shown that this model is somewhat over simplified. In research performed by Wallin et al.[6] it was shown that K is in fact not a size independent for materials suffering from cleavage failure. Here the critical K value was shown to decrease with increasing specimen size, which is most probably caused by weakest-link sampling effects. These effect are described by the Weibull modulus, which describes the variability in measured material strengths of brittle materials[7, 8]. According to Anderson [2] the thickness dependence in ductile failure is purely caused by the shear lips near the surface, and that side-grooved samples would take away this dependence.

2.2.2 Temperature dependence

In some materials, with ferritic steel being the best known, another mechanism influences the fracture toughness as well. In materials with a Body Centered Cubic (BCC) crystal lattice a so called 'Ductile-to-brittle transition temperature behaviour' (DBTT) occurs. . This means that below a certain critical temperature the fracture mechanism changes from ductile microvoid coalescence to brittle cleavage fracture, as seen in figure 2.6.

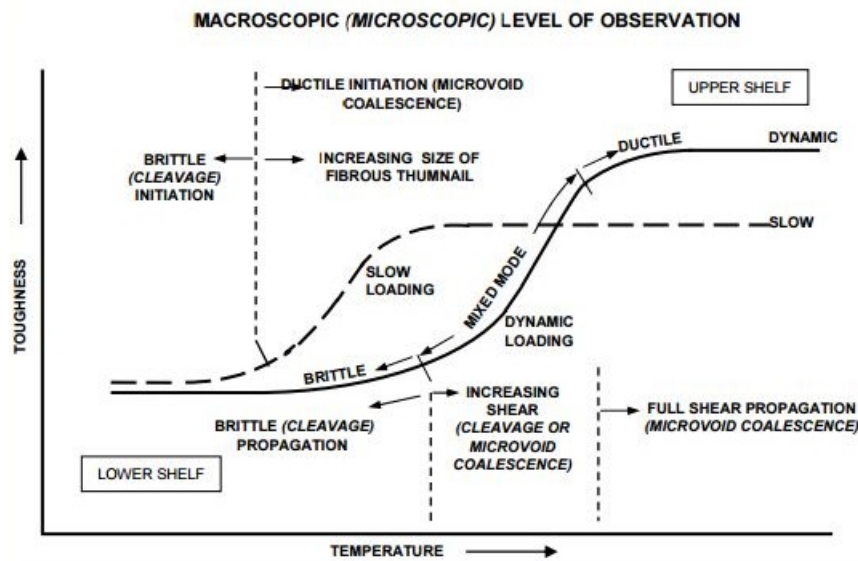


Figure 2.6: Schematic graph of the ductile-to-brittle transition [Cottrell 1958][9]

The reason this happens is that the motion of screw dislocations is very temperature sensitive because the rearrangement of the dislocation core prior to slip requires thermal activation. This leads to less plastic deformation during the fracture process. The criterion for a material to change from ductile fracture to brittle fracture is that the yield strength below the DBTT is higher than the stress necessary for the formation of a cleavage crack.

2.3 Fracture toughness testing

This chapter will deal with the practical aspects of fracture mechanical testing. Although some specifics may be different, all fracture mechanical tests operate from the same basis. They attempt to determine a valid fracture toughness parameter from a sample containing a pre-fatigue crack.

The first step will always be the preparation of the specimen. ASTM standards allow a total of five different standard specimens types, although no single standard allows the use of all five configurations, and even dimensioning differences exist between standards[2]. Three dimension are of importance: the crack length (a), the thickness (B), and the width (W). The great majority of tests is usually performed on either Compact Tension (CT) specimens, or Single Edge Notched Bending (SENB) specimens. Both of these have their specific advantages, the CT specimen is easier in use for plate material, while the SENB specimen is usually preferable for welded specimens.

Before the actual fracture toughness test can be performed the material must first be pre-fatigued in order to create a crack. This crack will usually be grown from the machined notch, which has a finite sharpness, operating as a stress concentration in the sample. The crack is grown by cyclic loading of the specimen, either in tension or in compression, depending on the particular test setup. Guidelines are in place which describe the exact loading condition during pre-fatigue.

After the crack is grown the actual test can be executed. The material is fractured and the load-displacement curve, and other required parameters, are determined. From the test data the most appropriate fracture toughness parameter must then be chosen. In order to qualify as a proper linear elastic critical plane strain stress intensity test (K_{Ic}) the test result must meet four criteria. These criteria are taken from ASTM E1820[10].

1. $B, a \geq 2.5 \left(\frac{K_{Ic}}{\sigma_{ys}} \right)^2$
2. $0.45 \leq \frac{a}{W} \leq 0.55$
3. $\Delta a \geq 1.3mm$
4. $P_{max} \leq 1.1P_Q$

Because K_{Ic} is a linear elastic parameter, most of these criteria are related to making sure the test stays within LEFM limits. The first rule gives a minimal thickness of the sample. This is done to make sure enough material around the crack is in high constraint, the thickness must be large compared to the plastic zone size to minimize the effect of the low constraint of the free surfaces. The second criterion is there to make sure the plastic zone around the crack tip is small compared to the crack length and uncracked ligament. The third criterion prevents any influence of the crack on fracture toughness. The final criterion is introduced in order to make sure the general material behaviour remains linear elastic, if this value would be higher significant plasticity occurred and LEFM would not apply. If any of these criteria is not met, EPFM fracture toughness parameters must be considered.

2.3.1 Conventional samples

In the standards set by the ASTM five official samples are recognized, the Compact Tension (CT), the Single-Edge-Notched Bending (SENB), the arc-shaped specimen, the disk specimen and the middle tension (MT) specimen. In practice the great majority of tests are performed on either the CT or the SENB specimen, these will therefore be shortly expanded upon in the next section.

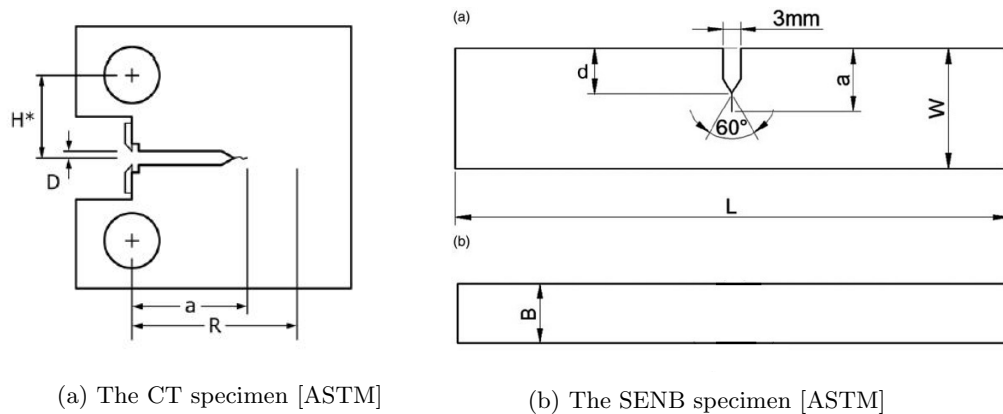


Figure 2.7

CT

The CT specimen, shown in figure 2.7a, is a somewhat square specimen with holes on the upper and lower flank and a notch in the center. The specimen is meant to be loaded in tension by applying a load to the two holes. The advantage of the CT specimen over the SENB is that it requires less material, it is however more difficult to machine, and therefore more expensive.

SENB

The SENB specimen, shown in figure 2.7b, appears as a long square bar with a single notched groove in the center. It is meant to be loaded in three point bending with a compressive force on the backside of the notch. Although SENB require more material than CT samples they are easier to machine due to their simpler geometry.

2.3.2 Non-conventional samples

More specimen types exist for testing fracture toughness than the five described in the ASTM standards, one of these is the Circumferentially Notched Tensile (CNT) specimen, shown in figure 2.8. Research in recent years have shown the CNT sample to be a good specimen for finding the fracture toughness of materials using relatively small specimens. The reason for this is the round shape of the sample, which offers a number of advantages; it makes the sample easy to machine, and the round shapes removes any free surfaces around the crack. Therefore, in theory, the desired plane strain condition is not limited by specimen size, allowing for the use of small specimen. Also the CNT specimen has a far higher constraint in the bulk material, allowing for higher loading before failure occurs.

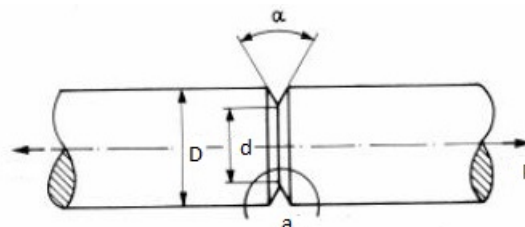


Figure 2.8: Geometry of the CNT specimen [Nath 2006][11]

2.4 Influence of welding on fracture toughness

Welding is defined as a fabrication process that joins two or more materials by causing fusion between them. This means that, different from brazing or soldering, the material along the line where it is fused together is actually brought into a molten state and allowed to solidify again.

Welding is a widely used technique in industry with many upsides, such as the low costs, high production rates and great flexibility in applications. It does however have a big downside from a material science point of view, that is that it locally alters the microstructure of a material, and with that its material properties and mechanical behaviour. Yield strength, corrosion and fatigue resistance and perhaps most importantly the fracture toughness of a material are drastically changed by the introduction of a weld. That is why it is very important to have good knowledge about the influence of welds on the fracture toughness of a material, and is also why extensive testing is being done in this field.

As said the most important quality of welding is the fact that the base material is molten, and in addition to the molten base metal in most forms of welding a filler material is also added to the welded joint to form a pool of metal, the so called weldpool. Along with this metal a shielding gas is usually used, to protect the weld flow and create a better weld. Many different types of welding exist, with gas metal arc welding (GMAW or MIG), gas tungsten arc welding (GTAW or TIG) and shielded metal arc (SMAW) being among the best known.

During the weld process the material next to the weld which is not actually molten will be subjected to a thermal cycle, consisting of very fast heating, followed by relatively slow cooling. This thermal cycle causes physical and chemical processes to take place in both the liquid and solid phase of the eventual weld.

2.4.1 Weld microstructures

When a material is welded there is always a zone just outside of the meltpool which is exposed to a high amount of heating and subsequent cooling. In material science it is well known that this kind of heat cycle has drastic effects on the local material behaviour, and this zone is therefore aptly known as the Heat Affected Zone (HAZ).

The extent and magnitude of the property change depends primarily on the base material, the weld filler material and the amount of heat input in the welding process. The thermal conductivity of the base material plays a large role, if it is high the cooling rate will be high too, and the HAZ will be relatively small. The materials in which the HAZ plays the most important role is in steels, in which the high-temperature phase transformations have great effects on its properties.

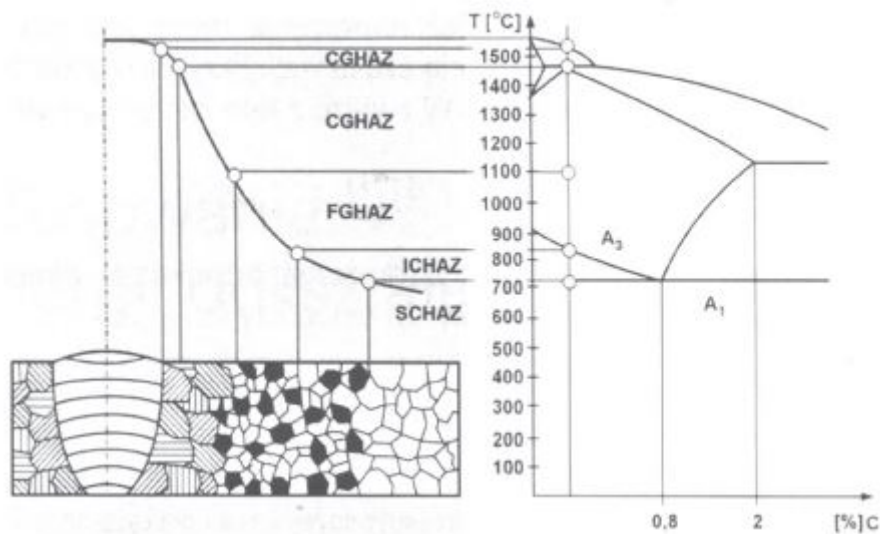


Figure 2.9: The different microstructures in the HAZ of steel, related to the iron-carbon phase diagram [Sloderbach 2015][12]

The HAZ in steel can be divided into a number of subzones, as shown in 2.9, which are the Course Grained (CGHAZ), Fine Grained (FGHAZ), Intercritical (ICHAZ) and the Subcritical (SCHAZ). Of these the CGHAZ has the most important effect on the fracture toughness of the weld, as this is where the heat has reached sufficient temperatures to let grain coarsening takes place. The effect of this is a reduction in the materials yield strength as well as a reduced fracture toughness

2.4.2 Heat affected zone simulation

Fracture toughness testing on actual welds is a very difficult process. The weld has to be extracted from the welded material, very precisely machined and then notched in the exact spot that is of interest. All of this makes it very interesting to find another way to do this.

When looking at fracture toughness of these welds the zone of primary interest is the CGHAZ, which is the weakest part of the weld, and although the area surrounding it is of some importance it remains the main problem. This fact then gives a lot of possibilities to circumvent most problems concerning fracture toughness measurements on welds. This is because it is possible to use a thermal-mechanical simulator to create a simulated HAZ in a specimen which will have the same properties as the actual CGHAZ, but then over a far greater area of material. These simulators use high amperage alternating electrical current to heat material, and can very accurately follow a pre-determined temperature path to create a desired microstructure in the heated area. A practical issue with this kind of simulators is the limits it sets on the geometry of the specimens, there is a limit in diameter due to the geometry of the mounts, and there is a demand that samples are fully cylindrical, as the current needs to be even throughout the specimen, this means samples can't be pre-crack beforehand.

2.5 High-strength steel

Steel is one of the most important and versatile engineering materials there are, the basic reason for this being the abundance of iron ore, the relatively low energy consumption and CO₂ production of production and its high recyclability. Use of high-strength steels (HSS) are one way to save energy and reduce life-cycle carbon dioxide emissions. Lighter construction means generally thinner wall thicknesses and, consequently, smaller welds or the possibility of replacing welds by bending plate sections. High-strength steels can also be advantageous to use from a cost perspective even for applications where weight considerations are less important.

2.5.1 Types

The tensile strength of steel at room temperature can vary hugely from less than 200 MPa to over 5000 MPa, however the range usable for welded structural applications is from about 200 MPa to 1300 MPa. The yield stress of a steel is governed by the stress needed to move dislocations sufficiently to produce a small permanent plastic strain. Dislocation motion is hindered by alloy element atoms in solid solution; grain, subgrain, phase and cell boundaries; other dislocations and precipitates. Higher strengths are obtained by reducing the distance between these obstacles. This can be done in numerous ways by controlling the alloying and processing. The phase transformation from austenite to ferrite on cooling offers many processing routes to high strength microstructures which are not available for other metals, making steel very versatile.

These strengthening mechanisms are attained by combining chemical compositions and processing routes, with many possible combinations. For hot-rolled steels the most common processing steps are normalizing heat treatments (N) or controlled rolling (CR), thermo-mechanical processing (TMP), reheating, quenching and tempering (RQT) and direct quenching with or without subsequent tempering (DQ/DQT).

The yield strength levels that are available through these different processes are:

- N and CR: 355 - 420 MPa
- TMP: 355 - 700 MPa
- RQT: 500 - 1300 MPa
- DQ: 890 - 1100 MPa
- DQT: 700 - 960 MPa

2.5.2 Challenges

High-strength steels offer many advantages, but also offer certain challenges, the most important of which will be expanded upon here:

Thick Sections HSS are formed by very accurately controlling the heat cycle of the material, specifically the speed of the austenite - ferrite transformation. Because of the thermal conductivity of steel the heat throughout the material can be assumed to be practically homogeneous for thin rolled plate material. For thicker rolled sections however this is no longer the case, because the cooling occurs on the outside of the material the inner parts are slower to cool than the outer parts. This inhomogeneity in cooling rate leads to a difference in microstructure as well, as the speed at which the austenite - ferrite transformation takes place is different throughout the thickness of the material. This difference in microstructure also has important consequences for the mechanical properties of the material; research by Popovich et al.[13] on thick-section S690QT

steel has shown a big differences in i.a. tensile properties, hardness and fracture toughness as can be seen in figure 2.10, 2.11, 2.12 and 2.13.

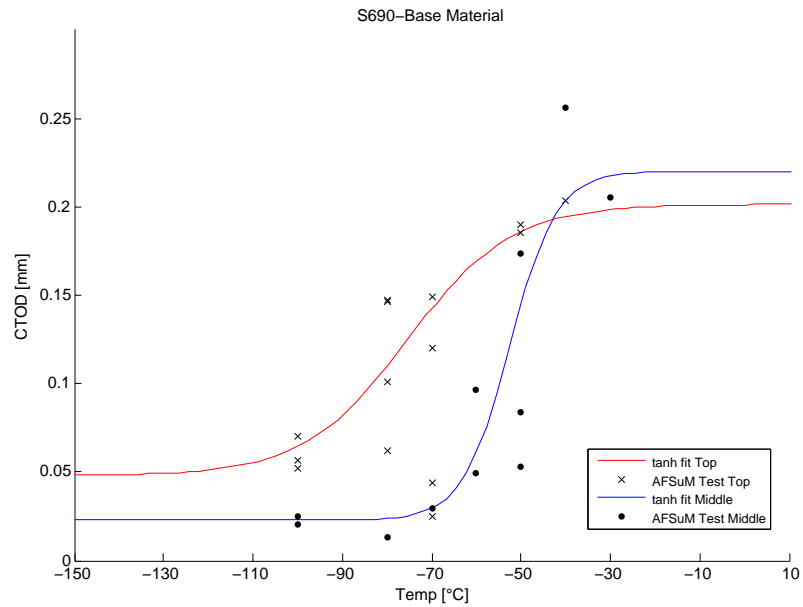


Figure 2.10: CTOD values for top and middle sections of 60 mm thick S690QT steel

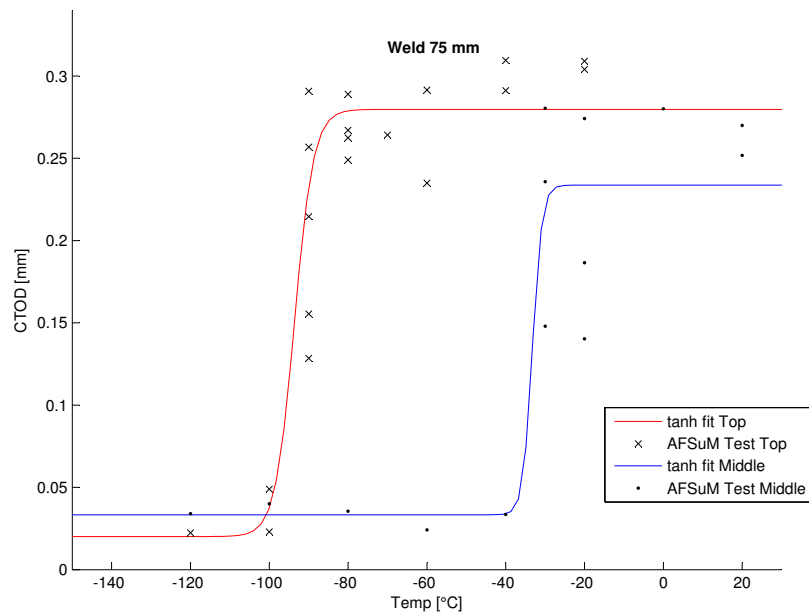


Figure 2.11: CTOD values for top and middle sections of the HAZ of 75 mm thick S690QT steel

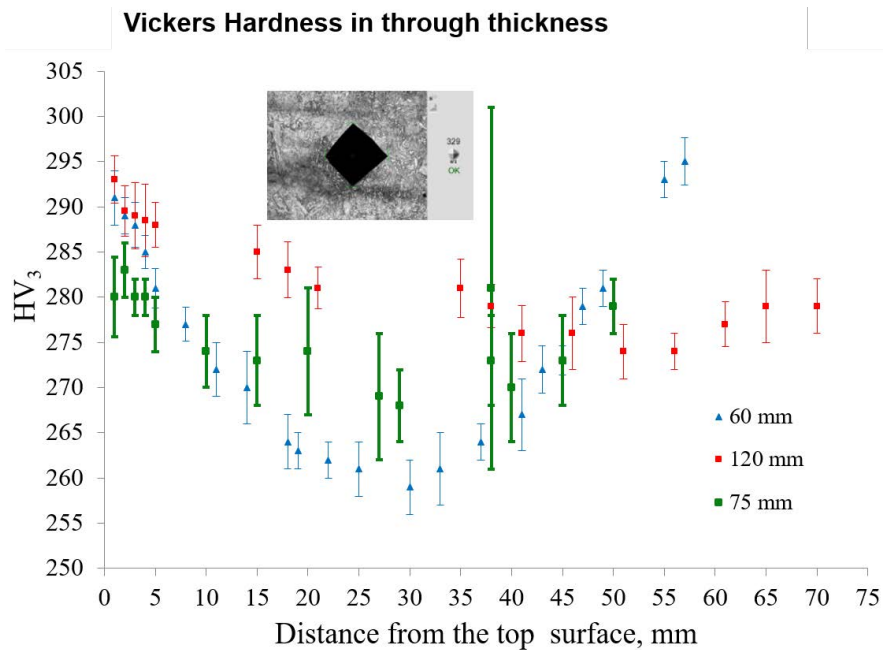


Figure 2.12: Hardness throughout the thickness of 60 mm, 75 mm and 120 mm S690QT steel

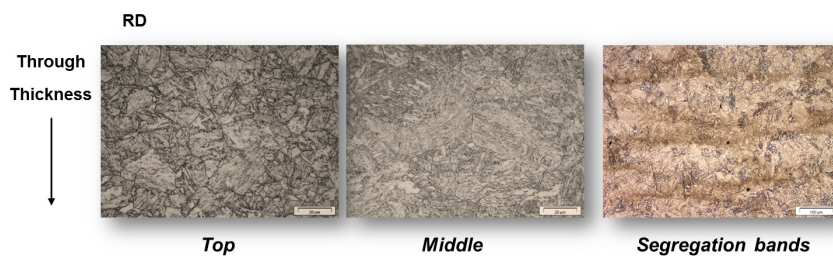


Figure 2.13: Differences in the microstructure in the through thickness of S690QT steel

Weldability As the strength of steel increases it becomes ever more sensitive to hydrogen embrittlement, atomic hydrogen concentrated around stress concentrations which reduces the local fracture toughness[14], where the hydrogen can enter the steel in two ways. During the liquid steelmaking process the hydrogen can enter the steel, this hydrogen can be prevented by both working on methods to minimise the exposure to hydrogen and by long heat treatments to remove it from the material. The other source of hydrogen is fabrication work on the material, during welding hydrogen can enter the material through the molten weldpool. Hydrogen embrittlement is already a problem in the HAZ of low-strength steels, but in high-strength steels special care must be taken to protect the material as much as possible.

Chapter 3

Literature background on the CNT specimen

In this chapter the available literature concerning the Circumferentially Notched Tensile (CNT) specimen will be reviewed, as well as other topics relevant to this topic.

3.1 CNT

Fracture toughness testing of the plane strain stress intensity factor K_{Ic} is a complicated affair, and the preparation of the specimens to accurately do it is costly and time consuming process. Another problem can be the impossibility to create specimens which adhere to the specimen size criteria set in ASTM E1820[10]. This can be caused due the absence of enough material, or a problem in the geometry of the material. This means however that it is then impossible to obtain a valid K_{Ic} value for this material according to the set standard.

One of the solutions proposed to counter this problem is the so called Circumferentially Notched Tensile specimen, or CNT as it will be referred to from here. The CNT specimen is a round bar with a circumferential notch around its surface. From this notch a pre-fatigue crack is then initiated into the sample. This pre-fatigue crack is then theoretically completely in plane strain, or the stress state all around the crack is triaxial, caused by the complete lack of free surfaces of the round bar. This would mean that the CNT specimen has only a very small plastic zone and no shear lips and is completely size-independent, thus allowing for far smaller samples than in conventional fracture toughness testing while still being valid.

3.1.1 Theoretical advantages of CNT specimen

According to literature the CNT specimen should offer the following advantages over conventional test specimens.

- There are no free surfaces, meaning the entire crack is in plane strain conditions.
- The samples are easily machined.
- The sample can be tested on a standard tensile testing rig.
- The axisymetrical geometry is easy to model in FEM simulations.
- Precracking a notched round bar can easily be done in several ways.

3.1.2 Geometry

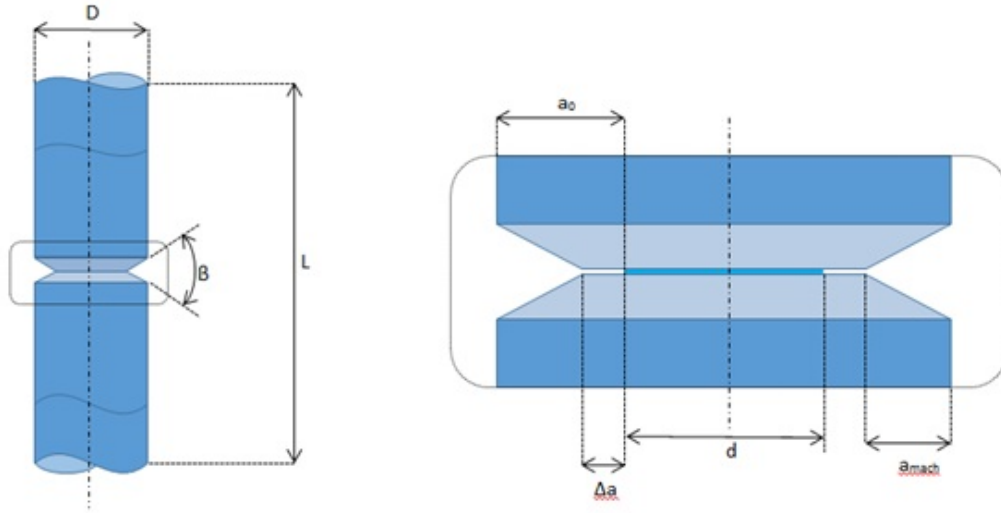


Figure 3.1: Geometry of the CNT sample [Slachter 2016]

The CNT specimen, shown including its variables in figure 3.1, consists of a round bar with the outer diameter D , and with a length L . This round bar is then radially notched, with a notch angle β and a notch radius ρ . This is usually done in a lathe, and after this the specimen is pre-fatigued. The remaining ligament is after applying the crack is called d , while the depth of the crack is a_0 , which is equal to $\frac{D-d}{2}$.

3.1.3 Dimensioning

In fracture toughness testing there are demands made on specimen geometry to ensure 'plane strain' conditions. This practically means the plastic zone in front of the crack can't be too large compared to specimen geometry. In the case of SENB and CT samples this demand is formulated as:

$$B \geq 2.5 \left(\frac{K_{Ic}}{\sigma_{ys}} \right) \quad (3.1)$$

with B being the thickness of the specimen.

Many authors have written on formulated theories on similar demands for the CNT specimen, nor are they all in agreement with each other. One of the defining factors in the CNT sample, the circumferential crack is also one of the potential downsides, if the sample is compared with similar size SENB samples. Whereas the SENB sample has only one crack passing through the sample, the CNT has two growing towards each other. Practically this means that the center line of the specimen can also be seen as the boundary, meaning the thickness of the sample might not be the ligament diameter D , but it's radius, meaning it is only half as big.

In 1985 Devaux [15] noticed a reduction in fracture toughness with a reducing diameter while testing A508 pressure vessel steel. Lucon [16] noticed that although the test were reasonably accurate for brittle specimen, a size dependency was found for ductile material, these test were performed according to the standard ASTM E399-90. It was noticed that the fracture toughness became smaller as the diameter was reduced. The explanation for this is that for small samples

the ratio of the plastic zone size to the diameter of the uncracked ligament becomes increasingly bigger. Because there is a circumferential crack there is also a plastic zone in front of it on all sides, which is moving inwards at crack extension. This means that at a certain moment the plastic zones will intersect each other and the fracture becomes a purely plastic event, thus reducing the measured K value. If the diameter is increased the ratio decreases, leading to elastic fracture in the ligament and thus a more accurate critical stress intensity. From finite element modeling it was then deduced the minimum diameter of the ligament should be:

$$d \geq 10 \cdot r_y \quad (3.2)$$

with the assumption that $d/D \approx 0.5$. This then leads to:

$$D \geq 1.1 \left(\frac{K_{Ic}}{\sigma_{ys}} \right)^2 \quad (3.3)$$

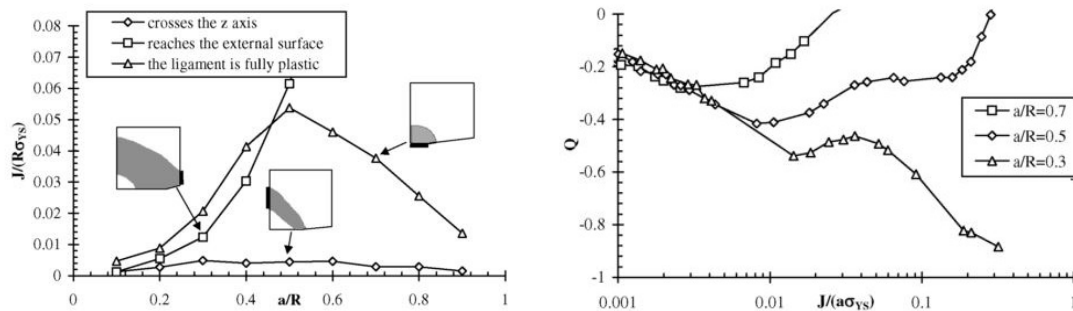
meaning the almost 2,5 times thinner than the SENB criterion. Lucon also proposes a minimum crack length of $0.265(K_{Ic}/\sigma_{ys})^2$.

Ibrahim[17] stated that because the entire crack is theoretically in plane strain the plastic zone size can be calculated in the same way as for conventional plane strain plastic zones. From this he stated the minimum diameter for CNT can be found when the crack tip is placed in the vicinity of the mid-point between the free surface and the center line, this lead to the following relation.

$$D \geq 32r_y \implies D \geq 1.7 \left(\frac{K_{Ic}}{\sigma_{ys}} \right)^2 \quad (3.4)$$

this means this research states the diameter must be approximately 1,5 times bigger than Lucon stated.

Neale[18] performed finite element calculation on a set of theoretical materials. From this he found the optimal geometry for $a/b(d/D)$ to be 0.5. Also his results show $L/b \geq 3$, thus giving a minimum length for the sample. Scibetta [19] and Ibrahim [17] are in agreement on the a/b ratio of 0.5. The reasoning behind this is that ratio of the plastic zone size should be as small as possible towards all other dimensions. This way the plastic zone will reach either the free outer surface or the center line as late as possible, which will ensure Small Scale Yielding for the longest amount of time. This theory applies for materials with any combination of fracture toughness and yield strength.



(a) Plastic zone evaluation for different 'crack length to bar radius' [Scibetta 2000] (b) Constraint values for three 'crack length to bar radius' [Scibetta 2000]

Figure 3.2

Scibetta also performed finite element calculations into minimum specimen size. Using the constraint factor Q as a guiding parameter, formulated as:

$$Q = \frac{\sigma_{zz}(r^* = 2) - \sigma_{zz}^{SSY}(r^* = 2)}{\sigma_{ys}} \quad (3.5)$$

with $r^* = r/(J\sigma_{ys})$ and SSY referring to small scale yielding. For brittle materials a Q -factor lower than -0.1 is considered significant and is sometimes used as a secondary parameter for failure. It was found that loss of constraint during loading occurred for shallow cracks, while it increased for deep cracks.

The most important conclusion from this research, shown in figures 3.2a and 3.2b, is however for the advised minimum thickness value, which was derived for a material with work hardening coefficient $n = 0,1$ and $E/\sigma_{ys} = 500$. For a negligible loss of constraint the minimum thickness would have to be:

$$a, b \geq 2500 \frac{(1 - \nu^2) K_{Ic}^2}{E \sigma_{ys}} \implies D \approx 10 \left(\frac{K_{Ic}}{\sigma_{ys}} \right)^2 \quad (3.6)$$

this means this criterion leads to a thickness more than nine time as high as for the criterion suggested by Lucon in equation 3.3. The reasoning behind this criterion is that the plastic zone very quickly reaches the center line of the specimen, and then loses a high amount of constraint, thus leading to invalid conclusions. A consideration here is that the modeling was done for only one type of material, making it hard to extrapolate the meaning of this data.

The most important conclusion from all authors however appears to be the fact that full ligament plasticity must be prevented for a valid determination of the critical stress intensity K_{Ic} . FEM calculations were performed on the results of the research by Hengeveld [5] and Slachter [20] on CNT measurements of *S690QT* steel. These calculation made it possible to say if the ligament became fully plastic, and could therefore be used as a tool for determining the validity of the tests. This method of combining test results with FEM calculations on the specific geometry and material properties of the test specimen appears to be a promising method for validity determination. It is however a far more time consuming process that a single statement on validity and should therefore be improved to improve its usability.

3.2 Solutions

In fracture mechanical testing specimens are usually tested by loading the crack until failure, leading to a form of load-displacement curve or a crack opening displacement measurement. To get from these measurements to a fracture mechanical parameter means a certain solution for this problem must be used, the next section will present a set of these solutions for the different fracture mechanical parameters.

3.2.1 K-solutions

Most of the proposed solutions relate to the linear-elastic stress intensity factor, K_{Ic} . Throughout the research done a large number of different solutions have been presented, and the most promising will be presented here.

The first apparent stress intensity function for a CNT specimen was found by Benthem[21] in 1973:

$$K = \frac{P}{2\pi d^2} \cdot \sqrt{\frac{\pi a d}{D}} \cdot \left[1 + 0.5\left(\frac{d}{D}\right) + 1.5\left(\frac{d}{D}\right)^2 - 0.363\left(\frac{d}{D}\right)^3 + 0.731\left(\frac{d}{D}\right)^4 \right] \quad (3.7)$$

with P being the axial load in Newtons

Tada[22] in 1985 gave the following solution in the analysis of cracks handbook:

$$K_I = \frac{P\sqrt{\pi b}}{\pi d^2} \cdot \sqrt{\frac{d}{D}\left(1 - \left(\frac{d}{D}\right)\right)} \cdot 0.5 \left[1 + 0.5\left(\frac{d}{D}\right) + \frac{3}{8}\left(\frac{d}{D}\right)^2 - 0.363\left(\frac{d}{D}\right)^3 + 0.731\left(\frac{d}{D}\right)^4 \right] \quad (3.8)$$

Dieter[23] in 1988 gave the following solution:

$$K_{Ic} = \frac{P}{D^{3/2}} \cdot \left[1.72 \frac{D}{d} - 1.27 \right] \quad 0.48 \leq (d/D) \leq 0.86 \quad (3.9)$$

What this illustrates is that there is no single value in use for K and some experimental comparison between these different approaches might allow for a more informed choice of K solution. It must be noted that the solution of Benthem was evaluated by Scibetta[19] using finite element modeling and was found to be very accurate.

3.2.2 CTOD

The last fracture toughness parameter to be discussed is the Crack Tip Opening Displacement, this parameter is not usually expressed in a formula, but is an directly observable quantity. Yet where measuring this in SENB and CT samples is relatively straight forward, due to the ease in measuring the CMOD, which is a straight face, the circular shape of the CNT makes accurately measuring the CTOD for these specimens far more difficult. Several techniques have been proposed to accurately measure CTOD, these will be discussed here.

Giovanola [24] used FRASTA (fracture surface topography analysis), a quantitative fractographic analysis method that can be used to reconstruct the microprocesses of fracture and establish the fracture kinetics, it also provides crack extension data and toughness estimates in terms of CTOD. Meaning it can characterize fracture surfaces to different stages of crack initiation, crack growth and blunting. It found the point of maximum load to be very near the point where crack

initiation takes place, and suggest using the maximum force as the critical parameter for J_{Ic} calculations. This technique was not found to be used in any other research relating to CNT samples.

Another important finding by Giovanola was related to the CMOD. Finite element calculations performed indicated the crack flanks remain essentially straight and parallel during loading. This means as that as long the plasticity is limited to the ligament the CMOD should be equal to the CTOD, thus allowing for easier measurement using extensometers on the outer surface of the CNT specimen. Giovanola then verified this by stopping and unloading CNT tensile tests before instability occurred, and then measuring the crack opening around the circumference using optical microscopy. These results were in agreement with the finite element calculations, thus proving the CTOD can be measured through the CMOD.

Pardoen[25] performed CTOD measurements on cold-drawn copper, CNT samples were loaded until cracking initiated and then unloaded. The cracked ligaments were then embedded and grinded and polished to show the crack length throughout the ligament, as seen in figure 3.3. It was argued that after unloading reverse plasticity occurred which would reduce the accuracy, so this effect was countered through a correction factor. It was found that if crack initiation can be detected the specimen is useful to determine δ_c , as long as the crack growth rate is not of interest. One interesting consideration was the size of the found plastic zone, which for an CNT sample was about 1,5 times smaller than in SENB samples.

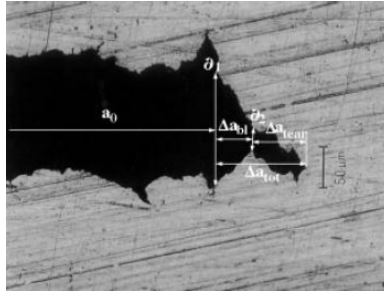


Figure 3.3: Measuring the crack opening through optical microscopy after unloading [Pardoen 2000A]

Wu [26] determined a function relation K_{Ic} and the critical CTOD δ_t for CNT specimens. By combining numerical modeling and experimental results using different materials the following general relation was defined:

$$K_{Ic} = \sqrt{E\sigma_{ys}} \cdot \sqrt{[451.58\delta_t^3 - 9.14\delta_t^2 + \delta_t]} \quad (3.10)$$

with δ_t in mm and E and σ_{ys} in MPa. Slachter [20] used unloaded tensile specimens to measure crack opening, finding uneven crack openings, possibly due to eccentricity in the ligament. It was found this also influenced the results gotten from extensometer measurements on two sides of the specimen, thus according to the author leading to an average CTOD at fracture, but not a critical CTOD at fracture. The other method used here was measuring stretch zone width (SZW) of the fracture. These measurements indicated the extensometer data underestimated the CTOD values at fracture. According to the author this meant either the use of SZW to determine the crack tip opening was incorrect, or an unforeseen error was introduced in the measurements. The author concluded however that determining the critical CTOD was not a viable for CNT samples, as any eccentricity would inevitably lead to measuring the average CTOD instead. An interesting case was made however for using and knowing the size of the plastic zone.

3.2.3 EBSD

In recent years an interesting case for measuring plastic zone sizes has been made using Electron Backscattered Diffraction methods. Research by Githinji [27] and Unnikrishnan [28] used different methods of EBSD measurements to measure the strain in several materials.

Githinji looked at strains surrounding welds, using different EBSD techniques. The techniques used were 'Kernel Average Misorientation' (KAM), which determines very local misorientations within each grain, 'Low Angle Misorientation Fraction' (LAMF), which measures the fraction of low angle grain boundary misorientations. 'Average Misorientation' (AMIS) evaluates the mean of all spatially uncorrelated misorientations in each grain, and doing this on a smaller scale than KAM and LAMF. If a threshold value is set for AMIS determination, it is possible to map an area into 'deformed' and 'undeformed' material. In this research it was found KAM is useful for strains smaller than 0.2, LAMF between 0.05 and 0.15 and AMIS up to a strain of 0.35. This makes it an interesting tool for mapping an area with both very small strains, as well as local very high strains, such as the plastic zone around a crack tip.

Unnikrishnan compared the measured plasticity around a reheat crack in a stainless steel steam nozzle in EBSD with hardness measurements. Both KAM and GROD (grain reference orientation deviation) were used in this research. It is visible that the hardness measurements agree well with the two EBSD techniques.

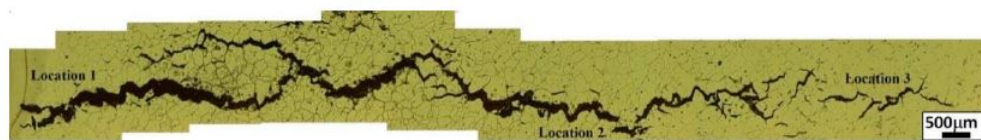


Figure 3.4: SEM photography showing the reheat crack in the nozzle [Unnikrishnan 2016]

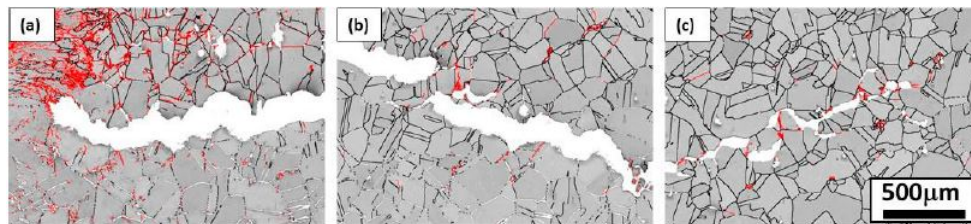


Figure 3.5: SEM photography showing the same reheat crack with black lines being high angle grain boundaries ($\theta \geq 15^\circ$ and red being LAGB ($2^\circ \leq \theta \leq 15^\circ$)) [Unnikrishnan 2016]

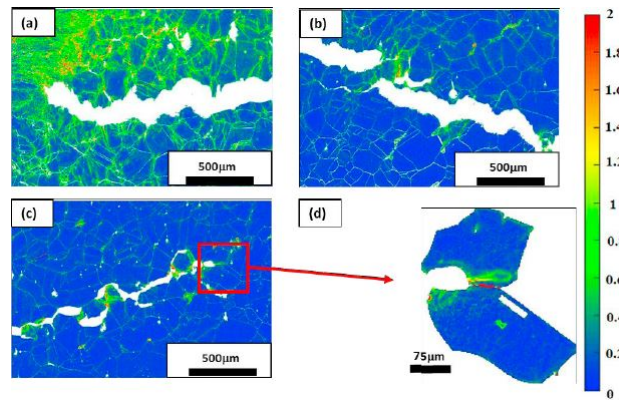


Figure 3.6: SEM photography showing the KAM at the three locations and zoomed in on the crack tip [Unnikrishnan 2016]

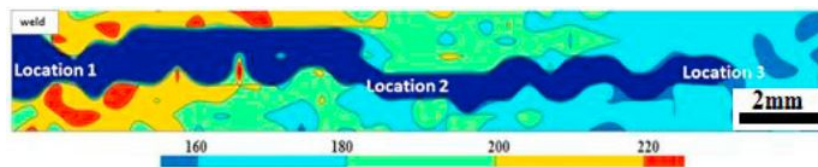


Figure 3.7: SEM photography showing the hardness measurements around the crack [Unnikrishnan 2016]

3.3 Experimental considerations

Besides the more fundamental parts expressed in chapter 3.2 there are also practical experimental considerations need to be taken into account.

3.3.1 Pre-fatiguing of CNT specimen

In order to create a cracked CNT specimen a pre-fatigue crack must be grown from the circumferential notch. In the previous sections it was already established that a crack/outer diameter a/D -ratio of 0.5 is desirable. To create this notch there are two techniques commonly used: rotational bending and compression-compression loading.

Rotational bending

The most common technique to create the pre-fatigue crack in a CNT specimen is by using rotational bending. The theory behind this system is that as the specimens are round they can be rotated around their axis by mounting one end in an electric motor or in a lathe. If a friction-less force is then applied to the other end leading to a cyclic loading in the specimen, meaning that in a single rotation every point on the specimen will be loaded in both tension and compression in a sinusoidal way. This is then the basis of rotational bending pre-fatiguing. Because the CNT specimen has a deep notch along its circumference this is the primary place where the fatigue crack will originate, this is both due to the fact that there is a significantly smaller cross section along the notch and the notch acting as a stress concentration.

Most researchers have worked on standard rotational bending machines, as described by Stark [29], which apply either a fixed bending moment on the specimen, or a fixed displacement, shown in 3.8a. In the first case the displacement will increase during fatiguing, in the second case the required moment will decrease, both of these can be used as a way to measure crack growth. Another method is described by Giovanola[30], where a purpose built compression casing is applied to a lathe with a CNT specimen mounted, as shown in 3.8b.

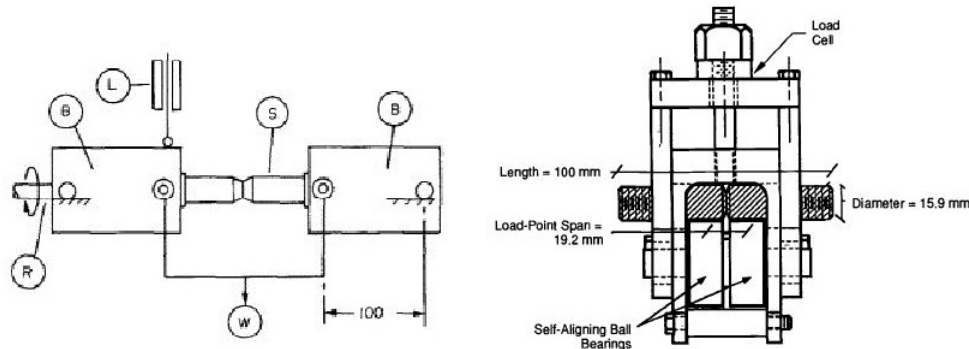


Figure 3.8: Two methods for rotational bending, left the method described by Stark [Stark 1986], right the lathe based system by Giovanola [Giovanola 1995]

The most critical aspects of rotational bending pre-fatiguing are crack length monitoring and preventing eccentricity in the ligament. There are several methods for monitoring the crack length of the specimen. As mentioned above it is possible to measure the increase in deflection in fixed force bending. The reduction of the ligament diameter leads to a decrease in stiffness, meaning the deflection will increase. Standard mechanical relations can then be used to estimate the crack depth. The system with fixed deflection uses the same relations, only with the force

reducing instead of the deflection increasing. In most materials it is also possible to use potential drop measurements. Finally the loss of stiffness can be measured by loading the material in tension and measuring the stiffness of the total specimen, the deeper the crack, the less the stiffness.

The other important aspect is the prevention of eccentricity. Lucon [31] found that the eccentricity of the ligament is dependent on the rotation speed and force applied to the specimen during pre-fatigue. This means that lower speeds and forces lead to less eccentricity. This does mean that the time required for pre-fatiguing increases. He advises a speed of 4000 RPM and a stress intensity of 60 percent of the expected K_{Ic} , as these stress intensity values are used as standards in conventional pre-fatiguing too.

Compression - Compression

In the research of Hengeveld [5] and Slachter [20] a different method to pre-fatigue the specimens was used. The so called Compression-Compression method (C-C), uses a single compressive overload followed by a cyclic compressive load. If the CNT sample is given a compressive load which creates a local stress which is above the yield stress of the ligament, but still below the yield strength of the full diameter of the specimen a local plastic zone will form around the notch tip, after removal of the external compression load. Because the stress applied is in compression, the local zone of residual tensile stresses will remain around the notch tip.

When a cyclic compressive loading is then applied to the specimen, no crack growth will occur, except in the local plastic zone around the notch tip. This part will experience cyclic tensile forces, thus allowing it to develop a pre-fatigue crack. This crack will be limited to the size of the plastic zone which was created by the compressive overload, making it self-retarding. An additional advantage is that by changing the notch tip geometry and height of the compressive overload it becomes possible to influence the depth of the pre-fatigue crack. This process is schematically visualized in figure 3.9. A more expansive visual explanation of this process, created by dr. Riemslag, for both CNT and SENB is given in appendix A

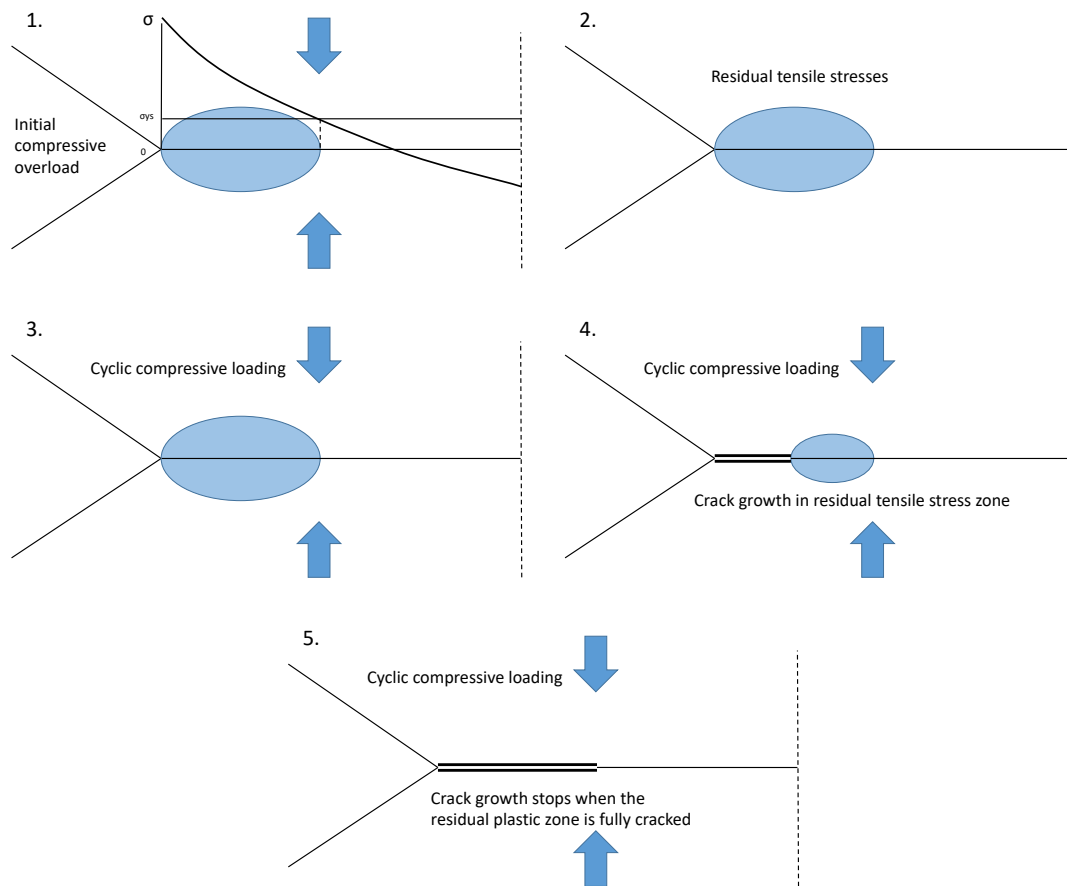


Figure 3.9: Schematic depiction of the Compression - Compression pre-fatiguing process

Effect of eccentricity on fracture toughness measurements and results

Both rotational bending and Compression-Compression have a tendency to form eccentric ligaments. This can be caused by a number of factors, such as flaws in the methods used and internal material properties. That is why it is important to study the effect of eccentricity on the results of CNT fracture toughness tests.

During tensile loading an eccentric ligament is able to cause a bending load on this ligament, this bending load will influence the local stress state. Ibrahim[17] formulated a formula to account for the influence of this bending load, where he added a stress intensity factor due to bending to the normal stress intensity factor. However, Slachter[20] found that this factor greatly exaggerates the effect of the bending load, thus causing far too high stress intensities. A possible reason for this was the use of brittle aluminium by Ibrahim, while Slachter used far more ductile high strength steel. A possible effect in ductile materials is load-line realignment, where the eccentric ligament realigns itself to the load-line, thus acting as a fully centric ligament, effectively canceling the possible effects of the eccentricity. This effect would most probably not take place in brittle materials, due to the lack of plasticity.

Two important observations were made regarding the testing of eccentric ligaments. The first is the failure mechanism involved, in tensile testing an eccentric ligament Slachter discovered that ductile crack growth initiated from the side of the biggest crack length, growing towards the

center of the specimen, and only then stopping when the remaining ligament failed from cleavage failure.

The other is measuring the CTOD of the specimens. This was measured by attaching a clip-gauge extensometer to two sides of the crack, exactly opposite from each other. The eccentricity caused the specimen to slightly bend during loading, meaning the values measured by the two extensometers was not equal, as can be seen in figure 3.10. This results in difficulties associated with finding the critical CTOD values.

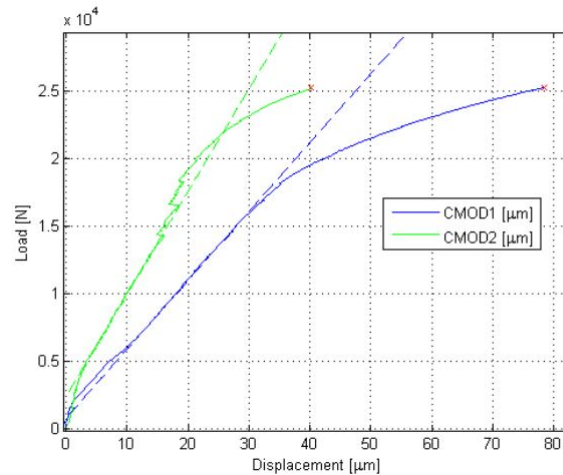


Figure 3.10: Graph showing the difference between the measured displacement of the two extensometers [Slachter 2016]

Influence of the notch geometry

The notch in the CNT sample has two important design parameters, being the notch tip radius ρ and the notch angle β . Both of these have great influence on the tensile behaviour of the specimen, due to the way they influence the stress concentrations on the tip of the notch. Yoda [32] discovered that once a crack initiates for the notch tip, the radius of the notch tip does not influence the fracture toughness of the sample. In CNT specimens, the notch geometry influences only the pre-fatiguing process. Further more Compression-Compression the notch geometry greatly influences the size of the plastic zone created during the initial overload, thus influencing the length of the pre-fatigue crack.

3.3.2 Equivalency to other test methods

As the CNT specimen is seen as a future possible standard test specimen it is important to establish equivalency to other test methods. Several researchers looked into this comparison, leading to different results. Stark worked on different steel types and found their critical stress intensities to be close to literature values, Lucon found good results for steel in the lower shelf. Li [33], worked on aluminium and found the resulting accuracy is very material dependent, while Londe [34] found tests on aluminium to come to a similar value as in literature. Giovanola worked with ductile pressure vessel steel and found a good result in the upper shelf, while lower shelf slightly overestimated the fracture toughness. Pardoen found the CNT sample to only be suitable for brittle and low-ductility materials.

Hence from previous research it appears that the CNT specimen performs better for brittle and low ductility materials, although some authors claim they found relevant results for ductile materials.

Plane strain of the crack tip

One of the claimed advantages of the CNT specimen is the state of plane strain all around its crack. Ibrahim[35] performed a finite element calculation on a medium steel type with a ligament size of 7 mm. It was found that even though it was 'a very small size specimen' for the material, it proved to be in plane strain. He also indicated the fatigue crack should be at least twice as long as the Irwin plastic zone size, otherwise the results will be higher due to a lack of triaxiality. Also the average stress in the ligament at fracture should not be higher than 2.5 times the yield strength of the material. Not following this would lead to a loss of constraint, and thus to an overestimation of K_{Ic} .

The constraint is an interesting value in relation to the CNT sample. It is important to note that there are two definitions of constraint used in literature, and thereby also in this thesis. The first is the plastic constraint factor C , which was introduced in equation 5.1. The other is the constraint factor Q , as seen in equation 3.5, which is referred to in this section. Several authors have done finite element calculations into the constraint on the crack tip during tensile testing. It was found that for a low amount of plasticity in the ligament the constraint quickly reduces and becomes lower than for an SENB sample. However if the plasticity increases further the CNT's constraint increases again, while the SENB will quickly lose constraint. This might mean that the CNT is better suited for highly ductile materials than the SENB, while the SENB would perform better for low- and medium ductility materials. Some disagreement occurs here, while some researchers have found the CNT to be in better constraint than the SENB, others disagree with this claim.

Slachter also attempted to experimentally verify the plane strain conditions. If the CNT's pre-fatigue crack is completely in plane strain it should have a smaller plastic zone than a SENB specimen, however Stretch Zone Width (SZW) measurements and stress intensity values at 2% showed comparable results between the plastic zones of the two specimens. This means that the CNT is not in fully plane strain conditions, however as mentioned before the SZW measurements on this specimen have sometimes given very scattered results, making it hard to fully confirm the plane strain conditions, without a further analysis of the plastic zone size around the crack tip.

Finally it is of importance to distinguish two effects of constraint on the specimen. The unique shape of the CNT specimen causes a fully constrained crack tip, leading to the assumption of plane strain stress conditions. The second effect is due to shape of the specimen itself. The bulk of ligament of the specimen is also constrained, allowing for higher forces to be applied before failure than in SENB specimen.

Loading rate effect on fracture toughness testing

An important parameter in tensile testing is the loading rate, or crosshead displacement rate. Slachter found out that the CNT specimen does not show any influence due to the speed of the crosshead, shown in figure 3.11. The tests showed that the fracture toughness of CNT specimen is dominated by geometry and stiffness of both the sample and the tensile machine. This means that fracture toughness testing of this specimen can be done on high crosshead speed without influencing the results.

An explanation posed for this by Slachter is in the way the material behaves under loading. It seems to be that before fracture the whole specimen is loaded and thereby stretched out, just

like a spring would. When fracture occurs the whole load of elastic energy is released, leading to a very high crack growth speed. A negative consequence of the behaviour would be that the CNT is not able to measure the crack growth speed. Results by Devaux[15] on the other hand contradict this finding, as stable crack growth was observed, and the crack growth rate was found.

The independence of the loading rate also plays an important part in the way the temperature dependent behaviour of the material can be determined. Research in the 'AFSuM' project by Walters [36] lead to the development of a fast and easy method of fracture testing sub-size fracture toughness specimens at low temperature. In conventional fracture testing at low temperature an SENB specimen has to be continually cooled by liquid nitrogen in a climate chamber, making for a cumbersome and slow testing regimen. In the AFSuM-method the sample is cooled to well below the desired testing temperature in liquid nitrogen, then mounted in the machine and left to warm up until the desired testing temperature. It can then be broken with a very high crosshead speed, making sure the sample does not change temperature during the actual test. As the CNT sample is also loading rate independent this means the AFSuM method can be applied for the low temperature testing.

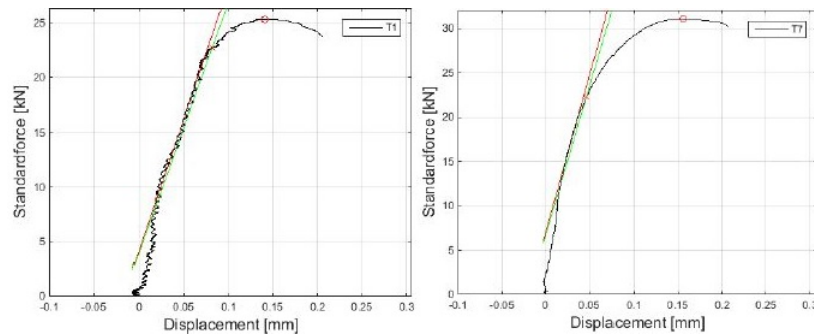


Figure 3.11: Load-displacement curve for low ($3 \text{ MPa}\sqrt{\text{m/s}}$) (left) and high ($571 \text{ MPa}\sqrt{\text{m/s}}$) (right) displacement rate show the equivalency between the load rates

3.4 Conclusions and recommendation

In the previous chapters it was shown that the CNT specimen shows a lot of potential as a fracture mechanical test specimen. However there are still a number of issues that should be addressed.

CNT

Theoretical advantages of CNT specimen described in section 3.1.1 indicate that this test could be very useful and a potential alternative to conventional tests. The advantages of the test regarding machining, modeling and application of tensile machine are all experientially verified in literature and not debatable. However, there are two issues still open for debate: 1) pre-cracking and 2) crack tip plane strain.

Solutions

Different solutions for K have been presented, where the solution by Benthem and Koiter (equation 3.7) seems to be used most and has been confirmed in finite element calculations to be very accurate. A J -integral solution for the CNT specimen has also been formulated, where several authors have also defined an η -function describing the plastic behaviour of the material. CTOD

has been shown to be difficult to measure on the CNT specimens, especially due to the eccentricity that often occurs, having been caused by the pre-fatiguing process. Possible techniques to improve the knowledge about the plastic zone size and the CTOD are using digital image correlation, EBSD and nano indentation hardness measurements.

Experimental considerations

One of two techniques is generally used to create the pre-fatigue crack in the CNT specimen. Rotational bending is used in most researches, where the specimen is sinusoidally loaded in compression and tension by applying a moment and rotating the specimen. The other technique is compression-compression fatigue, developed within the TU Delft, where the specimen is given a compressive overload creating a plastic zone around the notch where residual tensile stresses are present, this zone is then given a compressive cyclic load which creates a fatigue crack through the length of the plastic zone. If this crack is too short, tensile-tensile cyclic loading can be employed to further grow it. A major issue with both of these methods is the eccentricity, leading to uncertainty regarding the theoretical advantage of easy pre-fatiguing.

The other disputed theoretical advantage of the CNT specimen is the crack tip always being in the triaxial plane strain stress state leading to size-independence. The size-independence has been disproven by several authors, leading to the previously mentioned minimal size demands. In general it seems the size of the plastic zone around the crack could give an interesting new perspective on this discussion. It was also found that the CNT specimen is loading rate independent; allowing for the high speed low temperature tests developed in the AFSuM [36] project to be used.

High-strength steels

High-strength steels have many advantages over conventional steels, but also pose certain challenges. One of these is the fracture behaviour of the heat affected zone, as testing this is a difficult task. The CNT specimen might offer a relatively simple method of testing heat affected zone material, in particular the coarse grained heat affected zone material, which is the critical zone from a fracture toughness point of view.

3.5 Research Scope

A number of recommendations on the scope of the project concerning the CNT specimen can be formulated following this literature review.

1. Further development of pre-fatiguing method, in order to reduce eccentricity and increase crack length.
2. Find a method to easily and accurately measure the Cracktip Opening Displacement of CNT specimens.
3. Determine the equivalency between the CNT specimen and conventional fracture toughness specimens
4. Find a reliable method to test the fracture toughness of the coarse grain heat affected zone of steel using CNT specimens.
5. Measure the plastic zone around the crack in CNT specimens to give a better understanding of the constraint during loading

3.6 Research questions and test plan

Following this scope the research question and sub-questions have been proposed, along with the test plan required for answering these questions:

Are Circumferentially Notched Tensile test specimens suitable and applicable for failure assessment of (welded) S690QT steel?

- Use the CNT specimen to fracture test CGHAZ material. This means creating a simulated heat affected zone in a CNT specimen, pre-fatiguing it and testing it both at room temperature and at a lower shelf temperature.

the following sub-questions are formulated along with the main research question:

1. Can a pre-fatigue method be developed causing little or no eccentricity?
 - Use rotational bending to pre-fatigue the CNT specimen. This method has been shown to work and to create centric cracks.
 - Use the standalone compression - compression method to create the full pre-fatigue crack in the CNT specimen. In previous research this method was only used to initiate a crack, after which it was extended in cyclic tensile loading. It is hypothesized that the cyclic tensile part was the source of the eccentricity occurring in this method, so discarding this part should create a more centric crack. The absence of the pre-fatigue stage in tension means only a small crack would be created, therefore the compressive overload will be increased, and several notch geometries will be used, in order to find a sufficient crack length.
2. Can a convenient method be developed to measure the CTOD of CNT specimens?
 - Use several techniques to find the CTOD of the CNT specimen. Because the crack mouth opening displacement (CMOD) should be equal to the CTOD it should be possible to measure it using extensometers attached on the outside of the notch. In order to confirm this interrupted tensile tests are used to inspect the crack opening under the microscope. Furthermore digital image correlation (DIC) techniques will be used to optically measure the CMOD during tests, allowing comparison to load-displacement curves and inspection of the influence of eccentricity.
3. Can equivalency between the CNT specimen and conventional FM specimens be determined?
 - Test base material CNT specimen at room temperature and low temperature, these results can be compared to results from the AFSuM test program, to see if the results compare.
4. Can the plastic zone size of the CNT specimen be determined?
 - Use EBSD tests to find the size of the plastic zone ahead of the crack. This plastic zone size should allow an estimation of the plastic constraint factor to be made.

Chapter 4

Experimental methods

In this chapter all methods used in this research will be discussed. An overview of the sample preparation of the CNT specimens, the fracture toughness tests and the appropriate post-processing of the gathered data will be presented.

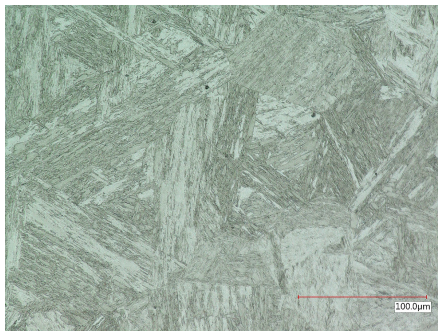
4.1 Material

The material used in this research was the high-strength S690QT steel, a type of steel often used in offshore applications. The samples were cut from a 60mm thick slab with the following composition (table 4.1), as measured using XRF.

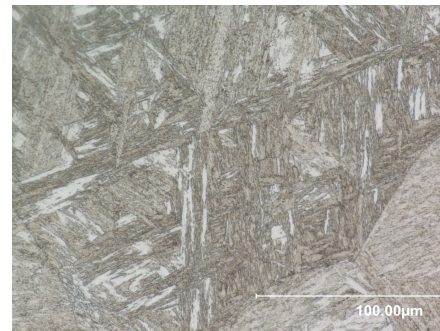
Table 4.1: S690QT steel composition

Element	C	Si	Mn	P	Cr	Mo	Ni	Cu	Al	Nb
wt(%)	0.162	0.2	1.3	0.01	0.36	0.45	0.01	0.081	0.093	0.029

The 60mm thick slab has been shown to have different hardness and microstructure through its thickness due to the non-uniform temperature distribution during cooling. Therefore the material used is cut from the top and bottom of the slab, thus not using the center part, in order to guarantee similar material properties for all samples. This material has a fine grain tempered martensite structure, as shown in figure 4.1a.



(a) Microstructure of S690QT base material



(b) Microstructure of S690 HAZ material

Figure 4.1

In this research simulated Coarse Grained Heat Affected Zone (CGHAZ) material was used as well. This material is comprised of martensite, austenite and some granular lath bainite. Martensite-Austenite (M-A) constituents can sometimes be found on prior austenite grain boundaries. This microstructure is shown in figure 4.1b. The mechanical behaviour of these materials are indicated in table 4.2:

Material	σ_{ys} (MPa)	σ_{uts} (MPa)	Hardness [HV ₃]
Base material	760	824	270
CGHAZ material	1110	1400	400-440

Table 4.2: Mechanical behaviour of base material and HAZ material

4.2 Sample preparation

CNT specimens were machined from a large slab of steel and subsequently pre-fatigued. All dimensions of CNT specimens are related to the outer diameter. The tensile machine and grips can sustain a maximum load of 100 kN, so this force should be never exceeded. Therefore the choice was made to base the outer diameter on the maximum diameter of unnotched bar of base material that could be broken below 100kN, which has a diameter of 12 mm. This lead to the dimensions shown in table 4.2.

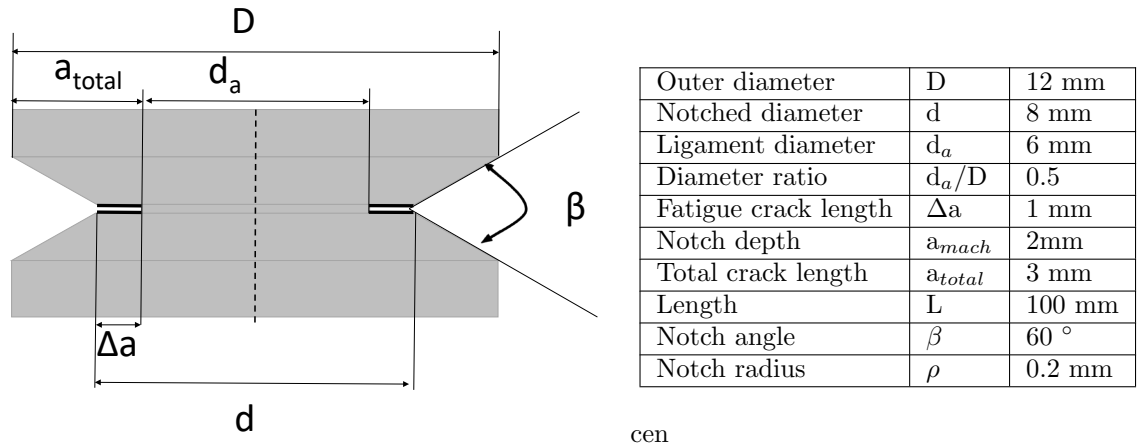


Figure 4.2: Parameters of the CNT specimen

4.2.1 Machining

The base material for the CNT specimens was cut in tranches in the T-L direction of the steel slab, as this is the direction known to have the lowest fracture toughness, shown in figure 4.3a. Then the top and bottom part of this tranche were cut by machined sawing into 15x15 mm wide bars with a length of 100 mm. These bars were turned to a diameter of 12 mm between two live centers in the lathe, this setup was used to insure the most uniform straight and round bars possible. These round bars were then notched in the same setup to a depth of 2 mm. For the compression-compression samples it is essential to have the top and bottom to be flat, and be as straight as possible, for mounting as shown in figure 4.5. Therefore the center holes were removed and the top and bottom of the samples were cut to be completely flat with the smallest

surface roughness achievable. During all these machining steps care was taken to prevent any heating of the specimen. The finished specimen is shown in figure 4.3b.

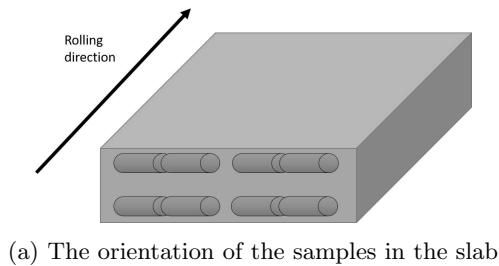


Figure 4.3

4.2.2 Pre-fatiguing

After machining the CNT specimens require a fatigue crack in order to qualify as a fracture toughness specimen, the next section describes the two methods used during this research.

Rotational Bending

Rotational bending (RB) is the conventional way of pre-fatiguing CNT specimens. The theoretical background of this method is explained in chapter 3.3.1. Calculations based on the formulas in Tada [22], indicate that an initial moment of 18 Nm would cause a stress intensity in the ligament of $15 \text{ MPa}\sqrt{\text{m}}$. A subsequent moment reduction of 10 % leads to a circumferential crack length of 1 mm for a gauge length of 120 mm, a reduction of 5 % is required for a gauge length of 50 mm.

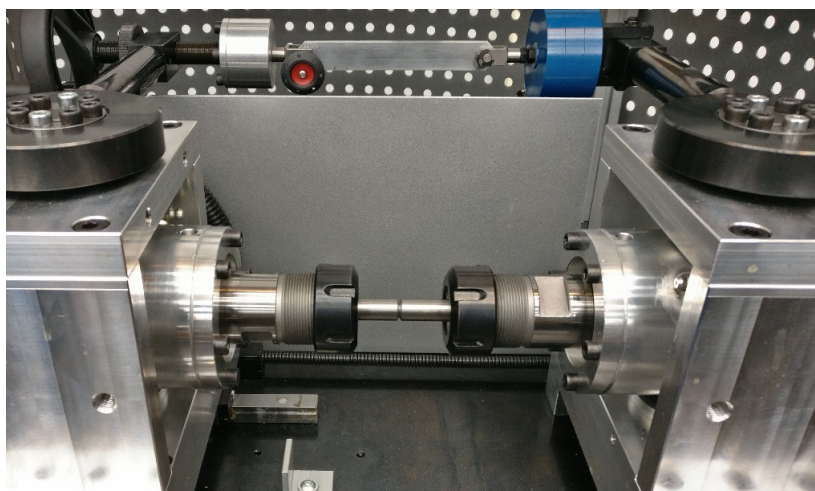


Figure 4.4: The Sincotec 50 Nm four-point rotational bending machine

For this research the "Sincotec 50 Nm four-point rotational bending machine", shown in figure 4.4, was used. This machine is able to apply rotational four-point-bending fatigue on specimens by gripping a round specimen in two cylindrical grips and applying a moment on the length between the grips. In this research a gauge length of approximately 50 mm between the grips was used when possible for the most consistence in results. No effect of the rotational speed is expected, therefore the specimens were fatigued at a speed of 2000 rpm (33.3 Hz), this was the maximum speed acceptable due to the excessive noise created at higher speeds. The machine was set to automatically stop the fatigue process once the pre-described drop in moment was achieved.

Compression - Compression

The Compression - Compression (C-C), fatigue method has been used in previous research as a method of initiating a small circumferential crack, which was then grown in tensile fatigue. This method is sensitive to misalignment and can lead to large eccentricities in the ligament, and was therefore rejected as a useful pre-fatiguing method. In this research it is proposed to discard the tensile fatigue part and optimize the C-C method. Because C-C has never been used to grow full-length cracks, attention will be given to the most important parameters governing this process.

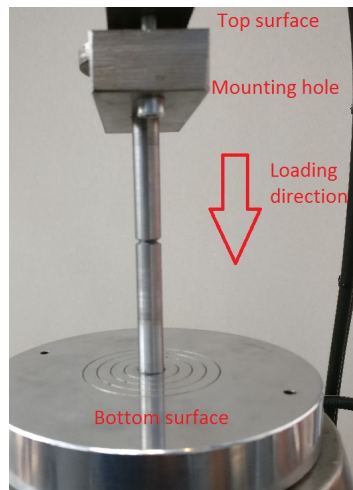


Figure 4.5: The C-C setup with a CNT specimen mounted

The Compression - Compression fatiguing was performed on a hydraulic MTS 350 kN fatigue testing machine, with a flat surface mounted in the bottom grip, and a metal bar with a hole with a diameter of 12.5 mm in the top grip. This metal part has a flat surface mounted beneath the hole, and the hole is used as an alignment method. The goal of this setup is to make sure both the top and the bottom part of the grips making contact with the specimen are completely flat and the specimen is loaded along its axis and not at an angle. This is important because the specimen is not gripped from the side, so the alignment must come from the top and bottom contacts, the whole setup is shown in figure 4.5.

When the specimen is mounted the compressive overload is applied. This overload must be lower than the yield stress of the main diameter, otherwise the specimen will bend. The size of the created tensile plastic zone depends on a number of parameters: the applied force, the d/D ratio of the ligament, the notch angle and radius and the strength of the material. To compare the effect of the overload on the crack length two overloads were used, 52.2 kN ($0.67 \sigma_{yse}$) and

72.9 kN ($0.89 \sigma_{yse}$). The σ_{yse} has been defined as a parameter describing the yield strength equivalent stress of the main diameter with a diameter of 12 mm. This means the σ_{yse} must always be below 1, as this would lead to general plasticity.

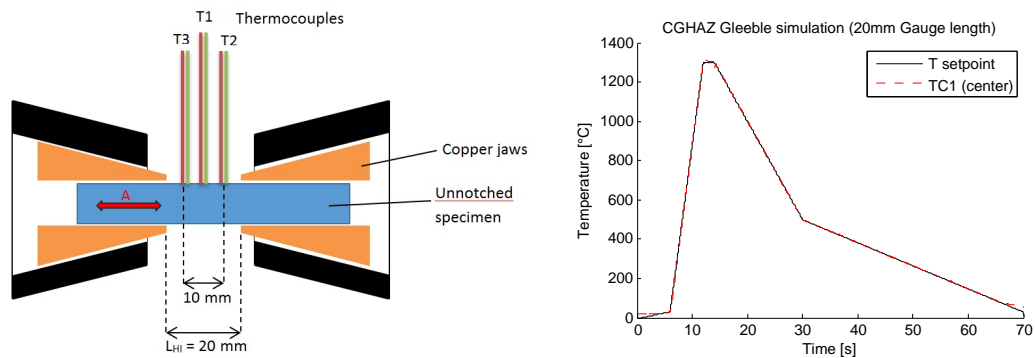
After the overload, the CNT specimen is fatigued using a sinusoidal compressive load. The force used is between 3.5 kN ($0.04 \sigma_{ys}$) and 27.8 kN ($0.36 \sigma_{ys}$), this to make sure no additional plasticity occurs. In this research all specimen had a ligament diameter of 8 mm, resulting in a force between 3.5 kN and 27.8 kN. The amount of cycles used was varied to investigate the minimum necessary amount of cycles. The amount of cycles used were 10.000, 20.000, 100.000, 500.000, 1.000.000 and 2.000.000 cycles.

For the C-C specimen used for the fracture toughness tests an overload of 72.9 kN was used, with 100.000 cycles of compressive cyclic loading, as this was found to give a crack of approximately 1 mm, with little eccentricity. The heat-treated material was also pre-fatigued using C-C. Here the material where the notch is applied will locally be stronger than the rest of the specimen. It is important to realize that the maximum compressive overload is dependent on the weakest material in the specimen, in this case the base material. Therefore the same overload was used for heat-treated material as for the base material, the amount of cycles used for these specimen was 500.000.

4.2.3 HAZ simulation

Specific HAZ microstructures are usually simulated by heat treating a sample using a pre-described thermal profile similar to that found in the real material. This thermal profile, which was measured during previous research, was determined using thermocouples attached to material being welded. Simulation of this microstructure was performed on the Gleeble 3800 thermo-mechanical simulator.

The Gleeble uses a high amperage alternating electrical current to heat up and control cooling of a metallic material. Because electrical current will create local hotspots and non-uniform microstructures on notched samples, these heat treatments were performed on unnotched bars. Using the pocket jaw method, shown schematically in figure 4.6a, the sample is clamped between the two jaws, consisting of 2 copper blocks, which fully grip both ends of the specimen. A length of approximately 20 mm between the two jaws was used for the CNT specimens and thermocouples are attached to the material to control heating and cooling. Because of the high amount of oxidation which occurs at the very high temperature used, the heat treatments are performed in a vacuum. After heating the specimens are cooled using Helium, both because it has a higher heat capacity than air and because it is inert and will thus cause no oxidation. The used temperature profile is given in table 4.3 and visualized in figure 4.6b.



(a) Schematic representation of the pocket jaw mode of the Gleeble [Slachter 2016] (b) Plot of the heat treatment with the control and measured temperature profile

Figure 4.6

Table 4.3: Temperature profile for CGHAZ simulations

Heating time from ambient to 1300 C (s)	Holding time at 1300 C (s)	Cooling time from 1300 C to 800 C (s)	Cooling time from 800 C to 500 C (s)	Cooling time from 500 C to ambient (s)	Heat Input (kJ/mm)
6	2	10	6	40	1.1

Because the Gleeble is not able to use notched or cracked specimens another method was attempted to create this microstructure as well. Using a Ultra High Frequency (UHF) induction coil and air cooling, shown in figure 4.7, the same temperature profile was simulated.



Figure 4.7: The Ultra High Frequency heating setup

4.3 Fracture Toughness testing

The main part of the research revolved around the fracture toughness tests, which will be described in the section below. The following three terms will be used below: Crack opening displacement (COD) is the opening of the actual crack; crack tip opening displacement (CTOD) is the opening of the tip of the crack; crack mouth opening displacement (CMOD) is displacement measured on the outside of the CNT specimen. However, if the crack flanks move parallel, all three of these values should be the same, making them interchangeable. Therefore the COD will be used in most cases, as this is the most correct of the three.

4.3.1 Crack Opening Displacement Measurement

Set-up

Measuring the Crack Opening Displacement (COD) was done using two universal testing machines. All fracture toughness tests performed at room temperature were performed on the Instron 5500R 100 kN universal testing machine. The displacement signal was measured using one or two Instron extensometers, depending on the accessibility of the specimen. These extensometers have a standard gauge length of 12.5 mm, which can be adjusted by changing the mounting position of the blades which contact the specimen, and are attached using rubber bands.

All low temperature tests were performed on the Zwick 100 kN universal testing machine. Two different extensometers were used on this machine. The Zwick makroXtens extensometer, which has a large range of possible gauge lengths. And the Zwick standard clip-on extensometer, which has a non-adjustable gauge length of 20 mm.

On both machines gripping was done by 100 kN mechanical wedge grips, which grip at four points around the circumference, at 90 °intervals. Because extensometers were used for all tests the grips were mounted with a certain amount of slack at the connection point of the tensile machine, which allowed them to compensate for any misalignment. The CNT specimen was shown to be crosshead speed independent, so for convenience all tests were performed at a crosshead speed of 2 mm/min and unless otherwise stated all specimens were loaded until failure.

Digital Image Correlation

Digital Image Correlation (DIC) was used to measure the CMOD during fracture toughness tests, this was a new method for testing CNT CTOD. DIC works by cameras tracking a unique speckle pattern on the surface of a specimen during testing, after which displacements and strains can be calculated and visualized. In this research the Limes 2000 DIC system was used, with two 5 megapixel cameras with a fixed zoom lens. The cameras were placed to exactly observe the full width of the notch, meaning the field of vision was 12x12 mm.

Before performing a DIC tests a high contrast speckle pattern has to be applied, this is done using a pressurized paint canister. The speckle pattern is applied by first creating a white paint background, then black paint is used to create the speckles. The pattern should be as fine as possible, so the canister is used from about a meter distance, which creates a very fine speckle.

As seen in figure 4.8b the cameras are placed at an angle of 90 °from the sample, this allows them to capture over 180°of the specimen circumference, which is enough to determine the possible eccentricity during testing, an extensometer is placed on the back of the sample to provide information about the displacement of that part. The cameras are calibrated using a 9x9 mm calibration grid. The correlation is performed using a coarse resolution, with a facet

size of 50 pixels and a grid spacing of 60 pixels. Post-processing then provides the displacement between the top and bottom part of the specimen, which is the CMOD.

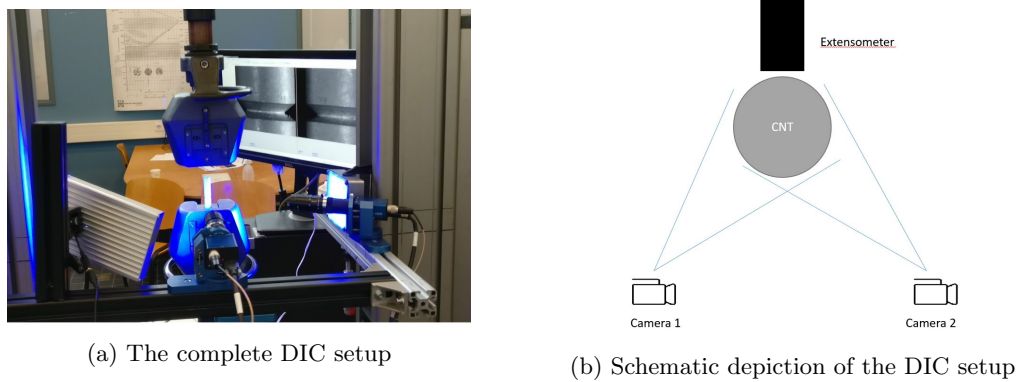


Figure 4.8

4.3.2 Unloading-compliance testing

One variation on the standard tensile fracture toughness test was the unloading-compliance fracture toughness test (UCFT). This test differs from a standard fracture toughness test in that at set intervals will unload part of the force before loading the specimen further. This test is used as a method of measuring the compliance of the specimen, which allows crack length predictions to be made. It means that at set intervals the material is unloaded to the higher of these two values: 50% of the previous load, or 20% of the maximum load. In this research it served another purpose as well, some specimen did not show standard elastic behaviour, so it was used as a method of proving the measurements were correct and to show that the unloading/reloading line did in fact show elastic behaviour.

4.3.3 Low-temperature testing

Part of the fracture toughness and tensile tests were performed at low temperature. Two methods were used to do this: the temperature chamber and the adapted AFSuM low temperature test.

The temperature chamber is a well insulated chamber, that can be mounted on the Zwick universal testing machine, which is cooled down by nitrogen evaporation. The CNT specimen is mounted in the standard grips in the temperature chamber with a thermocouple attached. Once the specimen has reached its desired temperature the test is executed using the clip-on extensometer. This method is easily controlled and kept constant, however it takes a long time, over 30 minutes per test, a lot of preparation and a lot of nitrogen. A practical concern was that the wedge grips used are loosened and tightened using a screw system. At very low temperatures this system froze, meaning it was impossible to mount or dismount the specimens, making it impossible to do a series of measurements.

In order to circumvent these problems the adapted AFSuM low temperature (AALT) test was developed. In the AFSuM research it was found that by fully cooling a specimen and quickly breaking it when the required temperature was reached it was far easier to perform low temperature tests than by using the temperature chamber. This principle was also applied in AALT tests.



(a) Specimen inside the temperature chamber



(b) The AALT method, the specimen is cooling in the nitrogen tank

Figure 4.9

The specimen, with a thermocouple and thermometer attached, is mounted in the top grip of the tensile machine and then lowered in a small tank of liquid nitrogen. When the sample is fully cooled, and has soaked in the nitrogen for a few minutes, the crosshead is moved up, the tank of nitrogen is removed and the sample is very quickly moved into the grip. After attaching the extensometer the sample will warm up quickly to the desired temperature, at which point it can be tested. This test has to be done very quickly in order to make sure the sample does not warm up too far, so a test speed of 50 mm/min was used, which allowed a temperature at fracture of -110°C .

4.4 Post-processing

After fracture toughness testing the results have to be processed and the processing methods are shown below.

4.4.1 Fracture surfaces

After fracture it is important to know the size of the pre-fatigue crack and how much eccentricity has occurred. This is done by measuring the fracture surface. Using an optical microscope a picture is made of the fracture surface. It is important to know the outer diameter of the specimen beforehand, as the outer diameter is set in the computer, after which the specimen is enlarged until the dimensions are correct.

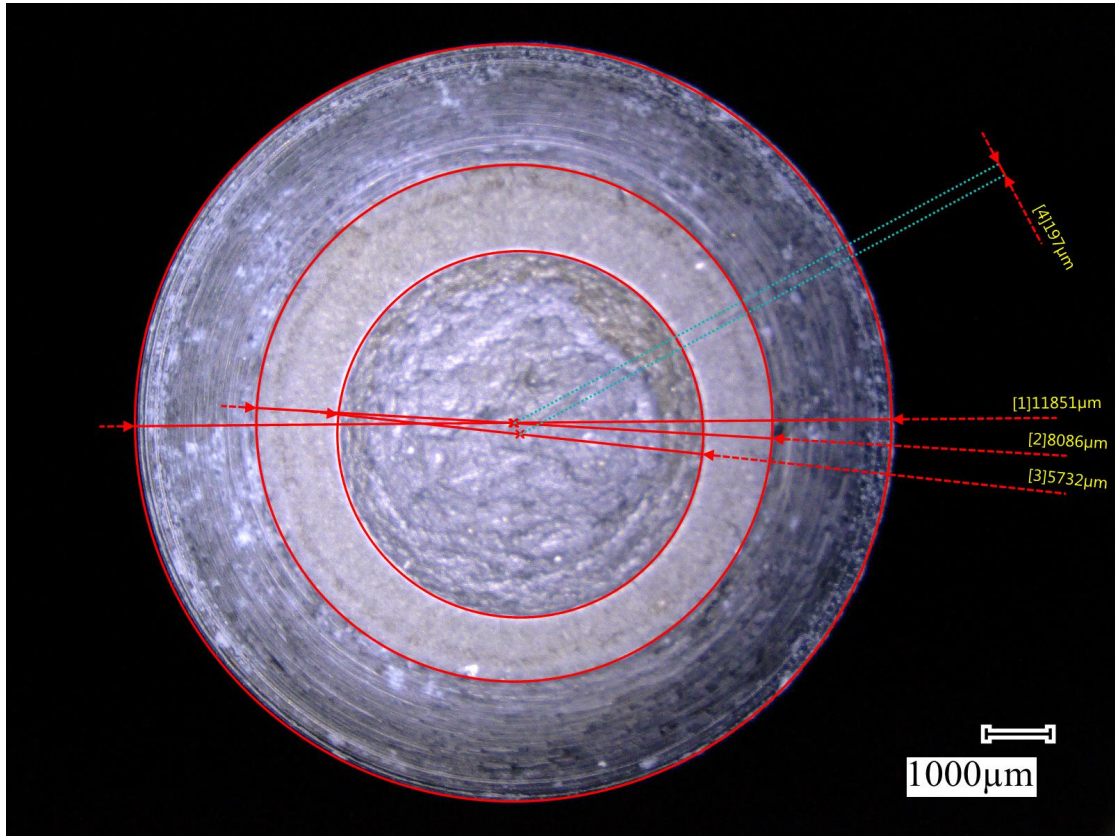
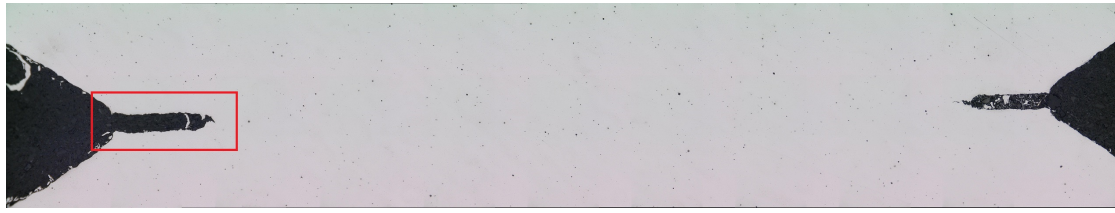


Figure 4.10: Fracture surface

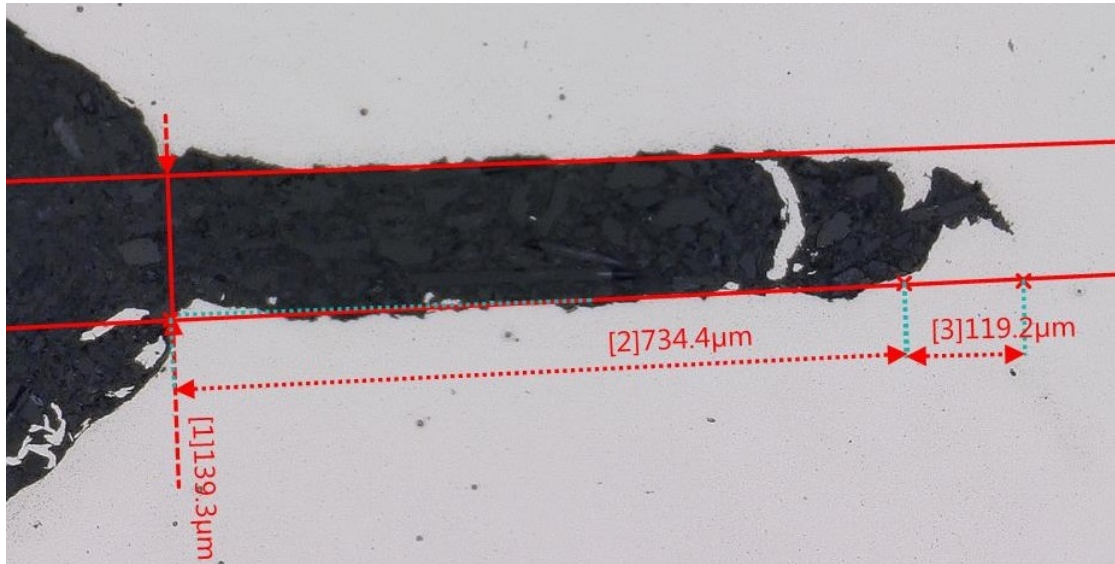
As shown in figure 4.10 four values are measured. The outer diameter, the diameter of the notch, the diameter of the ligament and the distance between the center of the ligament and the inner diameter. This value is defined as the eccentricity. The crack diameter is used to calculate the average crack length by $a_{av} = (d_{notch} - d_a)/2$. The maximum crack length is found by adding eccentricity to the average crack length: $a_{max} = a_{av} + ecc$.

4.4.2 Crack opening measurements

A number of samples were not tested until failure but interrupted at certain points during loading. These specimens were then cut in half along the vertical axis, to reveal a cross section of the specimen, as seen in figure 4.11a, with the notch and crack visible. After grinding and polishing this allowed for measurement of the plastic COD and crack length, seen in figure 4.11b. It could also be seen if stable crack growth had initiated. After measuring these values it was possible to break the specimen at low temperature, in order to measure the eccentricity and check the crack surface.



(a) Cross section of an interrupted loading specimen



(b) Measurement of COD and crack length

Figure 4.11

4.4.3 CTOD and compliance

Calculating the CTOD of conventional fracture toughness specimens requires a somewhat complicated approach, where the hinge effect has to be taken into account. For the CNT specimen literature states that the CTOD can be measured directly as the plastic displacement measured by the extensometer. This means that in order to find the permanent CTOD the elastic displacement must be subtracted from the total displacement measured. It is suggested that the critical CTOD is found at the maximum load, making this the point to calculate the CTOD at. Interrupted tests were performed, where the load was removed at maximum loading, to investigate this statement.

Because the CNT specimen does not have a uniform cross section the slope of the load-displacement curve in the elastic part will not be governed by the Young's modulus. Therefore the compliance is used to determine the elastic behaviour line, where the compliance is the inverse of the stiffness of the specimen. Because every specimen has a different crack length and amount of eccentricity the compliance of every specimen has to be calculated separately, as a function of its specific geometry. In literature three different approaches are given: the Koiter-Benthem compliance, the Scibetta compliance and the assertion that due to the present constraint the compliance is equal to the stiffness that would be present without a crack and notch.

The Koiter-Benthem compliance function is derived from the Benthem and Koiter, presented

in chapter 3.2.1, where:

$$C = \frac{\Delta}{P} = \frac{G}{E\pi R^2} \left[1 + 4\pi R \frac{1-\nu^2}{\Delta} H\left(\frac{d_a}{D}\right) \right] \quad (4.1)$$

with

$$H\left(\frac{d_a}{D}\right) = \frac{0.25}{x} - 0.35317171 + 0.168875x^2 - 0.1325521x^3 + 0.04880469x^4 - 0.001106345x^5 + 0.05044688x^6 - 0.003803811x^7 + 0.01669878x^8 \quad (4.2)$$

Where C is the compliance, x is d_a/D , P is the load, d_a is the ligament diameter, and Δ is the gauge length. This method is reported to be accurate up to 4,5 % from $G > D$

The Scibetta method is a further development of the K-B method, where a finite element fit was used to reduce minimum required gauge length to zero. This method is reported to be accurate within 0.5 % for all gauge length.

$$C = \frac{\Delta}{P} = \frac{\Delta}{E\pi R^2} + \frac{1}{ER} \left[4(1-\nu^2)H\left(\frac{d_a}{D}\right)(1 - e^{-2\frac{\Delta}{\pi}}) + \frac{a}{0.5d_a}I\left(\frac{d_a}{D}\right)e^{-2\frac{\Delta}{\pi}} \right] \quad (4.3)$$

with

$$I(x) = 0.635 + 1.14x + 0.926x^2 \quad (4.4)$$

These two methods and the assertion that ignoring the complex geometry will be compared in the results section to see which gives the most reliable result for calculating the CTOD.

Most of the specimen in this research have been measured using 2 extensometers, placed directly opposite each other. This means two COD's are measured during these test. Because the largest COD is the critical parameter in fracture mechanics, the larger of the two measured COD's will be used as the critical COD. When only one signal was available, this will automatically be used as the COD.

4.5 Plastic zone measurements

In order to measure the plastic zone of CNT specimen, EBSD measurements were performed, for which two samples were prepared. The first specimen was made of low carbon S37 steel, pre-fatigued in rotational bending, which was heat treated at 450°C for 45 minutes, in order to reduce the dislocation density of the material. The second specimen was a fully annealed S690 specimen which was pre-cracked using rotational bending before annealing. The annealing was performed at 930°C for 45 minutes in an envelope filled with inert gas. After heating the specimen was left to cool to room temperature.

The choice for these two different materials was caused by the high dislocation density of S690QT steel. These dislocations would make for small differences in measured signal between the background and the plastic zone, thus making it hard to detect plasticity. Low carbon steel has a far lower dislocation density, however fully annealing this material was undesirable because this material would exhibit a yield plateau, which would influence the results. The annealed S690 also has a lower dislocation density and does not present a yield plateau, thus allowing full annealing. These two materials should then have a larger difference between background dislocation density and plastic zone density.

The S37 steel was found to have a yield strength of 390 MPa, after heating, and was loaded to a force of 14.6 kN, equal to a stress intensity of $15 \text{ MPa}\sqrt{m}$ using equation 3.7. The annealed S690 has a yield strength of 288 MPa, and was loaded to a force of 5 kN, equal to a stress intensity of $8.15 \text{ MPa}\sqrt{m}$.

The two specimen were loaded to this set tensile force and then unloaded. After this they were cut in half along the central axis and grinded and polished using the following steps: P400, P800, P1200, P2000 sanding paper and 3 and $1\mu\text{m}$ polishing paste. The surfaces were then electrochemically etched to create a surface on which EBSD measurements could be performed. The EBSD measurements were performed at Ghent University, and used a step size of 5 nm.

4.6 Full test table

Test	Machine	Goal	Samples
Rotational bending fatigue	Sincotec 50 Nm rotational bending machine	Pre-fatigue crack creation	RB1- RB12 LTRB1 - LTRB5 S7 -S9
Compression - Compression fatigue	MTS 350 kN fatigue machine	Pre-fatigue crack creation	C1 - C25 GRT1 - GRT3 GLT1 - GTL3
Room temperature COD tests	Instron 5500R universal testing machine	COD determination	C9, C11, C13, C15 C18 - C22 GRT1 - GRT3 S7 -S9 RB1- RB6, RB8 RB12
Low temperature COD tests	Zwick 100 kN universal testing machine	COD determination	C23 - C25 GLT1 - GTL3 LTRB1 - LTRB5
Room temperature tensile test	Instron 5500R universal testing machine	Tensile behaviour determination	RTT1 - RTT2
Low temperature tensile test	Zwick 100 kN universal testing machine	Tensile behaviour determination	LTT1 - LTT2
Digital Image Correlation tests	Limes Instra4D DIC system	Visual CMOD determination	C13, C15, C18 G1
Heat treatments	Gleeble 3800 thermo-mechanical simulator	CGHAZ microstructure simulation	RTT1 - RTT2 LTT1 - LTT2 GRT1 - GRT3 GLT1 - GTL3 G2 - G4
	MTS UHF induction coil	CGHAZ microstructure simulation	T1300_6
Microscopy COD measurements	Keyence optical microscope	Plastic COD measurements	C19 RB3, RB5, RB6 LTRB2, LTRB3, LTRB5
Hardness measurements	Ecos hardness tester	Hardness mapping	G1, GLT1

Table 4.4: Full test table

Chapter 5

Results and discussion

In this chapter the results and their interpretation will be given. The first part will discuss the two pre-fatigue methods used,

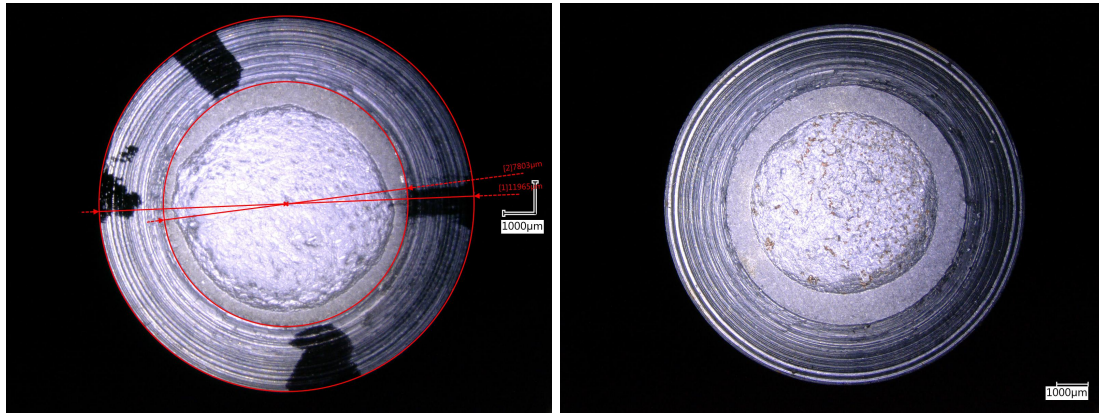
5.1 Pre-fatiguing

5.1.1 Rotational bending

As there was no prior experience working with the Sincotec rotational bending machine, this led to certain imperfections in the initial process. However with an average moment drop of 5% and an average initial moment of 17 Nm, a K value of $14 \text{ Mpa}\sqrt{m}$, the average crack length extension achieved was 0.85 mm and had an eccentricity of 0.1 mm. All rotational bending results can be found in appendix C.1.1.

Two important facts about the rotational bending procedure were found. In the first tests a load drop of only a 0.2 Nm was used, leading to very small crack extension with a certain eccentricity in the crack shape, as seen in the macrograph in figure 5.1a. This eccentricity is probably caused by terminating the process too early, as it appears to have a minimum required load drop in order to create centric cracks. If the load drop is not sufficient, the crack will initialize on all sides, but will not be able to form a centric crack before the set load-drop is reached.

This phenomenon might also have to do with the other issue encountered. Even though great precaution was used to make the notches as centric as possible, it was found that the specimens had a difference in observed moment along its circumference. When the moment was applied, it was found that some specimens had a difference in moment of over 3 Nm around its circumference. This might have been the cause of some of the imperfect cracks formed, and might be an interesting phenomenon to look into further.



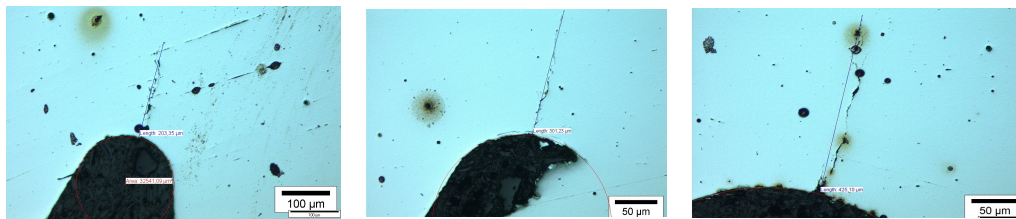
(a) RB specimen with a small crack length and an elliptical fracture surface (b) RB specimen with a larger crack length and round fracture surface

Figure 5.1

5.1.2 Compression - Compression

Compression - Compression was proposed as a standalone method for pre-cracking the specimen. In order to be able to use the C-C method for fracture toughness testing a created crack extension of approximately 1 mm is required. Several variables were tested and compared, and the complete C-C results can be found in appendix C.1.2. In this section the compressive overload will be expressed as the yield strength equivalent of the main diameter, meaning $0.67 \sigma_{yse}$ equates to $F = 0.67 \cdot \sigma_{ys} \cdot \pi \cdot \frac{d^2}{4} = 0.67 \cdot 760 \cdot \pi \cdot \frac{12^2}{4} = 57.2 \text{ kN}$

The first thing to be compared were the notch radius and notch angle. Three different notch radii were tested: 0.1 mm, 0.2 mm and 0.4 mm. These were given an overload of $0.67 \sigma_{yse}$, after which 2.000.000 cycles of compressive fatigue were applied. After this the specimen was cut in half in order to measure the crack extension, as seen in figures 5.2a, 5.2b and 5.2c. The average of the crack extensions measured is given in table 5.1 as a function of the radii.



(a) Crack with a notch radius of 0.1 mm (b) Crack with a notch radius of 0.2 mm (c) Crack with a notch radius of 0.4 mm

Figure 5.2

Table 5.1: Average crack extension for 3 different notch radii at a $0.67 \sigma_{yse}$ overload

Notch radius (mm)	Average crack extension (mm)
0.1	0.21
0.2	0.28 (+33%)
0.4	0.47 (+125%)

It can be seen that the larger the notch radius becomes, the larger the crack becomes.

The other specimen parameter that can be of influence is the notch angle. In order to verify this two notch angles were compared, seen in table 5.2, specimen with a notch radius of 0.2 mm and an angle of 30° and 60° were compared after using a $0.67 \sigma_{yse}$.

Table 5.2: Comparison of notch angles of 30° and 60° at a $0.67 \sigma_{yse}$ overload

Notch angle (°)	Average crack extension (mm)
30	0.28
60	0.53 (+89%)

The larger angle created a larger crack extension. This can be explained by considering the stress concentration values constituted by these notches. If the notch radius becomes larger, the stress concentration at the notch tip becomes lower, but will be present over a longer distance from the notch. This means a larger area will plastically deform and the residual tensile stresses will be present over a larger distance, thus leading to a larger crack. Similar for the larger notch angle. If the angle becomes larger the stress concentration at the notch tip will be lower, yet the distance will increase again and create a longer crack.

Because none of these samples reached the desired crack length extension of 1 mm, the compressive overload was raised to the maximum value which was considered safe: $0.89 \sigma_{yse}$, or 72.1 kN. It is assumed any higher load might start leading to plastic deformation, which could lead to bending or even the disastrous buckling of the specimen. For the $0.89 \sigma_{yse}$ overload, different amount of cycles were used, to determine their effect, the results are shown in table 5.3 and a selection of macrographs in figures 5.3a and 5.3b.

Table 5.3: The crack extension found using a $0.89 \sigma_{yse}$ overload and a varying amount of cycles

Number of cycles	Average crack extension (mm)
20000	0.57
50000	0.41 (-28%)
100000	1.09 (+91%)
1000000	1.49 (+161%)

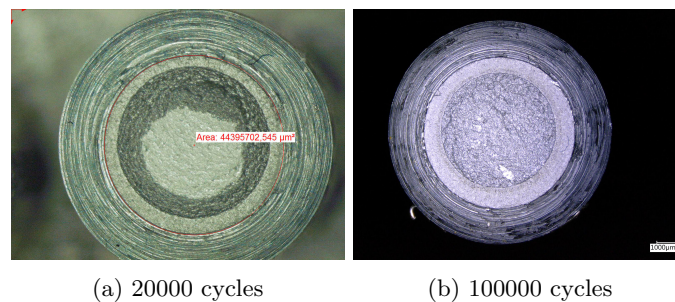


Figure 5.3

It can be seen that the 100.000 cycles at an overload of $0.89 \sigma_{yse}$ is the closest to the desired crack extension of 1 mm. For this reason this will be used as the standard for all other C-C samples. All specimen will have a notch radius of 0.2 mm and a notch angle of 60°.

5.2 Fracture Toughness testing

5.2.1 Crack Opening Displacement measurements

In order to measure the COD of CNT specimen two factors had to be defined: the load at which the critical COD is found, and determining the linear elastic part of the measured load-displacement curve. This is important as the measured elastic component is assumed to be the elastic deformation of the bulk material, and all plastic deformation is assumed to be the crack opening.

The first factor was the load at which the critical COD was measured, here the fracture initiation point. In accordance with Giovanola[37] it was assumed that fracture initiation occurred at maximum load. This assumption is certainly correct for the low temperature tests, as well as the cases with brittle fracture, such as the CGHAZ specimen. For ductile tearing it is somewhat questionable, and might slightly overestimate the fracture toughness due to additional crack growth before failure.

In order to further investigate this, test were performed at room temperature where the specimen was unloaded at 0.1% load drop, this was the lowest threshold at which it was possible to stop the machine. This means the test was aborted almost immediately after the maximum load was achieved. These specimen were then cut to investigate the crack opening, which showed a small amount of tearing at the crack tip, shown in figure 5.5. However because ASTM standard E1820 allows for some crack extension at a measured J_{Ic} this means the conclusion of Giovanola that the maximum load can be used as the crack initiation point can be followed.

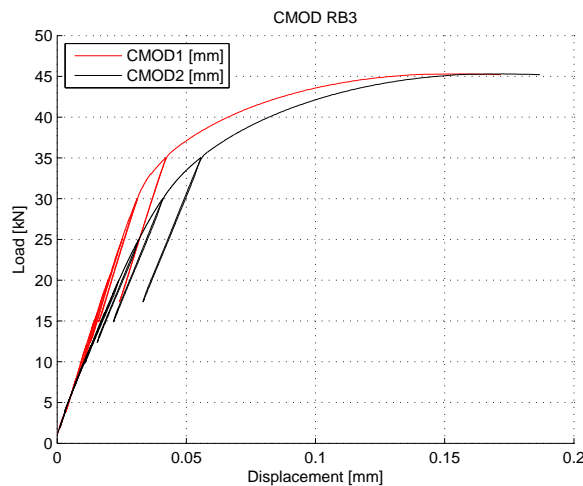


Figure 5.4: Tensile curve of an interrupted test at 0.1% load drop

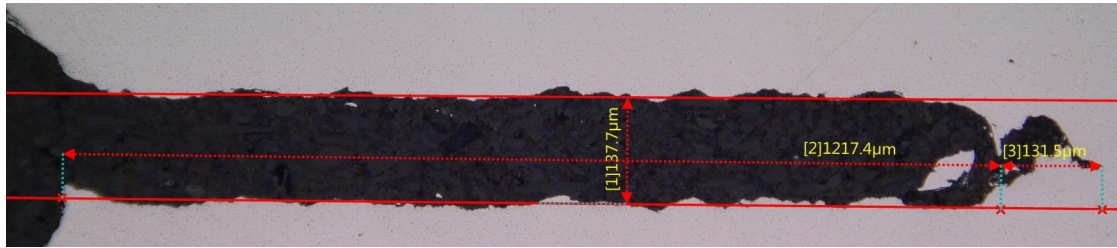


Figure 5.5: Measured crack growth at 0.1% load drop

Then in order to measure the plastic component of the displacement signal the elastic component of this signal must be defined. In cases where clear linear elastic behavior can be seen this is not a problem, as drawing a line from the maximum load, parallel to the linear elastic part of the load-displacement curve will easily show the plastic displacement measured. In cases where the elastic behaviour is not so easily visible, as will be shown for most C-C specimen, this method does not work. For this reason the compliance of the specimen needs to be calculated, as this should give the same slope as the slope of the linear elastic line. In order find the best approximation of the elastic behaviour the three methods (Scibetta, Koiter-Benthem and unnotched) mentioned in chapter 4.4.3 were investigated.

It was decided not to use the elasticity line for the measure of the elasticity, as this is not always exhibiting elastic behaviour. Instead unloading-compliance tests were used, as these should show pure linear elastic behaviour during the unloading part. The three methods were compared for several specimen, with the results for the sample shown in figure 5.4 below.

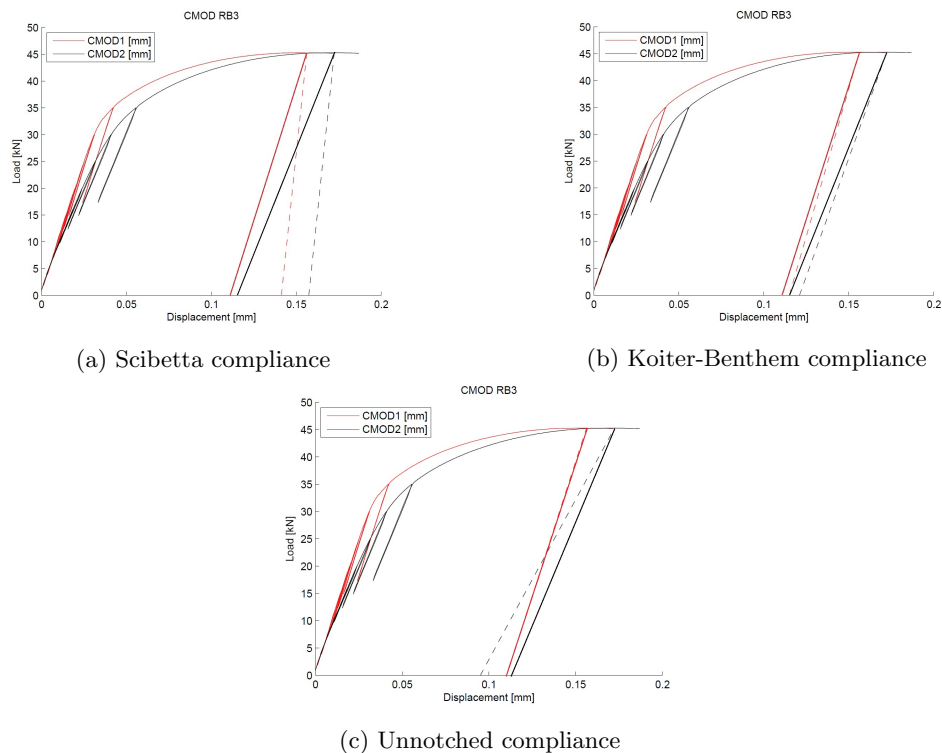


Figure 5.6

In these figures the whole lines show the actual linear elastic lines, while the dashed lines show the elastic behaviour calculated from the compliance formula's. From these and the other samples compared it was found that the Koiter-Benthem approach the true elasticity closest. It must be noted however, that none of the methods provides 100% accuracy.

5.2.2 Load-Displacement measurements

Fracture toughness tests were performed on base material S690QT in order to measure the COD. It should be noted that the tests were performed on both rotational bending and compression-compression specimen.

Rotational bending

An example of a rotational bending load-displacement curve was presented before in figure 5.4, and further detailed results can be found in appendix C.2.1. The average measured maximum COD was 0.12 mm. All rotational bending specimens showed relatively similar tensile behaviour, with deviation from the compliance line starting above 600 MPa. This means the applied stress during pre-fatigue (maximum of 350 MPa) was at all times less than 60% of the K_Q value, meaning the measurements are valid in this respect. However none of the samples were valid for the LEFM stress intensity factor K , as K_{max} was higher than $1.1K_Q$ for all tests.

Also it can be seen that relatively little difference is found between the average and the maximum crack length. This is caused mostly by the lack of eccentricity found combined with the plastic behaviour of the base material at room temperature.

Compression - Compression

The Compression - Compression load-displacement curves show a very different type of tensile behaviour than the rotational bending tests, as can be seen in figure 5.7.

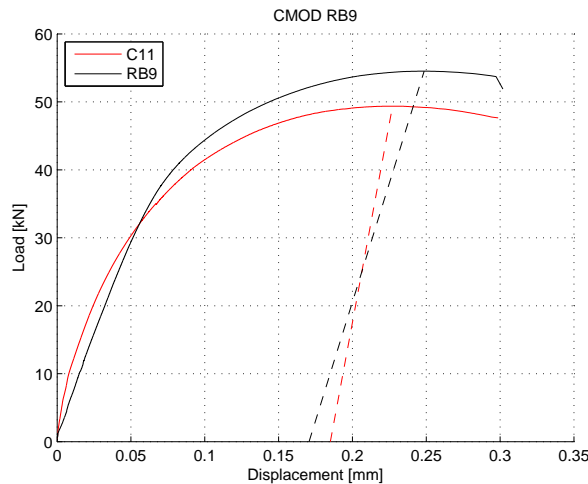


Figure 5.7: Load-displacement curve for a C-C specimen (C11) compared with a RB specimen (RB9)

As can be seen C-C samples show a load-displacement curve with no clear elastic behaviour at the start of the test. To exclude the possibility of this being caused by the extensometer slipping on the outside of the specimen unloading-compliance tests were introduced, as introduced in chapter 4.3.2.

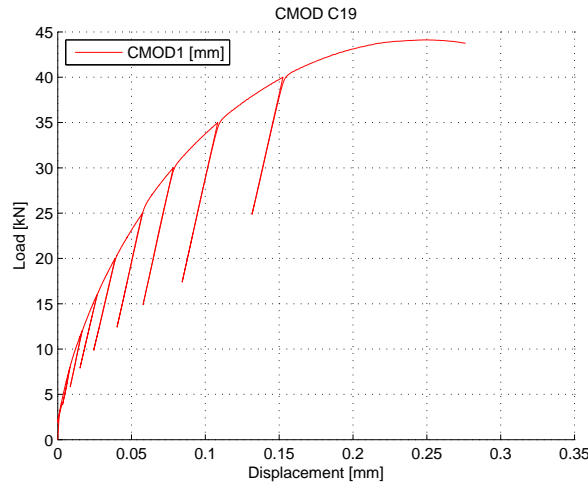


Figure 5.8: Unloading-compliance fracture toughness test for a C-C specimen (C19)

Clearly the extensometer signal was correct, as the unloading showed a straight line, as is to be expected for elastic behaviour. This behaviour then caused the need for an accurate compliance formula, so the plastic deformation at the maximum load could accurately be determined and the COD measured for all C-C samples. It would also be possible to incorporate unloading-compliance in all fracture toughness tests on C-C samples. These tests are more complex and time consuming than normal tests however.

All results for the fracture toughness tests can be found in appendix C.2.1. Using the Koiter-Benthem compliance formula to calculate the COD for the C-C tests an average maximum COD of 0.18 mm was found. As no linear elastic behaviour was visible the stress intensity factor clearly cannot be used. It can be seen that even though the eccentricities found here are larger, they have relatively little influence on the fracture toughness behaviour. It seems that the ductility of the base material allows it to compensate for eccentricity then, possibly because of load-line realignment as was proposed by Slachter [20].

Comparison of results

When comparing the load-displacement curves of RB and C-C samples, it can be seen that while the RB show almost fully linear elastic behaviour (a very slight curve appears to be present), the C-C samples do not show any linear elastic behaviour. The other major difference is the average critical COD found. For the C-C specimen the COD is 0.18 mm, while it is 0.12 for the RB specimen, a significant difference of 50%.

Two possible explanations are proposed. The first is the possibility that a certain amount of compressive residual stresses have remained after the pre-fatiguing, which possibly influences the tensile behaviour during the fracture toughness tests. The other possibility is that due to the principle in which compression-compression works, a stress-free crack has been created. This would mean that the complete tensile residual stress zone has been cracked and the material at the crack tip is completely undeformed and thus stress-free. The initial compressive overload, and the two possible crack-tip situations are visualized in figure 5.9.

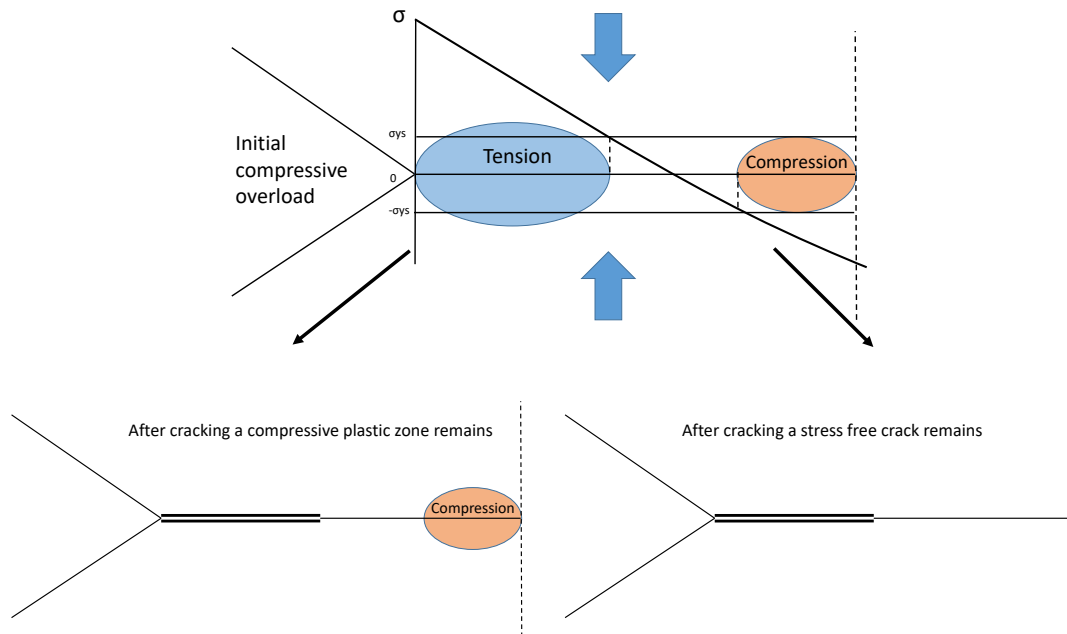


Figure 5.9: Schematic depiction of the two possible stress situations at the crack tip

In order to check this hypothesis RB and C-C samples were annealed at 930°C for 45 minutes in a stainless steel envelope filled with an inert gas. The samples were then left to cool down to room temperature. Because of the annealing these samples would also have a fully stress-free condition at the crack tip, allowing for comparison of the results to the C-C specimen.

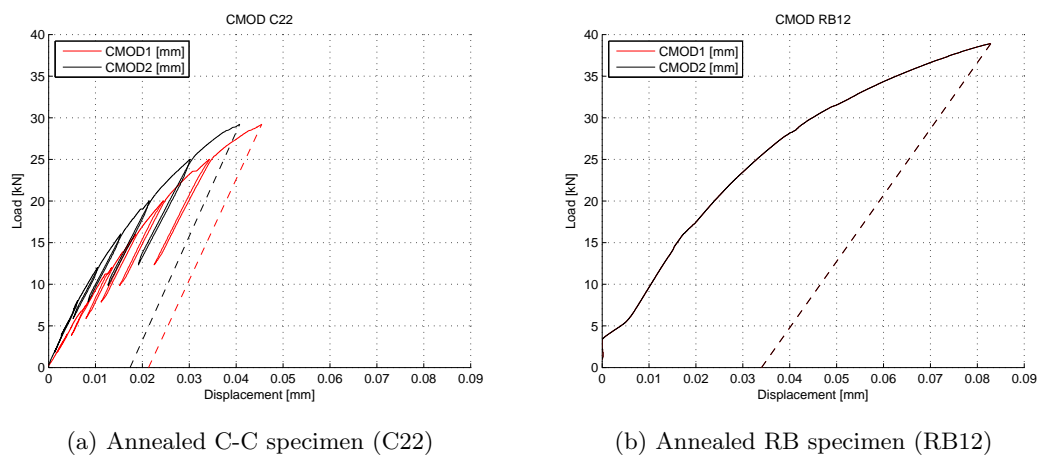


Figure 5.10

The results are shown in figures 5.10a and 5.10b. Because of the altered microstructure the material has become far less strong. It can be seen that both graphs follow the same curve, and both graphs show the curved initial part of the graph. This increases the belief that the unexpected load-displacement curves are caused by a stress-free condition at the tip of the pre-fatigue crack.

As a consequence of this, combined with the knowledge that the COD for the C-C specimen is 50% larger than that of the RB specimen, a further hypothesis can be formed. Rotational bending is similar to standard three-point bending fatigue methods in that it introduces tensile stresses in front of a crack.

These results have shown that these tensile stresses influence the fracture toughness behaviour, and reduce the measured CTOD value. Even though this means the normal way of measuring CTOD leads to a more conservative result, this could still mean the conventional method of measuring the CTOD is incorrect, as the pre-fatigue method influences the results.

Another important result is that CNT specimen are able to determine a COD for S690QT at room temperature. In the AFSuM project, it was found impossible to determine a reliable CTOD at room temperature because the measured values were not indicative of the fracture toughness, but just measured the plastic collapse of the material. This problem does not occur for the CNT specimen, because the constraint in the ligament is large enough to allow the material to sustain a far larger force before failure. Therefore the failure mechanism is dominated by the crack instead of by plastic collapse.

5.2.3 Optical microscopy

A second method of verifying the measured COD is by checking the opening of the crack under the microscope. This is done by cutting the specimen along its longitudinal axis and grinding and polishing the cross-section. In total seven samples were compared, leading to the results shown in table 5.4. It is important to note that the location of the extensometer was marked on the specimen, so the cut could be made on this location. This allowed proper comparison of measured extensometer value and the visible plastic COD.

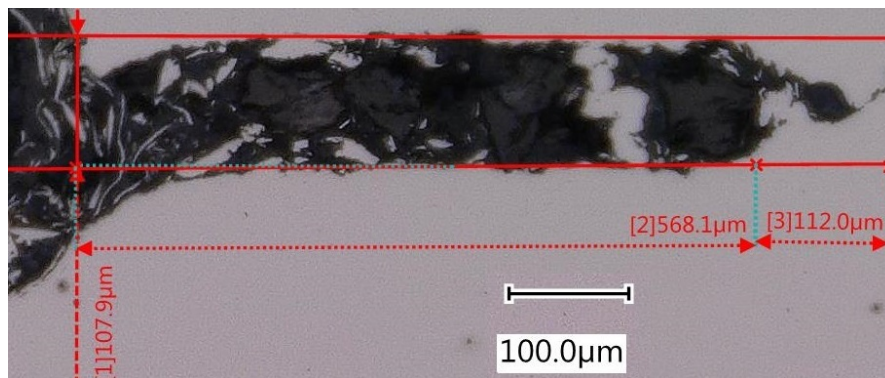


Figure 5.11: COD measurement under the microscope (LTRB2)

Table 5.4: Extensometer results compared with optical measurements

Sample	Extensometer (mm)	Optical microscopy measurement (mm)
C19	0.19	0.20
RB3	0.12	0.12
RB5	0.12	0.12
RB6	0.14	0.14
LTRB2	0.11	0.11
LTRB3	0.12	0.13
LTRB5	0.08	0.08

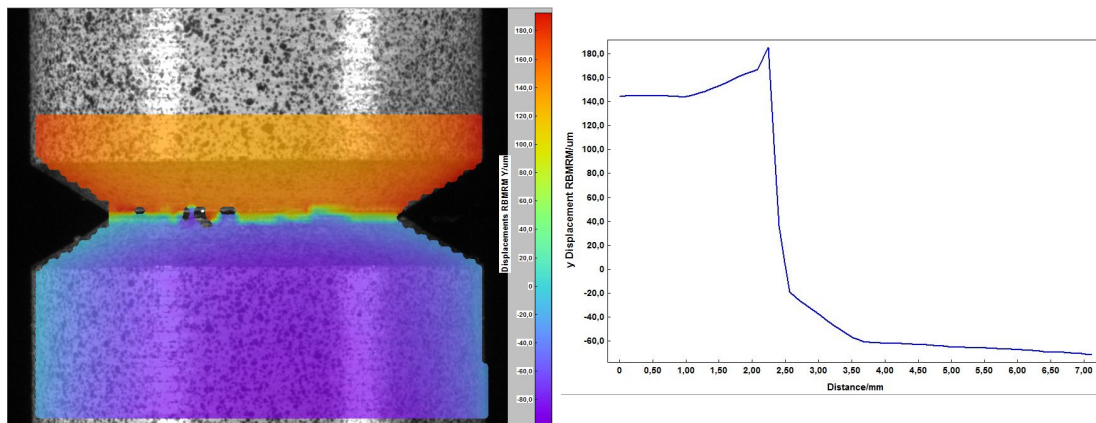
It can be seen that as assumed the crack flanks open parallel to each other, meaning that indeed the CMOD is the same as the COD. That is why combining the extensometer data with the compliance formula gives a reasonably accurate measurement of the plastic COD. One problem that remains here is the influence of the eccentricity on the COD, as now it is clear the extensometer signal is correct but it does not always measure the critical COD.

5.2.4 Digital Image Correlation

Because the plastic CMOD is a direct measurement of the COD, it should also be possible to optically measure the CMOD using COD. This would make it possible to measure the effect of eccentric ligaments on the COD. Optical measurement of the CMOD was done using digital image correlation, leading to the results in table 5.5. Due to the setup of the DIC system, all these tests were performed using only 1 extensometer and 2 DIC camera's.

Table 5.5: Results from DIC measurements

Sample	Extensometer (mm)	DIC (mm)
C18	0.22	0.22 - 0.25
GRT1	0.03	0.06 - 0.15



(a) Visual results for DIC measurement of C18

(b) Displacement measured figure in 5.12a

Figure 5.12

As shown in table 5.5 and figure 5.12b the results of the DIC measurement are close to the extensometer measurement. Samples C13 and C15 were also tested using the DIC system, but were invalid due to faulty calibration, while GRT1 shows a large scatter for the results.

Specimen GRT1 was a gleeble heat treated sample, which was pre-fatigued in Compression - Compression. After fracture it was found to have an eccentricity of 0.44 mm, which is considered large. When examining the data from the DIC system it was found that the minimum measured value occurred at the closest measurement to the extensometer, while to measurement of 0.15 mm was found on the opposite side. This means that the eccentricity for the heat treated material appears to play a more important role than for the base material, as for the base material tests such large differences have not been detected.

Going on the results of test C18, the DIC system shows to be a good way to measure the COD of CNT specimen. However the results measured should still be regarded as an indication, as issues surrounding the calibration and extensometer reference still need further attention. A different DIC-extensometer setup would also be advised, where 2 extensometers and 2 DIC cameras alternate each other every 90°, visualized in appendix C.2.5. This would allow for a better comparison between the measured data to be made, as the possible influence of eccentricity is reduced. Therefore further refining of this method is advised before employing it as a method of measuring the COD of CNT specimen. All in all DIC has shown to be a novel and promising method for measuring CNT COD values.

5.2.5 Temperature effect

Because fracture toughness test on AFSuM samples did not actually measure any fracture behaviour, but instead only measured the plastic collapse it is not possible to determine the equivalency between CNT specimen and AFSuM samples at room temperature. For that reason tests were performed at lower temperatures, allowing for valid AFSuM results to be compared to CNT results.

Two techniques were used to test at these low temperatures, the specimen tested at -30° using the temperature chamber, and the specimen tested at the lower temperatures using the adapted AFSuM method described in chapter 4.3.3.

Table 5.6: Low temperature COD test results

Sample	Temperature (C)	CTOD (mm)	Sample	Temperature (C)	CTOD (mm)
LTRB1	-30	0.11	LTRB3	-30	0.12
LTRB2	-30	0.11	LTRB4	-30	0.12
C24	-67	0.21	RB9	-60	0.16
C25	-91	0.11	RB10	-90	0.16
C23	-105	0.04	RB11	-110	0.15

As seen in table 5.4 the extensometer at low temperature is still able to measure the COD correctly (the LTRB samples in the table were found to be accurate). This allows for comparisons to be made to AFSuM results. In figure 5.13 the results of the all CNT measurements have been plotted along the results for S690QT SENB specimen performed in the AFSuM project.

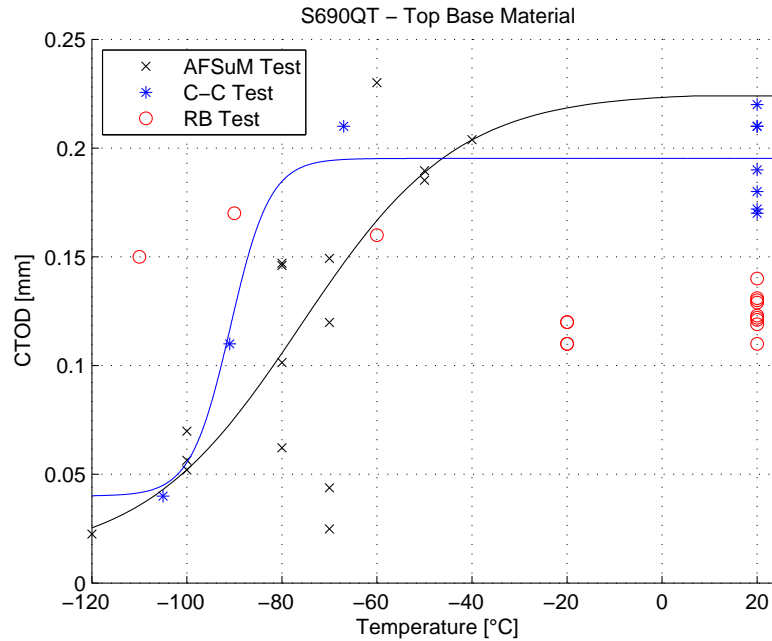


Figure 5.13: Extensometer results compared with AFSuM results.

It can be seen that the COD for the Compression - Compression tests appears to be close to the AFSuM fit, with the lower temperatures approaching the AFSuM data better. For the rotational bending tests this is not the case. The -30°C tests gave a result of 0.12 mm, which is in good accordance with the room temperature test, yet is lower than expected based on AFSuM results. The lower temperatures however gave a higher COD than for the -30°C samples. The COD measured on the low temperature C-C samples was close to the predicted values from the AFSuM tests.

Investigation of the fracture surfaces in the SEM showed the C-C samples to have a fracture surface dominated by cleavage, where no voids were detected. The RB specimen did show voids in the first part next to the crack, shown in figure 5.14, indicating plasticity occurred here before failure. This observation confirms that the RB specimen did not show fully brittle failure, as was already indicated from the load-displacement curves.

The red line drawn indicates the length of the ductile zone, which is about $70\text{ }\mu\text{m}$. This zone is known as the stretch zone width, and is an indicator for the CTOD. The stretch zone width is half the length of the CTOD, meaning the CTOD at the point measured was 0.14 mm. This can then be used as an indicator that the measured CTOD of 0.15 mm was indeed correct.

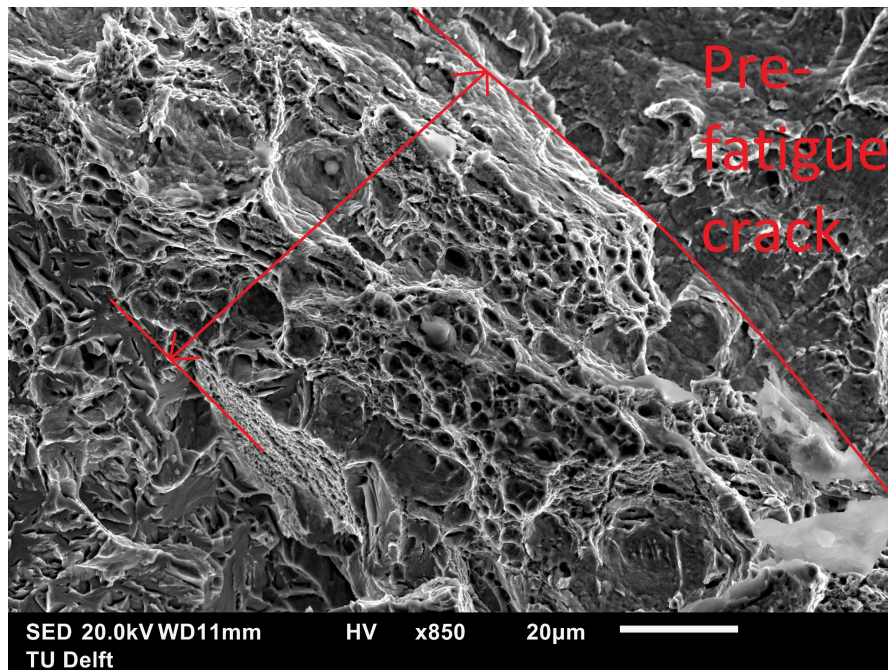


Figure 5.14: Fracture surface showing voids next to the crack (RB11)

One possible explanation for these results is the shape of the crack tip after the two types of pre-fatigue. The C-C should have a very sharp crack tip, due to an absence of tensile loading, and subsequent blunting of the crack tip, during pre fatigue. This blunting is presumed to happen in the rotational bending process, which shows as the difference in COD at room temperature. Because -30°C is still above the DBTT the same mechanisms still control fracture and the COD measured.

When the specimen is cooled to below the DBTT the absolute tensile strength is expected to increase up till a level when brittle fracture mechanisms take over. Instead of reducing the possible COD, the slight blunting of the crack tip would then reduce the stress concentration at the crack tip, allowing it to deform to a higher load than the sharper C-C specimen.

The general conclusion from these tests show that equivalency between CNT and SENB specimen can be found, with C-C pre-fatiguing method. Room temperature equivalency cannot be assumed, as no valid SENB data is available, but adding the room temperature C-C samples would lead to a plot following the plot in figure 5.13. Rotational bending specimens do not follow this curve, this could be caused by the combination of constraint with the more blunted crack tip.

The room temperature results for the C-C samples shows scatter, this was found to be caused by local brittle zones in the material. SEM analysis showed the fracture surface to contain mostly ductile failure, but showed local cleavage planes, as shown in figure 5.15. Because brittle failure (cleavage) has probabilistic nature, these local cleavage planes help explain the scatter in the results. The local brittle zones were not found in the RB specimen, explaining the lower scatter in the RB results.

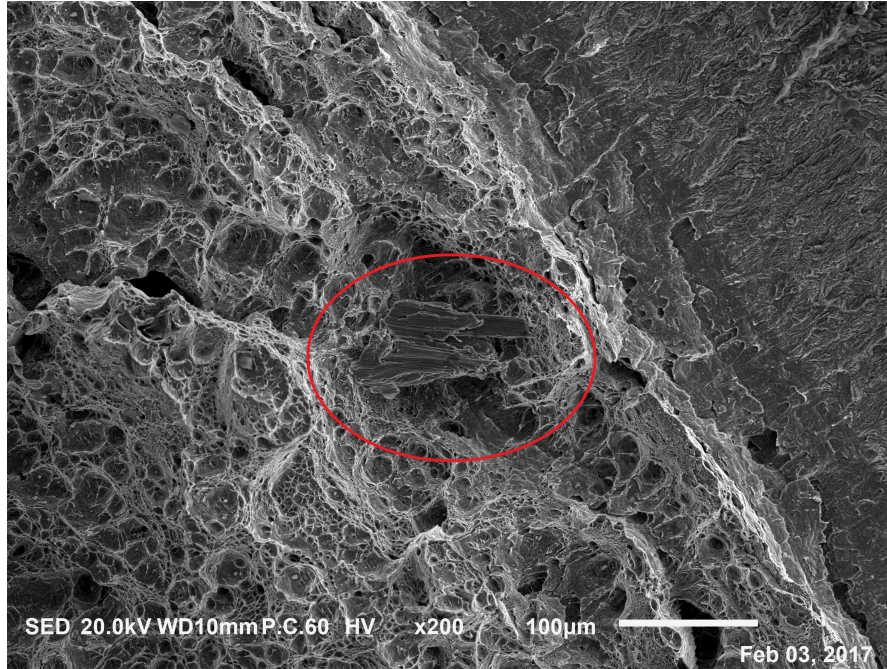


Figure 5.15: Fracture surface showing local cleavage zone (C17)

5.3 Plastic zone size

Two specimen were investigated using Electron Backscattered Diffraction in order to determine the size of the plastic zone in front of the crack tip. The goal here was to find the plastic constraint factor C' , where a full plane stress situation has a C' -value of 1, and plane strain a C' -value of 3. As mentioned in chapter 2.1.3 the plastic zone size in front of the cracktip can be determined by the following relation:

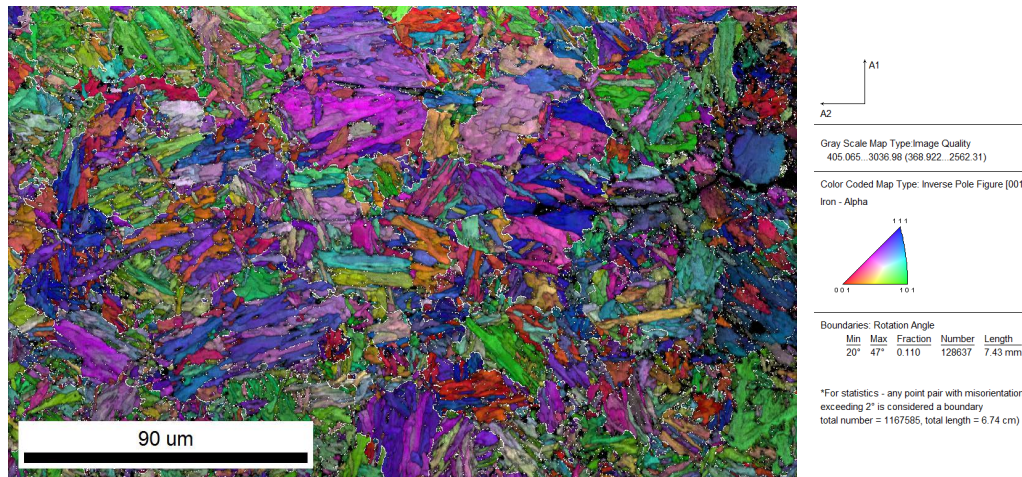
$$2r_y = \frac{1}{\pi} \left(\frac{K_{max}}{C\sigma_{ys}} \right)^2 \quad (5.1)$$

with C being the plastic constraint factor and $2r_y$ being the plastic zone size. Using this information the possible plastic zone sizes were calculated for both samples, which is shown in table 5.7

Table 5.7: Possible plastic zone sizes for the minimum and maximum value of C

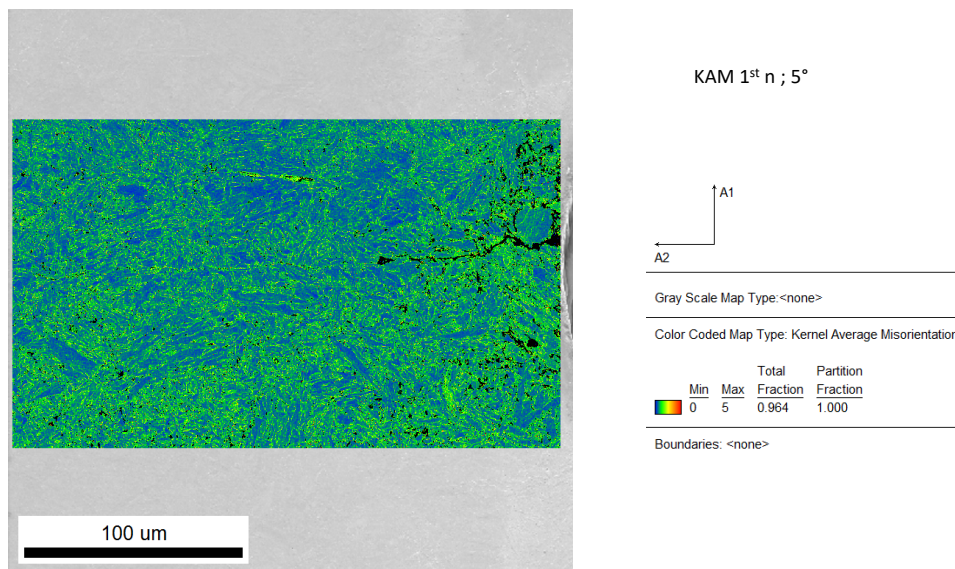
Sample	Force (kN)	K (Mpa \sqrt{m})	$2r_y$ (μm) C=1	$2r_y$ (μm) C=3
S37	14.6	15.0	470.8	52.3
S690 annealed	5.0	8.15	266.0	29.6

The results for the annealed S690 are shown below in figure 5.16



Color coded ND IPF. Prior austenite grain boundaries are in white.

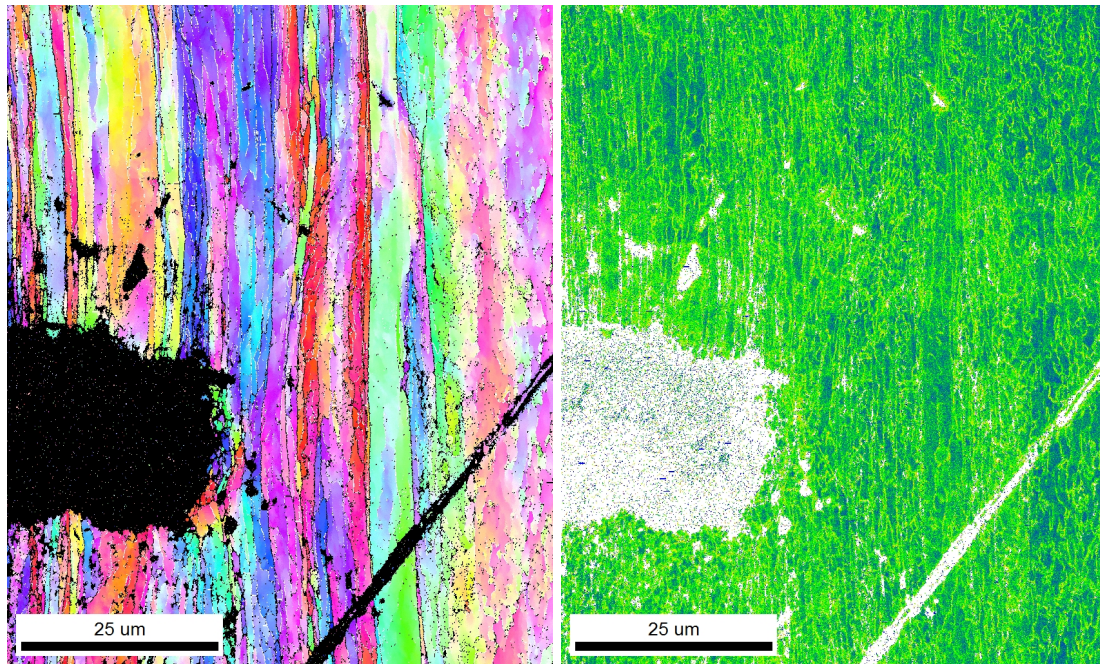
(a) Visualization of grains around the crack tip of the annealed S690 specimen



(b) KAM image of the crack tip of the annealed S690 specimen

Figure 5.16

Figure 5.16a shows the grains around the crack tip, with the austenite grains in white. The expected results for annealing the specimen would have been grains of the same size as the white outlines, this indicates that the sample was cooled at a too fast rate. Figure 5.16b shows the Kernel Average Misorientation (KAM), which is expected to show a higher value in the plastic zone in front of the crack tip. No clear difference can be seen between the area in front of the crack and at other locations. This means it is not possible to determine the plastic zone size in this measurement.



(a) Grains around the crack tip of the S37 specimen (b) KAM image of the crack tip of the S37 specimen

Figure 5.17

The EBSD measurement on the S37 material shows the material still has a clear rolling structure, as can be seen in figure 5.17a, also it can be seen the crack has opened further than for the S690 material, due to the higher stress intensity applied. Figure 5.17b shows a higher KAM for around $30\text{ }\mu\text{m}$ around the crack tip, this could be indicator of plasticity. The minimum plastic zone according to Irwin is $52.3\text{ }\mu\text{m}$, this means that this could not be the complete plastic zone. For this reason it is not possible to use this results to determine the C -factor.

A number of observations can be made based on these results. The S690 measurement shows the annealing to have been incomplete, meaning the cooling at room temperature lead to a super critical cooling rate. This means the microstructure is finer than desired, and means the resolution of the test has become to low to be able to distinguish plastic zone. The S37 sample was subjected to a far larger force, meaning a lot of plasticity occurred which caused the crack to open around $25\text{ }\mu\text{m}$, yet the results from the KAM displayed only small amounts of plasticity.

In research by Ghodrat et al [38], it was found that in 6061 aluminum the largest part of the plastic zone of a fatigue crack had a plastic strain level which was below the detectable limit of the EBSD. This might have occurred in these steel samples as well, and could explain why the measured plastic zone in the S37 material was smaller than the theory predicted. Another possible explanation for the inability to find the plastic zone would be that there is no plastic zone, as no plasticity occurred. The large amount of crack opening in the S37 sample would contradict this theory however.

5.4 Application of CNT specimen to CGHAZ material

An important goal of this research was to find a method to measure the fracture toughness of the Coarse Grained Heat Affected Zone (CGHAZ) microstructure of S690 steel using CNT specimen. Several steps were taken towards this goal. The start was made by comparing two methods of creating the simulated microstructure: using the Gleeble and Ultra High Frequency setup. After that tensile tests were performed to measure the tensile behaviour at both room and low temperature (-30°C), after which both pre-fatiguing methods were tested. Finally fracture toughness tests were performed at both room temperature and low temperature.

5.4.1 Gleeble

Two types of specimen were created using the Gleeble, short samples with a gauge length of 20 mm, and long samples with a gauge length of 35 mm. Thermocouple measurement on the short gauge length, shown in figure 5.18, shows the signal of the temperature setpoint, control thermocouple and a second thermocouple located close to the copper jaws.

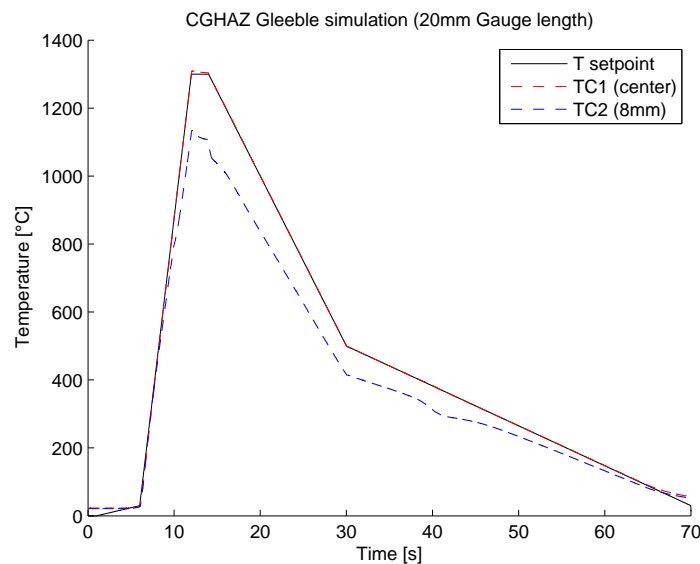


Figure 5.18: Thermocouple measurement of Gleeble heat treatment

The center thermocouple shows that the material is following the setpoint almost exactly. The outer thermocouple shows some deviation, this is caused by the cold copper grips, which have an influence up to a certain distance of the gauge length. Microstructure and hardness were measurements were performed in order to examine the uniformity. Image 5.19 and 5.20 show the result of a series of hardness measurements across the surface of the CGHAZ CNT specimen.

Around 8.5 mm from the cracked surface a line can be seen where the hardness suddenly drops from over 400 HV_3 to below 300 HV_3 , which is the hardness of the base material. This means a length of roughly 17 mm has a uniform hardness and microstructure. For the long gauge length samples, which the tensile specimen will be made from, this distance was found to be around 29 mm in total. The grain size found was around $80\text{--}100\text{ }\mu\text{m}$, matching results from the AFSuM project, these images can be found in appendix C.3.1.

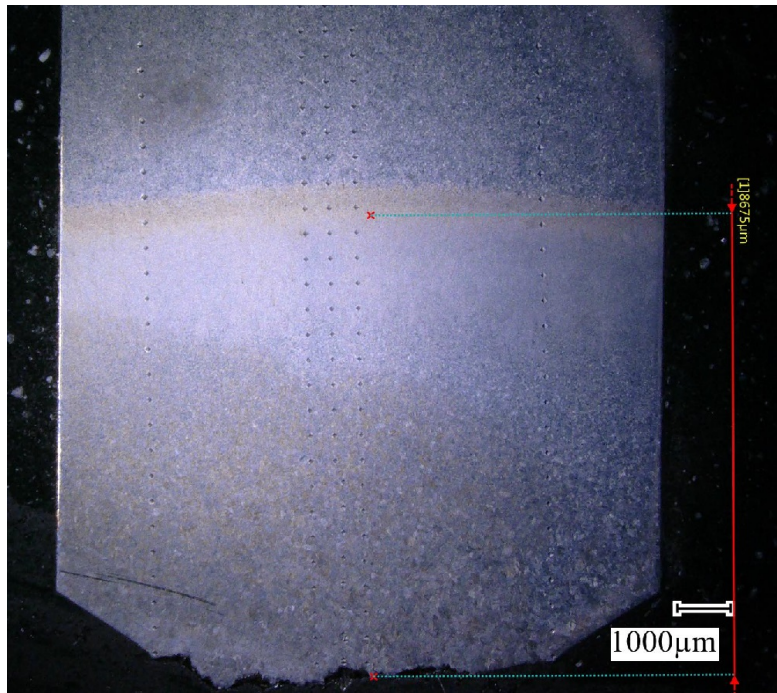


Figure 5.19: Image showing the microstructure crossover line at around 8.5 mm from the cracktip, the little marks are the hardness indentations

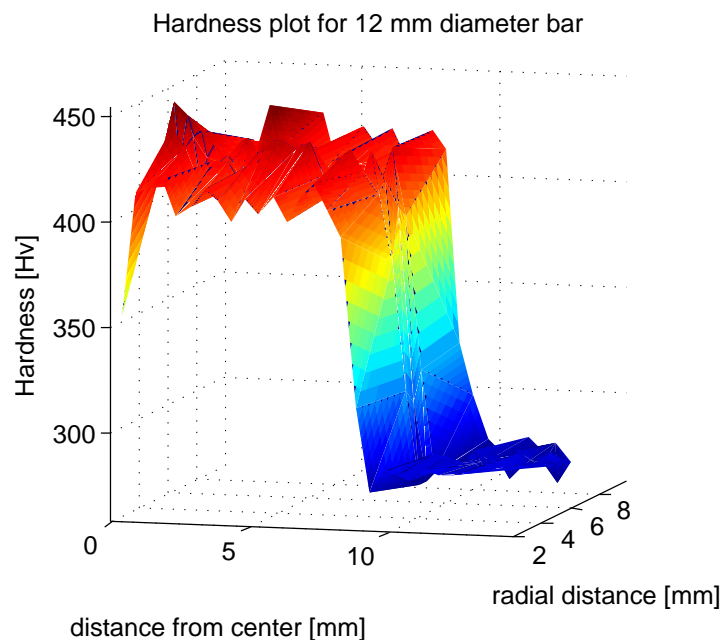


Figure 5.20: 3d-plot of Hardness measurements on the sample shown in figure 5.22

5.4.2 UHF

Due to the risk of hot spots, Gleeble specimen always need to have a uniform diameter. This means it is not possible to give the CNT specimen a heat treatment after notching and pre-fatiguing. A proposed alternative is using Ultra High Frequency (UHF) induction heating. This method is not affected by non-uniform cross-sections and could improve the ease of using CNT specimen for CGHAZ material tests.

Tests were performed on a uniform, 12 mm diameter piece of S690 steel, mounted in a vice and positioned in the UHF coil. Cooling was provided using three air nozzles mounted along the coil and additional cooling from a pressurized air nozzle. Thermocouples were placed in the center of the coil and about 15 mm from the center.

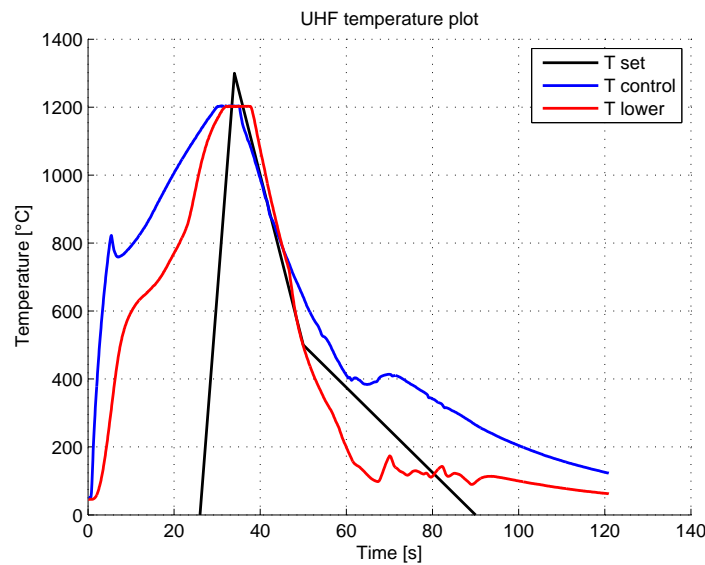


Figure 5.21: Thermocouple measurement of UHF heat treatment

It can be seen that the measured temperature does not fully follow the setpoint, as the cooling rate appears too low. Also the speed at which the specimen is heated is far too low, however this should not have any real influence on the microstructure or hardness. Also because the specimen is not heat treated in a vacuum and cooled using air a thick oxide scale forms around the surface.

Many of the problems encountered could be resolved, by creating a more advanced cooling rig, with better nozzles and using helium for cooling. Unfortunately further UHF experiments were not feasible on the UHF material during the timescale of this project.

Hardness measurements and microstructure studies were performed for this material as well. An average hardness of around 367 Hv₃ was found, for an average grain size in the same range as for the Gleeble samples (100 μm). All hardness measurements and microstructure photos can be found in appendix C.3.2.

Table 5.8: Average hardness for UHF sample

Location	UHF Center	UHFEdges	Gleeble
Hardness (Hv ₃)	367	368	400
Equivalent strength	1180 MPa	1184 MPa	1290 MPa

5.4.3 Tensile tests

In order to determine the mechanical behaviour of the heat treated material tensile tests were performed both at room and at low temperature. For these tests the long gauge length samples, with a heat treated material length of around 29 mm were used. After Gleeble heat treatment the specimen were manufactured in the lathe according to ASTM E8M,, with a reduced diameter of 6 mm, a shoulder radius of 5mm and a gauge length of 20 mm.

Room temperature tests were performed on the Instron tensile machine with crosshead speed of 2 mm/min and an extensometer gauge length of 20 mm. Low temperature tests were performed in the temperature chamber using the Zwick tensile machine at a temperature of -30 °C. Because of a geometrical problem preventing the usage of standard zwick clip-on extensometer, the macroXtens extensometer was used, with a gauge length of 18 mm. This extensometer has a less stable signal and its gauge length cannot be measured very accurately. Therefore post processing was applied to correct the signal and correct for the gauge length by correcting the slope of the graph to match the Young's modulus of 210 GPa.

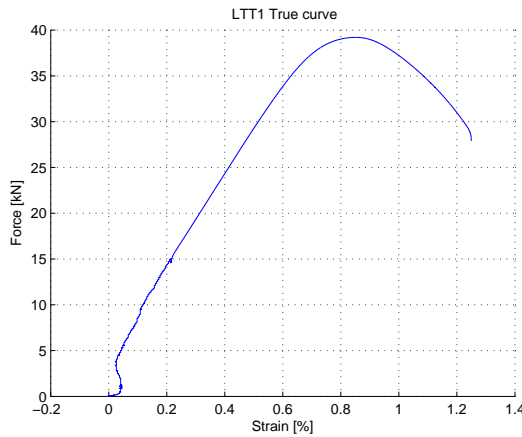


Figure 5.22: Extensometer signal

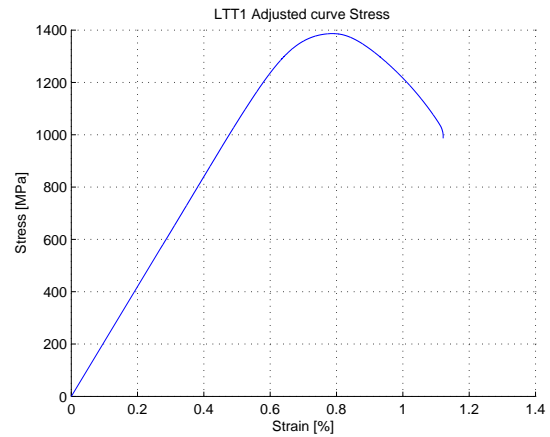


Figure 5.23: Corrected signal

Table 5.9: Tensile data found for CGHAZ material

Sample	T (°C)	σ_{ys} (Mpa)	σ_{uts} (Mpa)	ϵ_{max} (mm/mm)
RTT1	20	1114	1387	0.104
RTT2	20	1111	1416	0.113
LTT1	-30	1325	1387	0.0125
LTT2	-30	1302	1444	0.0126

This data is of importance for the potential use of Linear-Elastic fracture mechanics, as this requires an accurate yield strength.

5.4.4 Fracture toughness testing

After tensile testing, fracture toughness tests could be performed for these test it was of importance to get a centric circumferential pre-fatigue crack, as the research by Slachter showed the data was not usable when the pre-fatigue crack was not adequate. After cracking temperature and low temperature fracture toughness tests could be performed.

Pre-fatigue

Because of the large difference in strength between the heat treated material and the base material it was decided to attempt using rotation bending as the pre-cracking method. Different bending moments were tried, but none of these lead to a centric crack, an example is shown in figure 5.24. Therefore it was decided to abandon RB pre-fatigue.

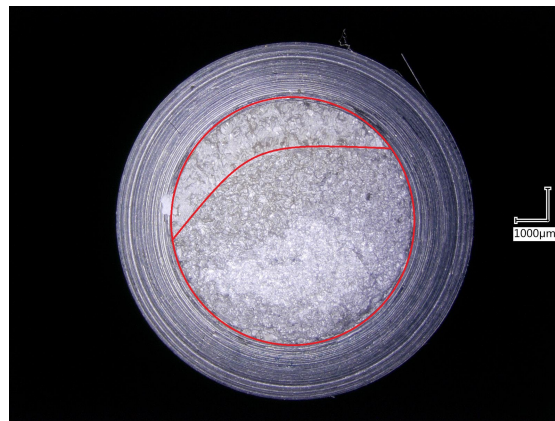


Figure 5.24: Eccentric crack due to RB pre-fatiguing

A number of observations were made during this process. The most important one was the amount of deformation that occurred in the bars during gleeble heat treatment. This caused the load that was applied at the notch to differentiate between 15 Nm and 35 Nm for a single specimen. It was therefore found necessary to remachine the samples, to make them completely straight again, as the misalignment was found to be up to 0.2 mm across a 120 mm long specimen. Although this did change the difference in load to less than 2 Nm, which was in the same range as base material specimen, it did not solve the problem of a crack forming on one side and not forming circumferentially. Having made sure the samples were as cylindrical as possible, the probable cause of this problem is the microstructure itself. The CGHAZ microstructure very coarse and contains local brittle zones which could be large enough the cause large scale inhomogeneity resulting in imperfect cracking.

Another possibility is a homogeneity problem in the circumference of the bar, caused by a local difference in cooling in the gleeble. Microstructure and hardness measurements were therefore done on the eccentrically cracked samples, these showed no visible differences in the material. The conclusion then is that the microstructure does not combine well with this type of pre-fatigue, due to the local brittle zones in the material. These seem to initiate cracking locally, and the low crack growth resistance of the material does not allow time for the self balancing of the crack, which occurs in more ductile materials.

Because rotational bending is not an option the other possibility is using Compression - Compression fatigue. The heat treated specimen only has the harder microstructure in the center of the specimen where the notch is located, and still has the base material at the top and bottom

of the specimen it is important to choose the correct parameters for C-C fatigue.

Because the initial overload cannot be increased, as it is already limited by the bulk diameter yield strength of the base material, the same parameters are used for the initial overload. The amount of compressive cycles is increased to 500.000 cycles, to make sure the crack can grow to its full extent.

Table 5.10: Results of Compression - Compression pre-fatigue on heat treated material

Sample	Δa (mm)	ecc (mm)
GRT1	0.80	0.44
GRT2	0.34	0.00
GRT3	0.59	0.25
GLT1	0.38	0.30
GLT2	0.44	0.13
GLT3	0.41	0.00

The results shown in table 5.10 show that a crack extension of on average 0.5 mm was achieved, with differing amounts of eccentricity. These results show that it is possible to create good circumferential cracks in heat treated CNT specimen. Eccentricity remains an issue for some of the samples, while others showed very centric cracks, the most probable explanation would be the influence of inhomogeneously distributed brittle zones. These samples were evaluated in SEM, shown in figure 5.25, which showed a brittle fracture surface, but the brittle zones in the cracked area could not be detected

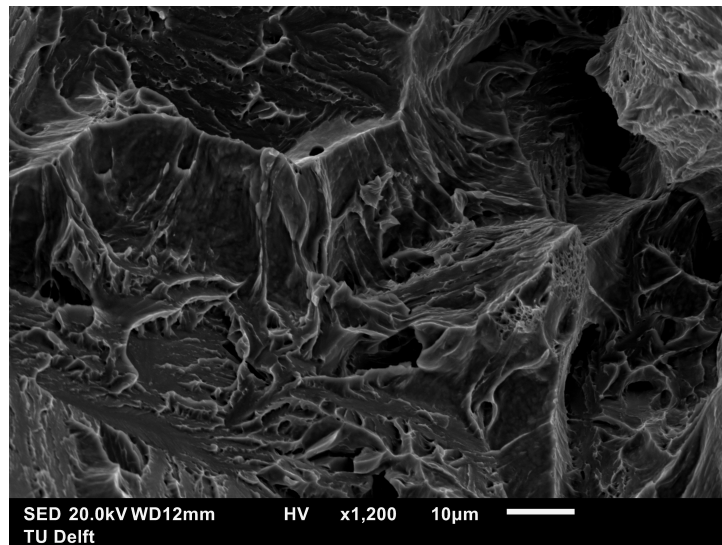


Figure 5.25: SEM image of fracture surface of GRT2 (1200x enlarged)

The crack extension of 0.5 mm is not as long as could be desired in this geometry. Further research could focus on methods to increase the crack length. At this moment the crack length is governed by the relative yield strength ratio at the notch tip created by a compressive overload which is limited by the strength of the base material in the main diameter. Both of these parameters could be changed to grow the crack length.

If the diameter of the ligament is reduced the applied force would lead to a higher stress, thus causing a larger residual tensile stress area, and thus leading to a bigger crack. The other option is to increase the strength of the entire specimen, for instance by annealing and quenching, before applying the local CGHAZ microstructure in the gleeble. An advantage of this method would be that it is possible to retain the same geometry as for base material samples. The specimen could then be subjected to a higher compressive overload, leading to a longer crack length.

CTOD testing

Fracture toughness tests were performed at room temperature and at -30°C , on the C-C pre-fatigued samples, the results are shown in table 5.11.

Table 5.11: Results for room and low temperature fracture toughness tests on heat treated material

Sample	Final load (kN)	Crack extension(mm)	CTOD (mm)	ecc (mm)	Temperature ($^{\circ}\text{C}$)
GRT1	56.18	0.80	0.03	0.44	20
GRT2	83.27	0.34	0.10	0.00	20
GRT3	77.41	0.59	0.03	0.25	20
GLT1	45.80	0.38	0.02	0.30	-30
GLT2	60.20	0.44	0.04	0.13	-30
GLT3	74.60	0.41	0.04	0.00	-30

AFSuM	15.88	1.84	0.13	-	20
AFSuM	12.30	1.99	0.056	-	-20

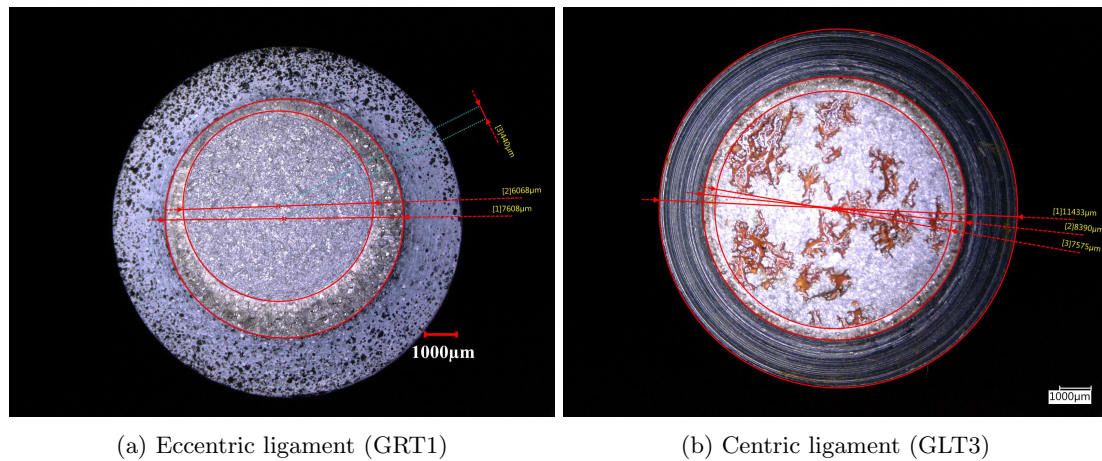


Figure 5.26

One of the observations made in the DIC tests was that eccentricity appeared to play a larger role in heat affected zone material than in base material. When looking at the load-displacement curve of specimen GRT2 in figure 5.27, it can be seen that the difference between the two signals is relatively large (0.07 mm vs 0.10 mm), while the visible eccentricity was too small to measure. Because the other tests were performed using only 1 extensometer it is not possible to guarantee if the measured value is close to the maximum COD or not.

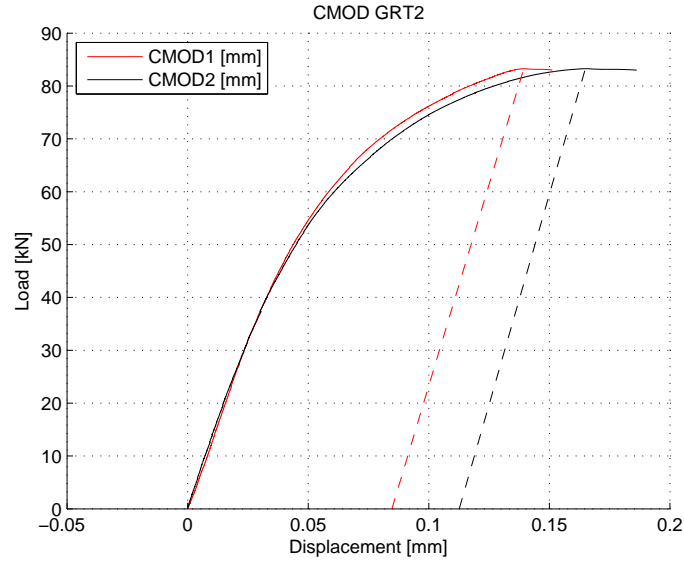
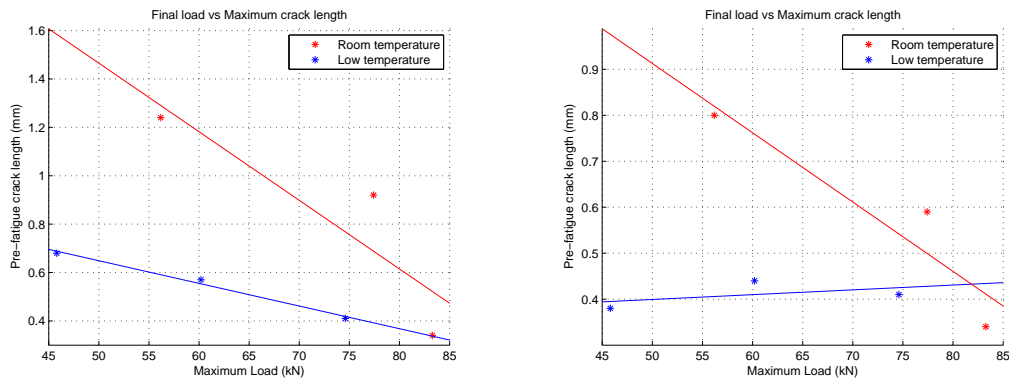


Figure 5.27: Load-displacement curve of room temperature specimen GRT2

When plotting the final load against the average crack length as has been done for most of this research it can be seen that no clear relation can be found between the measured data, as shown in figure 5.28a. What is important to note here is that for the heat treated material the eccentricity appears to be of larger importance, and that it is also larger than for most base material pre-fatigue cracks. Therefore it makes sense not to look at the average crack length, but at the maximum crack length

$$a_{max} = a_{av} + ecc \quad (5.2)$$

Hence the length of the eccentricity is added to the average crack length, thus giving the maximum distance from the ligament to the notch. When this is plotted, as in figure 5.28b, it can be seen that a far better relation between the final load and crack length is obtained. The reason for this would be that the heat treated material is far more brittle than the base material, and therefore performs closer to linear-elastic fracture mechanics, which is more driven by crack length than the elastic-plastic fracture mechanics most of this research is based upon.



(a) Maximum load vs. average crack lengths

(b) Maximum load vs. maximum crack lengths

Figure 5.28

The test results can also be compared to AFSuM results. These gave a COD of 0.056 mm at -20°C and 0.035 mm at -60°C . The results at -30°C fit this data very well, increasing the validity of the test results. All CNT results have been plotted together with the AFSuM results in figure 5.29.

Room temperature results have given a lower than expected value, as the average COD in AFSuM heat treated specimen was 0.14 mm. When looking at the visual data from the DIC results they imply the measured data was the minimum COD, and the actual maximum COD lies somewhere between 0.12 mm and 0.16 mm. This value would match the COD from AFSuM, but because the accuracy of the DIC measurements is considered imperfect these results cannot be considered fully correct. Adding a second extensometer on the other side of the circumference such as for specimen GRT2 would already reduce the difficulty caused by the eccentricity, as the odds of measuring close the the maximum crack greatly increase.

Hence it can be concluded that CNT specimen can be used to measure the fracture toughness, but a two, or even more, extensometer setup is advised, to reduced the effect of the eccentricity on the COD.

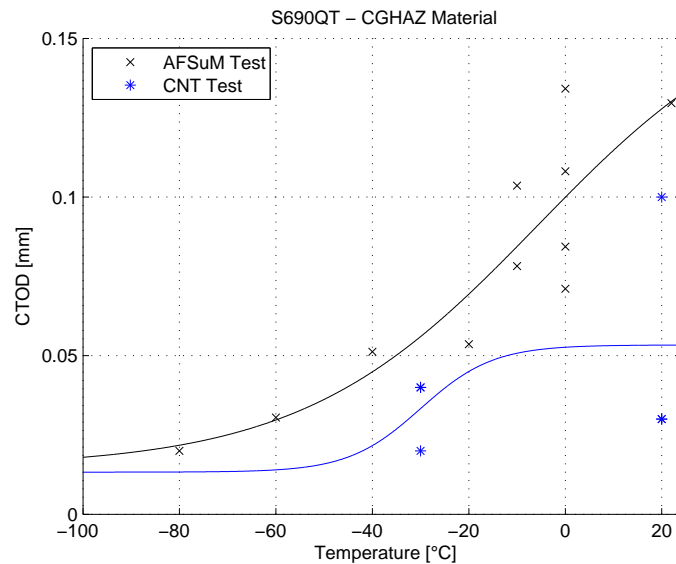


Figure 5.29: Comparison of AFSuM CTOD values for CGHAZ material with CNT results

5.5 Summary of results

This chapter will further discuss and summarize the conclusions found in the previous chapter, and will try to answer the research questions formulated in chapter 3.5.

Pre-fatiguing

Both rotational bending and Compression - Compression were successfully used to create pre-fatigue cracks in the CNT specimen. As in literature rotational bending formed cracks with little eccentricity and at a high speed. When the load drop was insufficient elliptical cracks formed, leading to the conclusion that a minimum load drop is present for centric cracks.

The new Compression - Compression method performed well as a method of pre-cracking CNT specimen. By varying the specimen geometry and compressive overload different crack lengths can be achieved, with comparative eccentricity to the rotational bending method.

Fracture toughness testing

Room temperature fracture toughness tests on S690QT are best performed using the CTOD as the fracture toughness parameter as too much plasticity is present to use the linear-elastic stress intensity factor, this is the case for both upper and lower shelf temperatures. Measuring with two extensometers, the CTOD can be taken as the maximum plastic deformation measured at the peak load, where the elastic component is calculated using the Koiter-Benthem compliance formula. This method is confirmed by comparing the visible COD of samples unloaded after reaching maximum load with the extensometer signal. Limiting eccentricity is useful here, as it will make testing easier. Because of the relatively large plasticity which occurs during the test, the effect of the eccentricity is limited however. This has been confirmed by using Digital Image Correlation to visualize the effect of eccentricity on the extensometer results.

One of the most important findings in this research is the difference found in fracture toughness behaviour between RB and C-C pre-fatiguing cracks. Whereas RB crack have a linear-elastic behaviour at the start of the fracture toughness tests, the C-C specimen appear to have no linear-elastic behaviour. A possible explanation for this is that the C-C method creates a stress-free crack, meaning the material in front of the crack is not plastically deformed. This is fundamentally different from normal pre-fatiguing methods, where the crack is always grown using tensile stress, meaning local plasticity is always present.

When comparing the measured crack opening displacement, the COD measured for C-C is 50% larger than for the RB. This could be explained by this being the extra plasticity a crack can sustain in if no plasticity is present on the crack tip. If this is so, it also has consequences on the method in which CTOD is normally measured according to the official testing norms, as the value measured in this way would not be the true COD but a underestimation. Another possibility is that the crack formed by rotational bending suffers from some immediate blunting, leading to a reduced COD.

A big difference with conventional fracture toughness test on S690QT is that a valid COD was found at room temperature without plastic collapse occurring. In the AFSuM project it was found that only plastic collapse could be measured at room temperature. Because the CNT specimen has high constraint in the ligament this problem did not occur, and valid COD's were found. This difference has to do with the far higher forces which can be applied to the material, due to the constraint of the ligament.

Tests were performed at low temperature in order to measure the behaviour of the CNT specimen and to allow for comparison to conventional fracture toughness tests results of S690QT. Large differences were found between the low temperature behaviour of the RB specimen and the C-C specimen, where the COD of RB samples was up to three times higher than for C-C at -100°C . RB specimen might be influenced by some possible blunting of the crack tip in the pre-fatigue process, which would increase the resistance to tearing and combined with the higher material strength at low temperature would lead to a higher COD.

C-C specimen at low temperature show similar behaviour to conventional fracture toughness specimen at low temperature, and the results found lead to equivalent COD's to be found.

Plastic zone size

Two EBSD measurements were performed in order to measure the plastic zone size of the CNT specimen. The annealed S690 specimen did not show plasticity, this could have been caused by improper annealing causing a too high dislocation density in the background, so the actual plasticity was measured as noise. The other possibility is that the plastic strain level stayed below the lowest detectable value of the EBSD, thus not showing in the results. This theory is supported by literature where the same issue was encountered in aluminium. This would also explain why the measured plastic zone of around $30\text{ }\mu\text{m}$ in the S37 specimen was smaller than the minimum size predicted by Irwin.

Application to heat treated material

Two methods were used to create the Coarse Grained Heat Affected Zone (CGHAZ) microstructure in the S690 steel. The gleeble thermo-mechanical simulator was able to exactly create the required temperature profile and thus lead to homogeneous CGHAZ material. During the gleeble heat treatments the material was deformed, making remachining necessary in order to make them perfectly straight again.

The other method used an Ultra High Frequency (UHF) induction coil to heat up the material, after which it was cooled using compressed air nozzles. This method did not manage to achieve the required cooling rate, however it is believed that with certain adjustments this technique too should yield the required microstructure.

Rotational bending was not viable as a pre-fatigue method for the heat treated material, as no circumferential centric cracks were created. Because the specimens were machined after the heat treatment to be perfectly cylindrical, the inability to properly crack is almost certainly caused by local brittle zones in the material.

Compression - Compression formed the required cracks, although the crack lengths were shorter than desired. Increasing the crack length could be done by reducing the notched diameter of the specimen, or by increasing the strength of the total specimen before heat treatment.

Fracture toughness tests showed a larger influence of eccentricity on the measured results. The increase in brittleness causes a larger influence of the crack length, meaning an eccentric ligament will cause a larger difference in the COD measured.

At low temperature the heat treated CNT specimen showed close agreement with the results from the AFSuM tests. The room temperature specimen showed a large spread of results, which appears to have been caused by the larger eccentricities of the ligaments, which were present in this set of samples.

Chapter 6

Conclusions

This chapter will summarize the conclusions found in the previous chapter, and will answer the research questions formulated in chapter 3.5.

Are Circumferentially Notched Tensile test specimens suitable and applicable for failure assessment of (welded) S690QT steel?

- CNT specimen can measure the COD of S690QT steel at both room and low temperature. Too much plasticity was present at any temperature to use the stress intensity factor. Room temperature COD tests can be performed on CNT specimen, this is not possible for conventional test specimen due to excessive plasticity.
- CNT specimen allowed the COD of S690 CGHAZ material to be measured at room and low temperature. Heat treatment using the Gleeble thermo-mechanical simulator, combined with Compression - Compression pre-fatiguing give results which are in agreement with previous research.

Sub-questions:

1. Can a pre-fatigue method be developed causing little or no eccentricity?
 - Rotational bending pre-fatiguing gives centric circumferential cracks if a minimum load drop is applied.
 - The new Compression - Compression pre-fatiguing method leads to centric circumferential cracks, where both the specimen geometry and loading conditions can be varied to influence the crack length.
2. Can a convenient method be developed to measure the CTOD of CNT specimens?
 - Using extensometers to determine the plastic displacement at the peak load the COD can be measured. When using two extensometer the maximum plastic displacement value is used, these results are confirmed by measuring the plastic crack opening under the microscope.
 - C-C and RB specimen show different load-displacement curves. RB shows clear linear-elastic behavior, for C-C no linear elastic behavior is found during testing. C-C specimen have a COD of 0.18 mm, while RB have a COD of 0.12mm. This is caused by a stress-free material condition at the cracktip of the C-C specimen. Because the crack is grown in compression, no residual stresses are present. A consequence of this finding is that conventional CTOD testing might give underestimations of the true COD.

-
- Digital Image Correlation is able to successfully measure the optical CMOD and determine the effect of eccentricity during testing.
3. Can equivalency between the CNT specimen and conventional FM specimens be determined?
 - Low temperature tests are performed to determine the equivalency between AFSuM and CNT results. C-C samples show a comparable result to the AFSuM samples, while the RB samples show an increase in fracture toughness.
 4. Can the plastic zone size of the CNT specimen be determined?
 - Using EBSD scans on annealed S690 and low carbon steel S37 it was not possible to measure the plastic zone.

Chapter 7

Recommendations

During this research issues were encountered that could not be investigated due to time constraints, or did not fit the scope of this project. This chapter will give some recommendations on these issues and on future research objectives.

- Expand the Compression - Compression pre-fatiguing method to other materials. This method has only been shown for S690 so far, expanding the method to other materials is necessary to further verify the method.
- Compression - Compression pre-fatiguing is far more time consuming than rotational bending. In order to reduce the time it would be useful to find a method that would allow for more than one specimen to be subjected to the compressive cyclic loading. An example would be a system that clamps multiple samples from their side on either the top or the bottom. That way the length of the specimen is not critical and up to 10 S690QT specimen could be pre-fatigued in one go, while still using the current setup.
- Further develop the UHF induction heating method. Using an improved cooling setup, using better nozzles and helium cooling, would allow for higher cooling rates and would allow this method to be used instead of the Gleeble. This would also allow the possibility of performing the pre-fatiguing, heat treatment and fracture toughness test on the same machine.
- Further develop the Digital Image Correlation CMOD measuring technique. The setup used in this research used 1 extensometer and had the cameras at at 90° angle. Using two extensometers and positioning the cameras at a 180° position, as depicted in figure 7.1 would allow for a further improvement in the system. This way the effects of eccentricities could be measured more accurately, and it would create a more robust method. Once these results are fully understood, testing using just the two cameras should be possible.

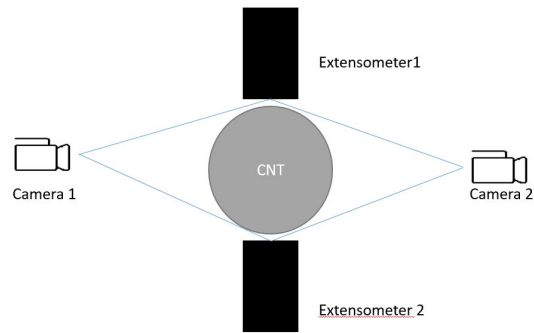


Figure 7.1: Top view of the improved DIC setup

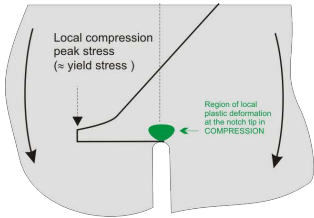

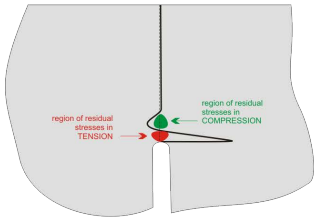

- Use CNT specimen for fracture toughness testing brittle materials. In brittle materials the stress intensity factor is a valid parameter and this will allow a far more direct comparison of CNT and SENB equivalency.
- Perform further COD tests on CGHAZ material samples with longer crack lengths. Comparing these results will shed more light on the requirement of a minimum crack length. Longer crack can be created by hardening the base material or reducing the diameter of the ligament.
- Improve gripping arrangement for the Adapted AFSuM Low Temperature testing method. The method used during this research needed the operator to move really fast, by creating a gripping system with a pin-hole connection some of this need for speed can be reduced.
- Nanoindentation measurements should be performed in order to measure the plastic zone size, these have been shown to give good results in aluminum and would be interesting for steel too.
- Perform the EBSD measurements with a different material. If the dislocation density of the background material is very low, the required strain level needed to detect plasticity would be lower, and the KAM results should show larger differences. Using an EBSD with a higher resolution could also help in this aspect.

Appendices

Appendix A

Compression - Compression fatigue

This is the schematic explanation of the C-C pre-fatiguing method created by dr. Ton Riemsdag

DESCRIPTION	- RESIDUAL STRESS REGIONS AT NOTCH TIP - STRESS DISTRIBUTION IN LIGAMENT	BENDING MODE OF 3 POINT SENB SPECIMEN
<p>1ST STEP APPLICATION OF A SINGULAR HIGH LOAD LEVEL IN REVERSED BENDING, CAUSING PLASTIC DEFORMATION IN COMPRESSION AT THE NOTCH TIP STRESS CONCENTRATION.</p> <p>THE RISK OF BRITTLE FAILURE BY LOCALLY EXCEEDING THE YIELD/FRACTURE STRESS IS LIMITED BECAUSE IT HAPPENS IN COMPRESSION.</p>		<p>Reversed monotonic bending mode (Single overloading in compression)</p> <p>MTS 25 kN hydraulic testing machine</p>  <p>B = 6.5 mm (thickness) W = 12.1 mm (height) S = 51 mm (span)</p> <p>Notch depth $a_0 = 5.5$ mm $F_{max} = -3500$ N ($K_{max} = -50 \text{ MPa}\sqrt{\text{m}}$)</p>
<p>SITUATION AFTER REMOVING THE EXTERNAL LOADING RESIDUAL TENSILE/COMPRESSIVE STRESSES RESPECTIVELY AT AND AHEAD OF THE NOTCH TIP.</p>		<p>Unloaded</p> 

2nd STEP: subsequent initiation, growth and arrest of a fatigue crack.

A (MODERATE) FATIGUE LOAD IS APPLIED IN REVERSED BENDING, PARTIALLY RELIEVING THE RESIDUAL TENSILE STRESSES AT THE NOTCH TIP.

THIS CONSTITUTES (LOCAL) CYCLIC TENSION STRESSES ($\Delta\sigma$) RESULTING IN CRACK INITIATION AND GROWTH.

INITIALLY, DURING THE VERY EARLY STAGE OF CRACK GROWTH, THIS IS CONTROLLED BY ΔK IN TENSION (i.e. the crack growth driving force when the crack length is still small compared to region of residual tensile stresses).

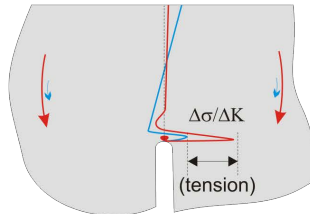
A CRACK CANNOT TRANSMIT TENSILE STRESSES, AND GRADUALLY THE RESIDUAL TENSILE STRESS REGION DISAPPEARS, CAUSING THE CRACK TO ARREST.

THE ARRESTED CRACK TIP IS NOW SURROUNDED BY A STRESS FIELD CHARACTERIZED BY THE STRESS INTENSITY (K), HOWEVER IN COMPRESSION.

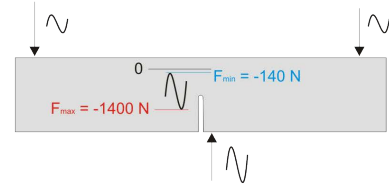
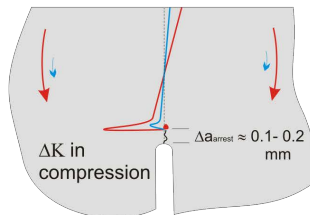
THE MAXIMUM CRACK EXTENSION WILL BE IN THE ORDER OF THE NOTCH TIP RADIUS, WHICH USUALLY IS SMALL (0.1 mm).

THE AUTOMATIC CRACK ARREST IS ESSENTIAL TO KEEP THE WHOLE PROCESS UNDER CONTROL.

Initial crack growth stage



Situation of crack arrest



Reversed bending fatigue mode (MTS Hydr. mach.)

Notch depth $a_0 = 5.5$ mm.

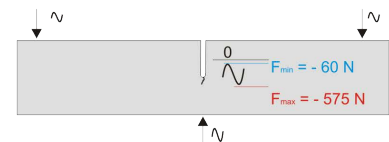
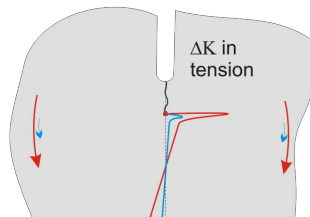
$\Delta F \approx -1250$ N \Rightarrow after crack initiation ($\Delta K \approx -17$ MPa \sqrt{m})
30 Hz, $N_{tot} = 250.000$ cycles (crack arrest).

The crack extension Δa_{arrest} is very small, in the order of the notch tip radius, i.e. about 0.1 mm.

3rd STEP: fatigue crack growth in normal bending mode.

THE ARRESTED CRACK TIP IS SUBJECT TO A RELATIVE LOW ΔK VALUE IN TENSION. ($\Delta K_{cr} < \Delta K < K_{IC}$)

THE CRACK EXTENDS IN A CONTROLLED WAY, TO A TOTAL EXTENSION OF $\Delta a \approx 1-2$ mm.



Normal bending fatigue mode (MTS Hydr. mach.)

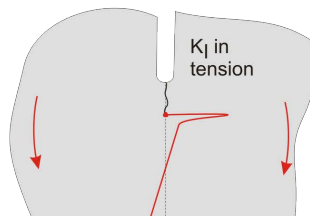
Final crack length ≈ 6.5 mm

$\Delta F \approx 500$ N, 30 Hz, $N_{tot} = 250.000$ cycles.
 \Rightarrow after crack initiation ΔK at $a = 6.5$ mm $\approx +9$ MPa \sqrt{m}

FINAL STEP: CONSTANT LOADING IN DEAD WEIGHT CONSTANT LOADING SET-UP (RECONFIGURED HARDNESS TESTER)

THE FATIGUE CRACK IS SUBJECT TO A HIGH POSITIVE (MODE I) K VALUE OF ABOUT $K_I = 0.95 K_{IC}$.

THE CRACK LENGTH IS MONITORED AT REGULAR INTERVALS BY MICROSCOPIC OBSERVATION OF THE CRACK TIP AT THE POLISHED SPECIMEN SURFACES (AT HIGH MAGNIFICATION)



Constant Load in normal bending (Dead weight set-up)

Starter (pre-fatigued) Crack Length ≈ 6.5 mm

$F = 774$ N \Rightarrow after crack initiation ($K \approx +14$ to $+17$ MPa \sqrt{m})

Appendix B

Stress intensity factor calculations

As shown in chapter 5 none of the tested specimen allowed for the use of the linear-elastic stress intensity factor K , because load at which plasticity occurred did not occur within 1.1 times the maximum load, thus not satisfying criterion 4 in chapter 2.3. One of the issues with this criterion is that this severely limits the applicability of K , as load-displacement curves which do not fit within this limit are automatically considered too plastic to be expressed as a K value.

A different interpretation of this criterion is also possible. P_Q could be determined as in normal specimen, and consequently used to calculate the stress intensity factor this would satisfy all demands which are made for applying this method. This means that for calculation purposes the specimen failed at P_Q , and a valid K value can be calculated. The only difference would be that in practice the specimen would have failed far later, thus giving a more conservative value for K . An example is given below in figure B.1

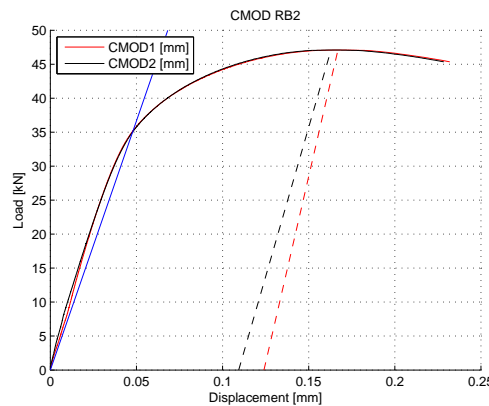


Figure B.1: Location of P_Q in the load-displacement curve of sample RB2

If the Koiter-Benthem method for calculating K , found in equation 3.7, with P_Q is 35 kN, is then used the K -value found would be $61.82 \text{ MPa}\sqrt{m}$. This would have been a valid result for the stress intensity factor if the specimen would have failed below 38.5 kN.

In this case the specimen did not fail below 38.5 kN, officially invalidating the found K value. However, according to this alternative interpretation the only difference this would make is that the found K value is an over conservative value, and would be acceptable as a value to use in calculation. This method would greatly increase the applicability of K for many purposes.

Appendix C

Full experimental data

C.1 Pre-fatigue

C.1.1 Rotational Bending

Table C.1: All results of the rotational bending pre-fatiguing

Sample	D (mm)	d (mm)	Δa (mm)	a/R	ecc (mm)	Initial Moment (Nm)	Moment drop (%)	Amount of cycles
RB1	11.92	7.90	1.25	0.45	0.15	17.5	8.6	34000
RB2	12.02	7.90	1.05	0.48	0.15	17.6	4.5	50600
RB3	12.00	7.90	1.05	0.48	0.12	17.7	5.1	36800
RB4	11.97	7.80	0.56	0.56	0.15	18.4	3.3	67500
RB5	12.00	8.00	1.19	0.47	0.10	14.9	3.4	54200
RB6	12.00	8.00	0.73	0.54	0.21	15.6	2.6	37400
RB7	11.88	7.85	0.80	0.53	0.12	15.7	3.8	76700
RB8	11.98	7.99	0.78	0.54	0.23	15.7	4.5	38500
RB9	11.76	7.77	0.87	0.51	0.00	17.2	3.5	76300
RB10	11.76	7.71	0.43	0.58	0.00	17.6	3.4	17300
RB11	11.80	7.88	0.60	0.57	0.13	16.8	3.0	26400
RB12	11.90	7.94	0.54	0.58	0.05	17.6	4.5	21800
LTRB1	12.00	8.00	1.00	0.50	0.04	14.4	4.2	63800
LTRB2	12.00	8.00	0.69	0.55	0.03	15.3	2.0	37600
LTRB3	12.00	8.00	1.05	0.49	0.05	15	4.0	53000
LTRB4	12.00	8.00	1.00	0.50	0.15	15	4.0	25700
LTRB5	12.00	8.00	0.85	0.53	0.00	15	4.0	40900

C.1.2 Compression - Compression

Table C.2: All results of the rotational bending pre-fatiguing

Sample	D (mm)	d (mm)	Δa (mm)	a/R	ecc (mm)	Amount of cycles	$F_{overload}$ (kN)
C1	11.71	7.81	0.33	0.61	0.05	20000	53.21
C2	11.76	7.88	0.48	0.59	0.00	50000	53.26
C3	11.69	7.73	0.59	0.56	0.14	100000	54.26
C4	11.69	7.67	0.61	0.55	0.08	20000	76.40
C5	11.81	7.94	0.85	0.53	0.13	50000	73.26
C6	11.76	7.95	1.16	0.48	0.16	100000	75.83
C7	11.76	8.07	1.49	0.43	0.85	1000000	76.32
C8	12.00	7.32	1.00	0.44	0.18	100000	70.65
C9	11.76	7.92	1.09	0.49	0.12	100000	72.10
C10	12.00	7.46	1.21	0.42	0.29	500000	72.10
C11	11.82	8.02	1.04	0.50	0.00	100000	72.10
C12	12.00	7.64	0.95	0.48	0.13	1000000	72.10
C13	11.92	7.94	1.05	0.49	0.00	100000	72.10
C14	12.00	7.41	1.27	0.41	0.40	500000	72.10
C15	11.85	8.09	1.18	0.48	0.20	100000	72.10
C16	12.00	7.66	0.87	0.49	0.22	1000000	72.10
C17	12.00	7.28	1.29	0.39	0.45	100000	72.10
C18	11.92	8.02	1.11	0.49	0.16	100000	72.10
C19	12.00	8.00	1.15	0.48	0.15	100000	72.10
C20	11.86	7.93	1.14	0.48	0.13	100000	72.10
C21	11.86	7.94	1.15	0.48	0.33	100000	72.10
C22	12.00	8.16	0.93	0.53	0.00	100000	72.10
C23	11.90	8.00	0.95	0.51	0.14	100000	72.10
GRT1	12.00	7.81	0.80	0.52	0.44	500000	72.10
GRT2	11.58	7.96	0.34	0.63	0.00	100000	72.10
GRT3	11.81	8.43	0.59	0.61	0.25	250000	72.10
GLT1	11.41	7.96	0.38	0.63	0.30	500000	72.10
GLT2	11.49	7.80	0.44	0.60	0.13	500000	72.10
GLT3	11.43	8.39	0.41	0.66	0.00	500000	72.10

C.2 Fracture toughness tests

C.2.1 Rotational bending

Table C.3: All results for fracture toughness tests on RB samples at room temperature

Sample	Final load (kN)	Crack extension (mm)	a/R	CTOD (mm)	ecc (mm)
RB1	40.78	1.25	0.45	0.12	0.15
RB2	47.09	1.05	0.48	0.12	0.15
RB3	45.30	1.05	0.48	0.12	0.12
RB4	58.92	0.56	0.56	0.13	0.15
RB5	50.14	1.19	0.47	0.12	0.10
RB6	57.44	0.73	0.54	0.14	0.21
S7	49.15	1.09	0.49	0.13	0.15
S8	29.97	1.82	0.38	0.13	0.46
S9	17.09	2.42	0.27	0.11	0.06

C.2.2 Compression - Compression

Table C.4: All results for fracture toughness tests on C-C samples at room temperature

Sample	Final load (kN)	Crack extension(mm)	a/R	CTOD (mm)	ecc (mm)
C11	49.37	1.04	0.50	0.19	0.00
C13	48.00	1.05	0.49	0.17	0.00
C15	46.06	1.18	0.48	0.17	0.20
C18	45.23	1.11	0.49	0.22	0.16
C19	44.11	1.15	0.48	0.21	0.15
C20	44.67	1.14	0.48	0.19	0.13
C21	44.37	1.15	0.48	0.18	0.33

C.2.3 Comparison between RB and C-C specimen

Table C.5: Results for the annealed specimen used for the comparison between RB and C-C specimen, all tested at room temperature

Sample	Final load (kN)	Crack extension (mm)	a/R	CTOD (mm)	ecc (mm)
RB8	31.33	0.78	0.54	0.03	0.23
RB12	38.92	0.54	0.58	0.03	0.05
C22	29.23	0.93	0.53	0.02	0.00

C.2.4 Optical microscopy measurements

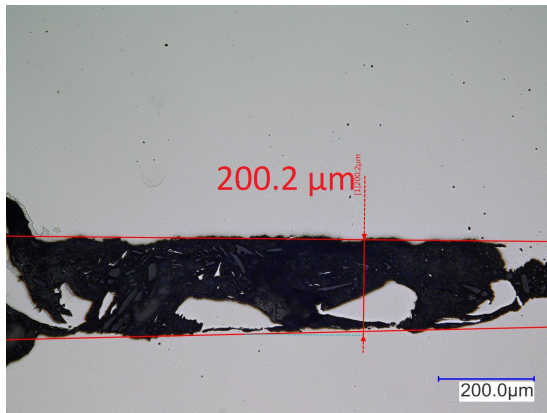


Figure C.1: C19: extensometer measurement result 0.19 mm

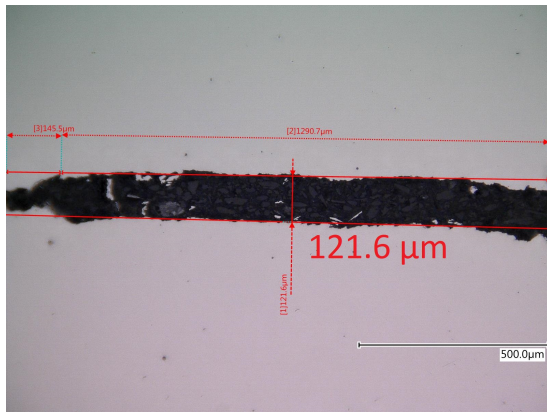


Figure C.2: RB5: extensometer measurement result 0.12 mm

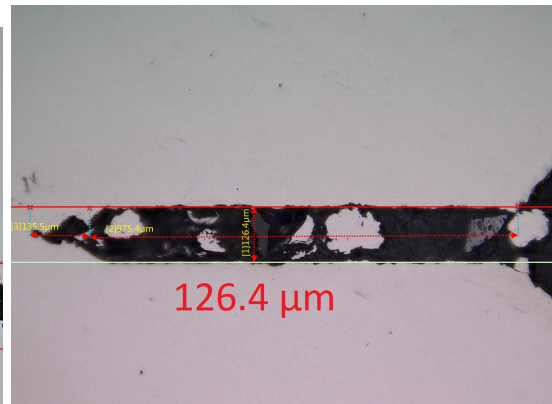


Figure C.3: RB3: extensometer measurement result 0.12 mm

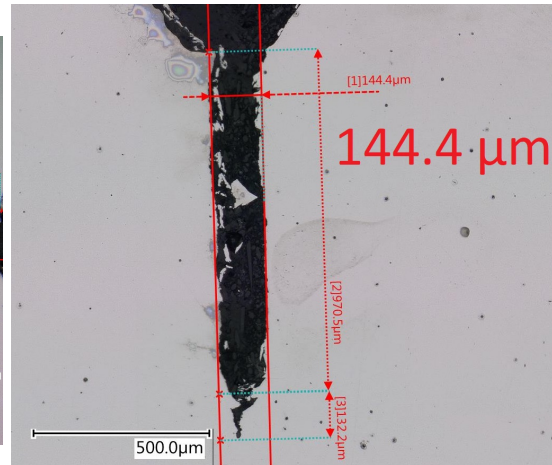


Figure C.4: RB6: extensometer measurement result 0.14 mm

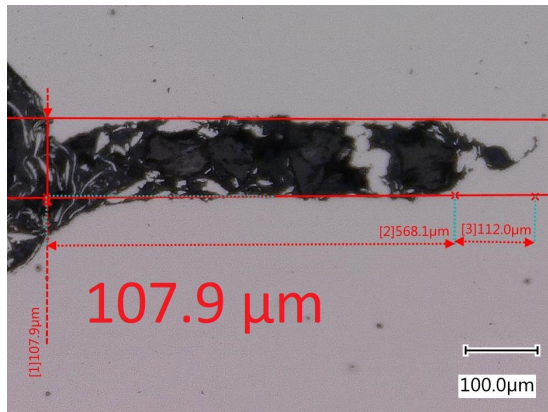


Figure C.5: LTRB2: extensometer measurement result 0.11 mm

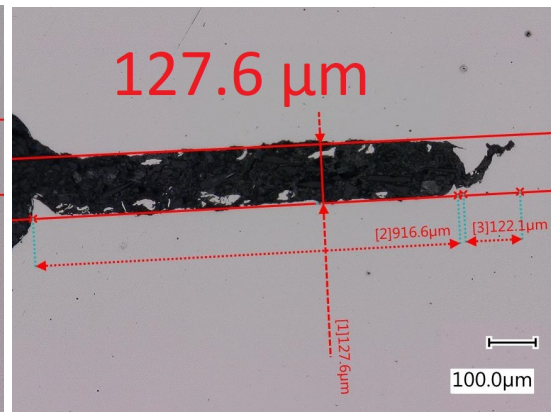


Figure C.6: LTRB3: extensometer measurement result 0.12 mm

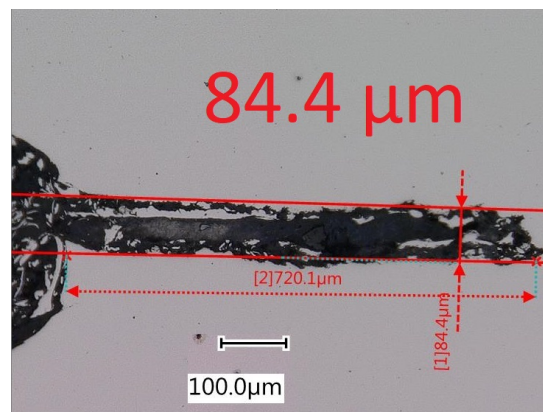


Figure C.7: LTRB5: extensometer measurement result 0.08 mm

C.2.5 DIC

These are the results of the DIC measurements. The first picture will show one of the two camera images, while the second image shows the line depicting the measurement.

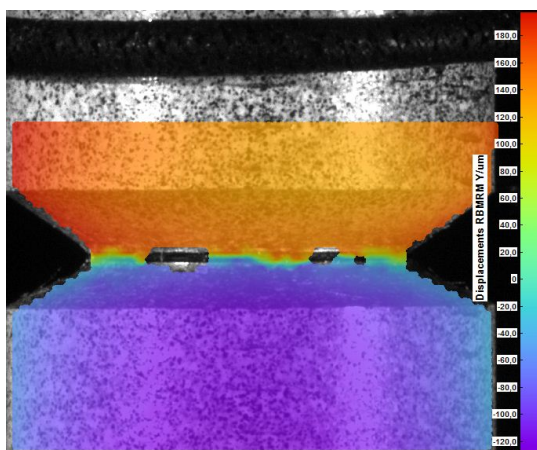


Figure C.8: C13: camera image

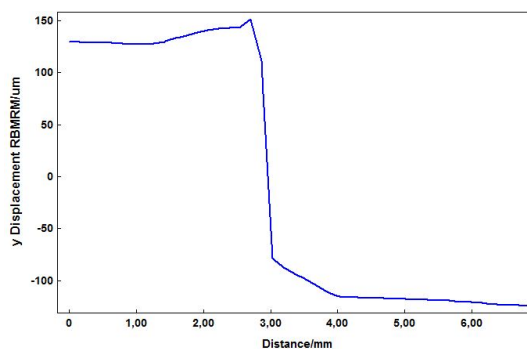


Figure C.9: C13: measurement line

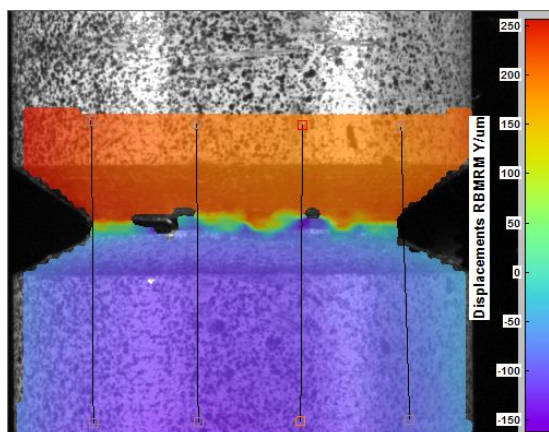


Figure C.10: C15: camera image

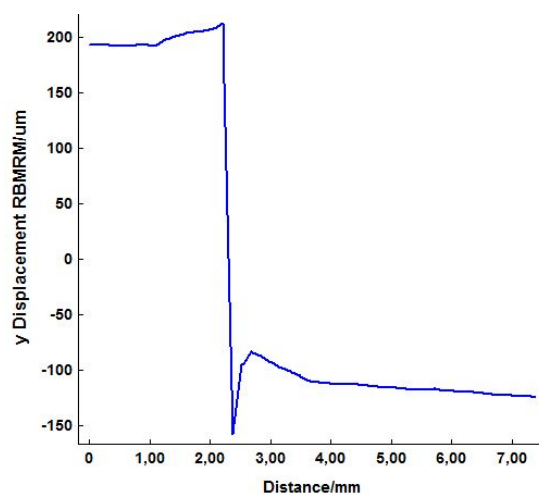


Figure C.11: C15: measurement line

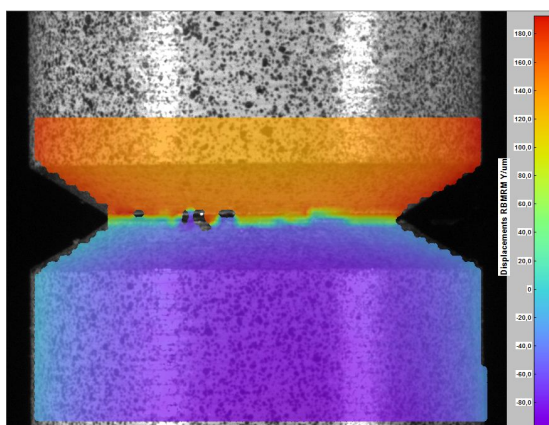


Figure C.12: C18: camera image

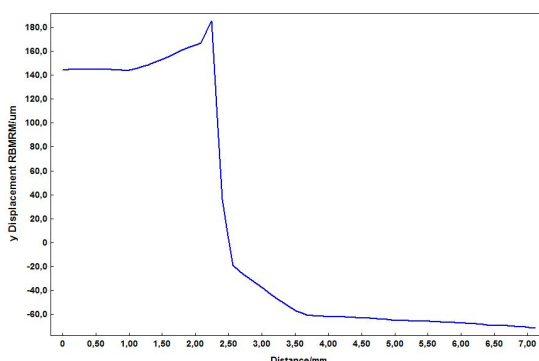


Figure C.13: C18: measurement line

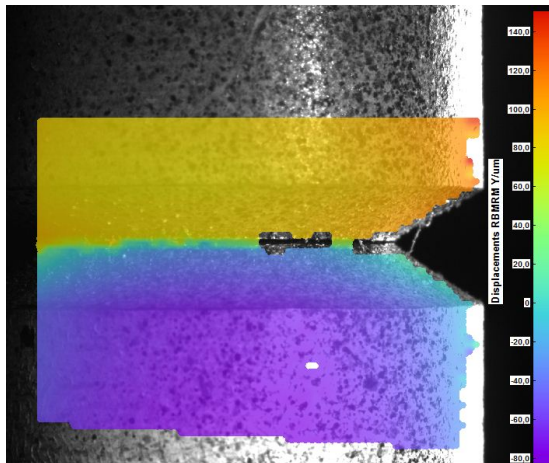


Figure C.14: G1: camera image

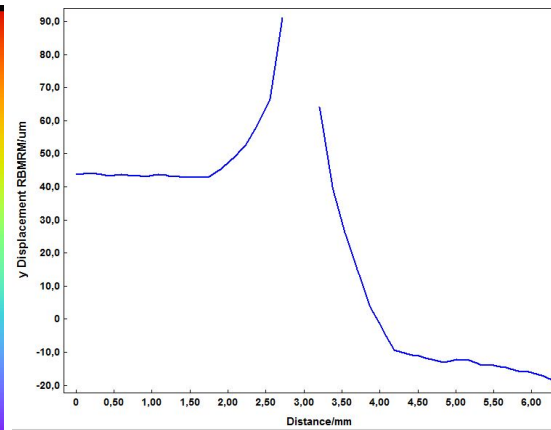


Figure C.15: G1: measurement line showing minimum value

C.3 CGHAZ material

C.3.1 Gleeble heat treatment



Figure C.16: CGHAZ microstructure from the center of the bar (250x)



Figure C.17: CGHAZ microstructure from the edge of the bar (250x)

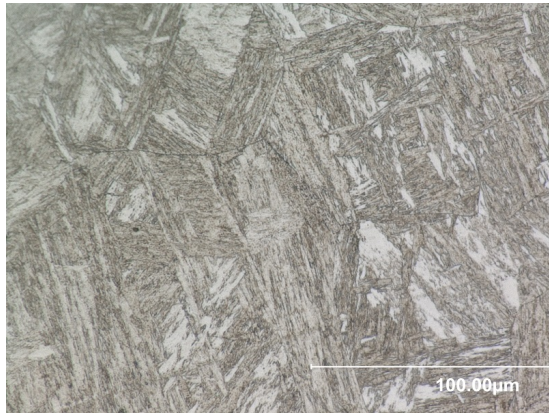


Figure C.18: CGHAZ microstructure from the center of the bar (1500x)

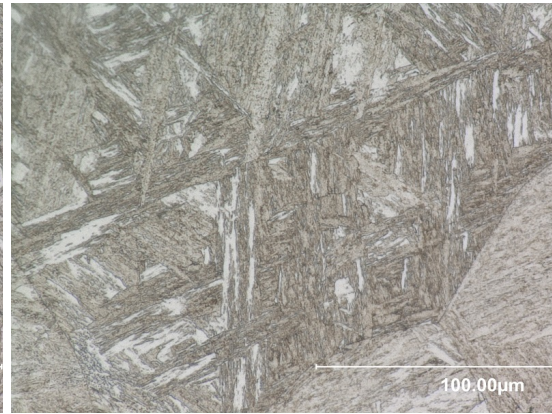


Figure C.19: CGHAZ microstructure from the edge of the bar (1500x)

C.3.2 UHF heat treatment

Hardness (Hv ₃)				
Center	Right	Under	Left	Top
363	375	356	387	370
383	380	345	361	361
351	376	352	368	380
356				
361				
355				
387				
382				
368				

Average hardness (Hv ₃) / Equivalent strength				
367	377	351	372	370
1180 Mpa	1211 MPa	1128 Mpa	1196 Mpa	1190 Mpa

Table C.6: Hardness measurements on UHF heat treatment material

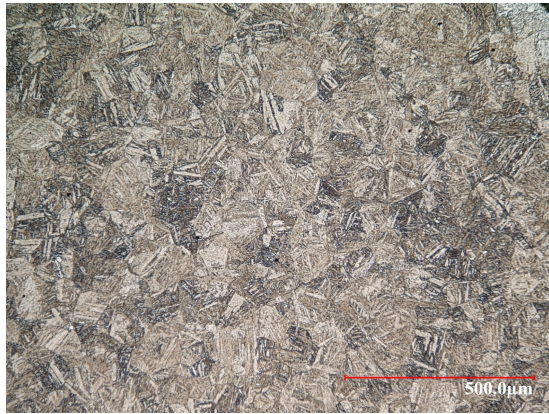


Figure C.20: Microstructure created using the UHF induction coil (250x)

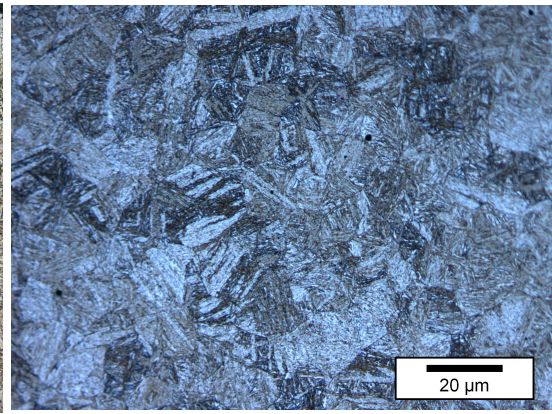


Figure C.21: Microstructure created using the UHF induction coil (1500x)

C.3.3 Tensile curves

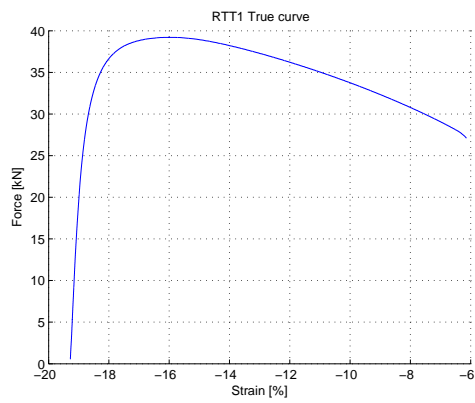


Figure C.22: RTT1: Extensometer signal

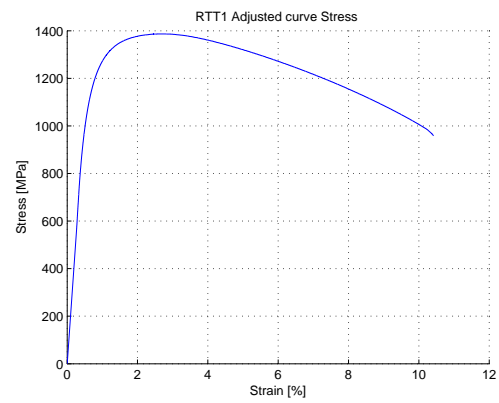


Figure C.23: RTT1: Corrected curve

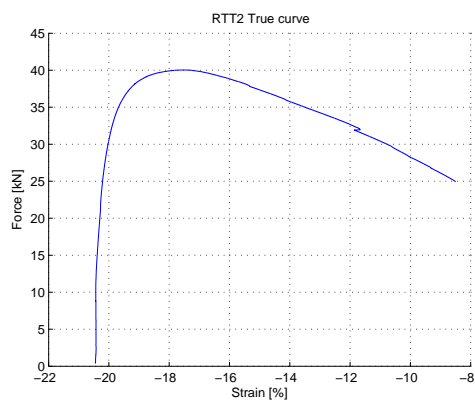


Figure C.24: RTT2: Extensometer signal

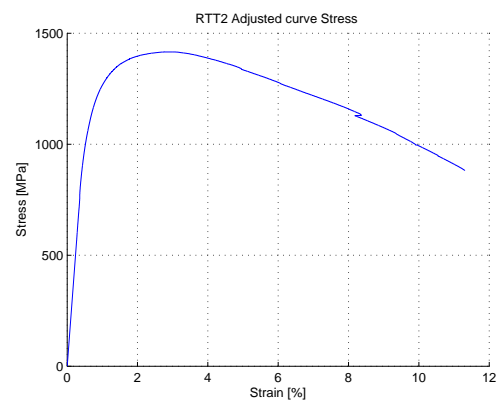


Figure C.25: RTT2: Corrected curve

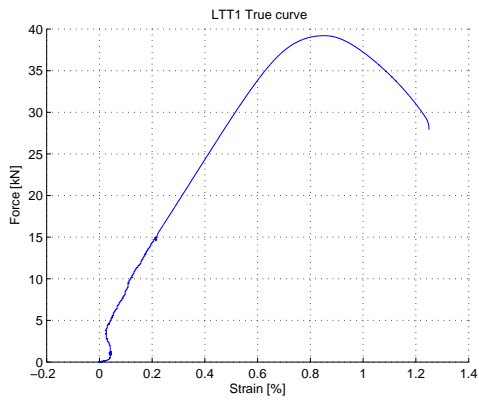


Figure C.26: LTT1: Extensometer signal

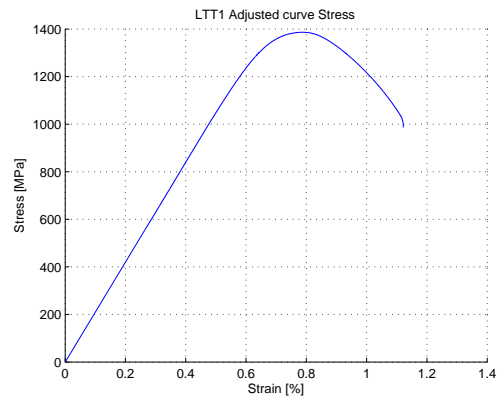


Figure C.27: LTT1: Corrected curve

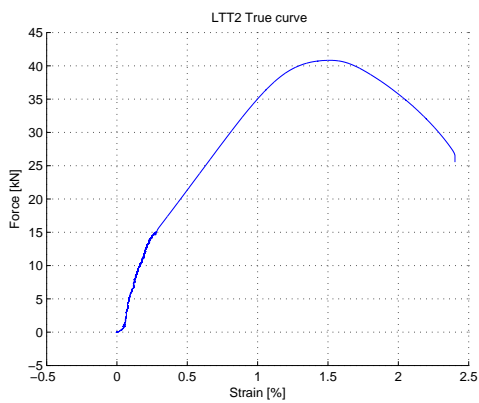


Figure C.28: LTT2: Extensometer signal

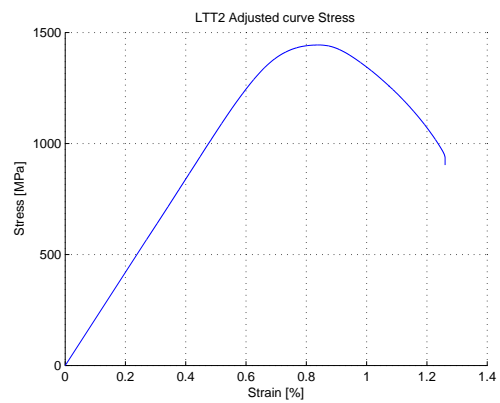


Figure C.29: LTT2: Corrected curve

C.4 Fracture surfaces and Load-displacement curves

C.4.1 C1 - C25

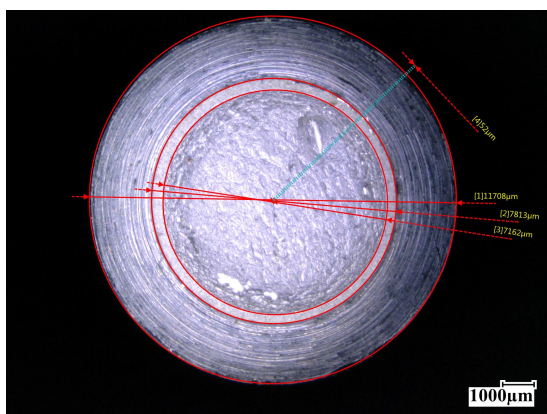


Figure C.30: C1: fracture surface

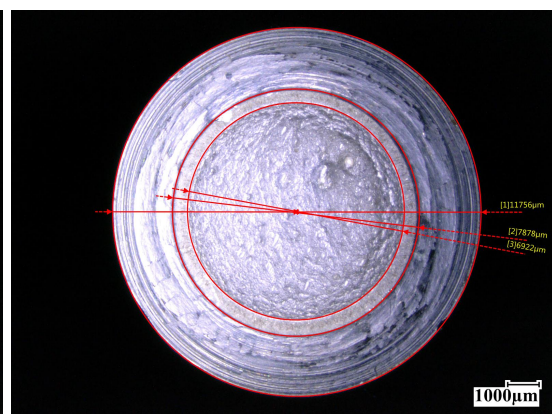


Figure C.31: C2: fracture surface

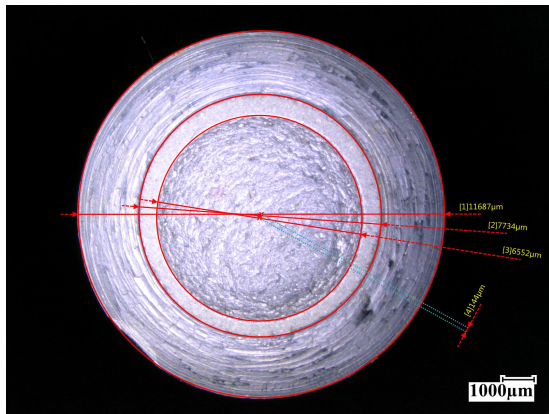


Figure C.32: C3: fracture surface

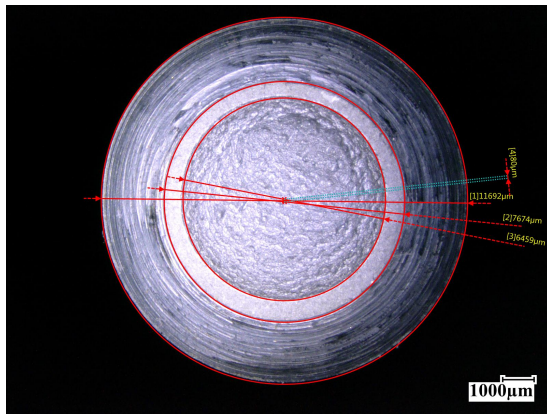


Figure C.33: C4: fracture surface

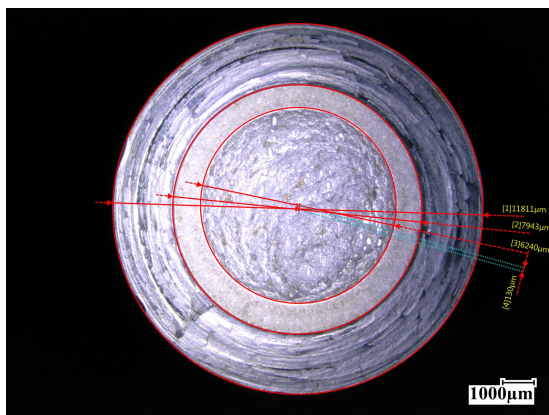


Figure C.34: C5: fracture surface

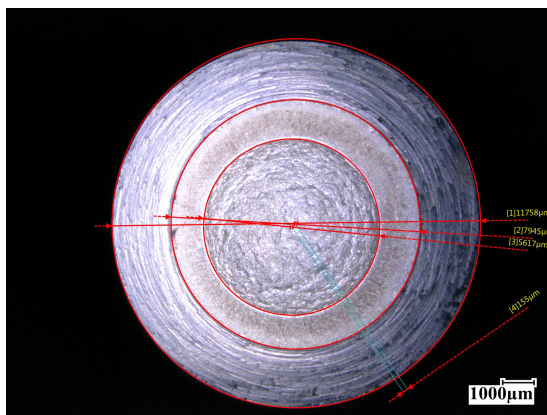


Figure C.35: C6: fracture surface

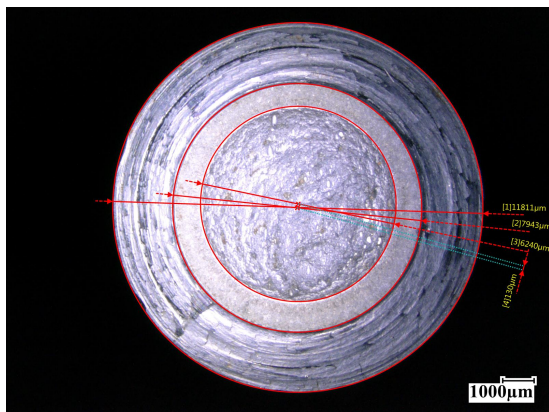


Figure C.36: C7: fracture surface

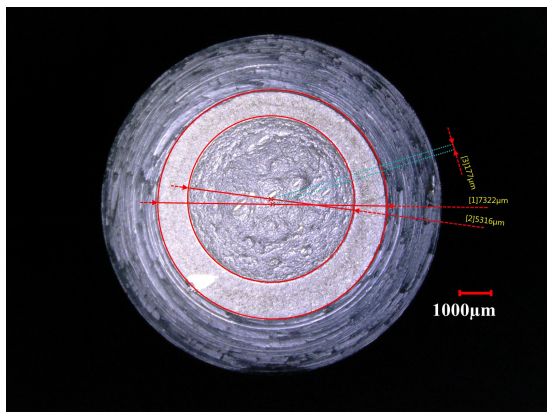


Figure C.37: C8: fracture surface

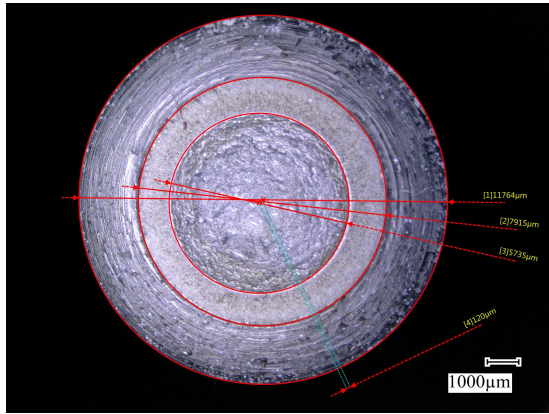


Figure C.38: C9: fracture surface

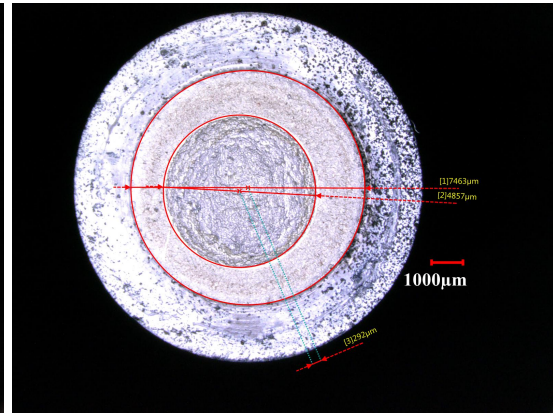


Figure C.39: C10: fracture surface

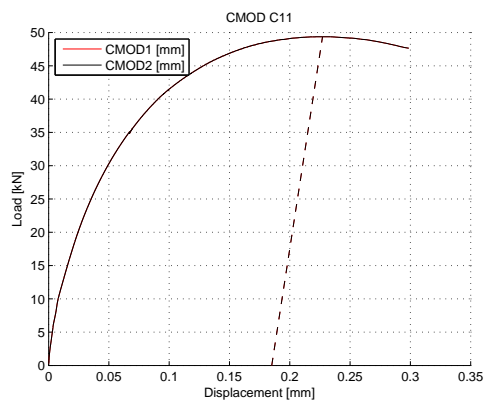


Figure C.40: C11: load-displacement curve

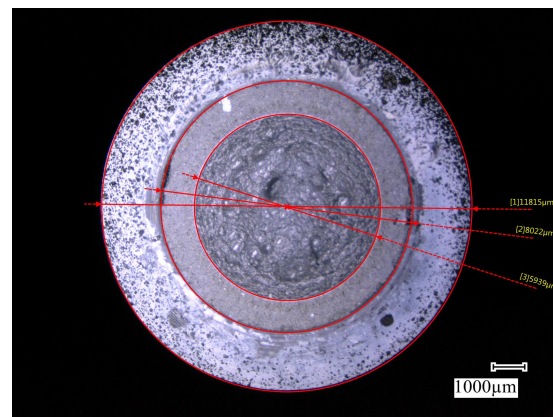


Figure C.41: C11: fracture surface

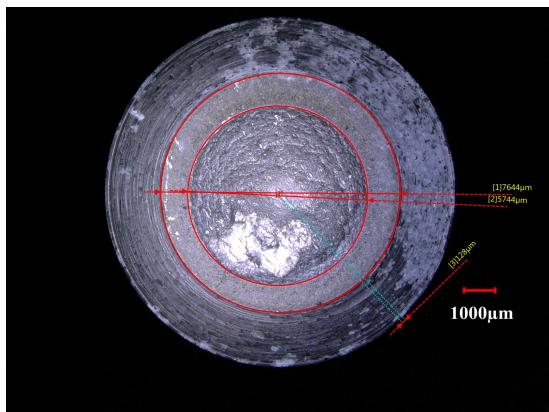


Figure C.42: C12: fracture surface

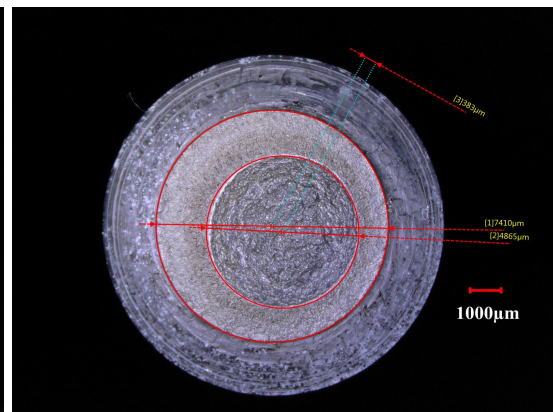


Figure C.43: C14: fracture surface

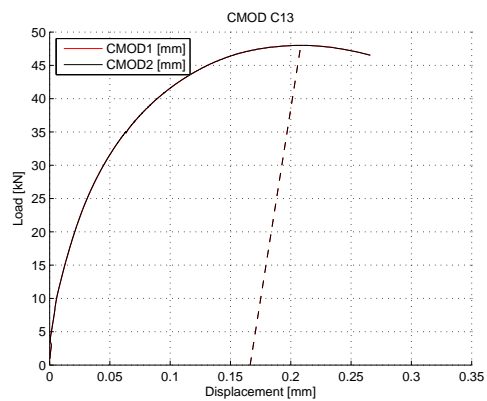


Figure C.44: C13: load-displacement curve

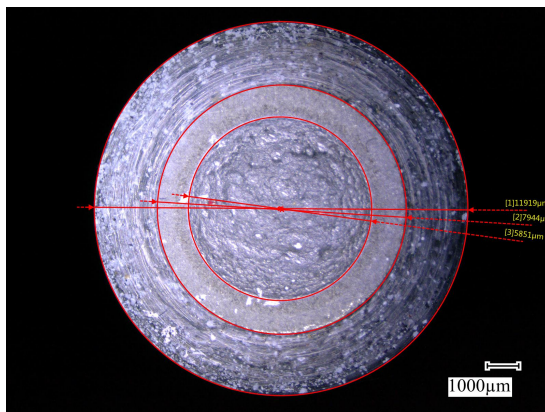


Figure C.45: C13: fracture surface

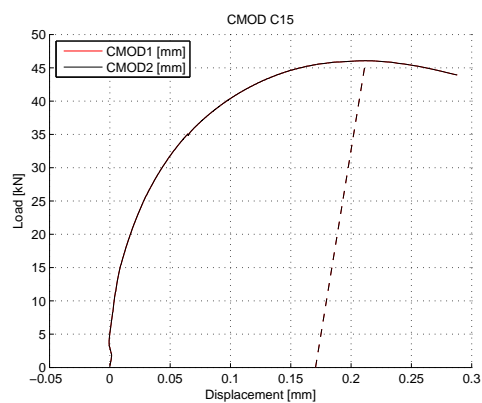


Figure C.46: C15: load-displacement curve

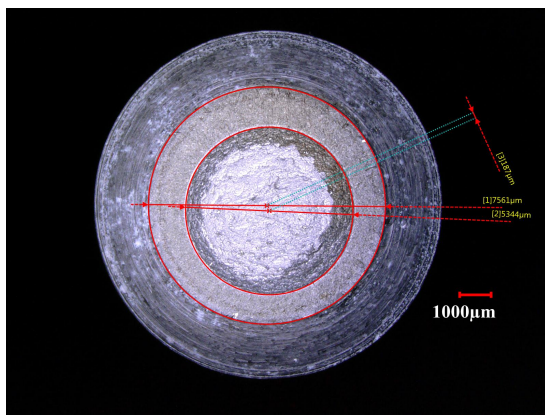


Figure C.47: C15: fracture surface

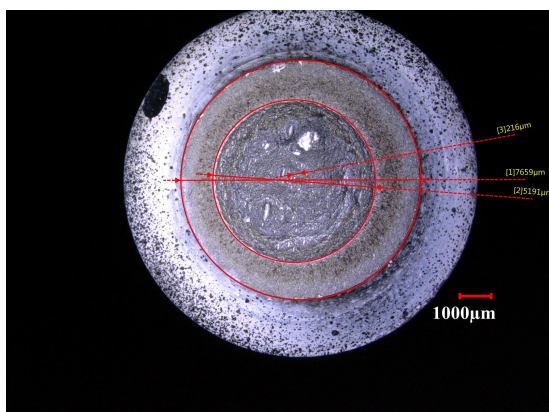


Figure C.48: C16: fracture surface

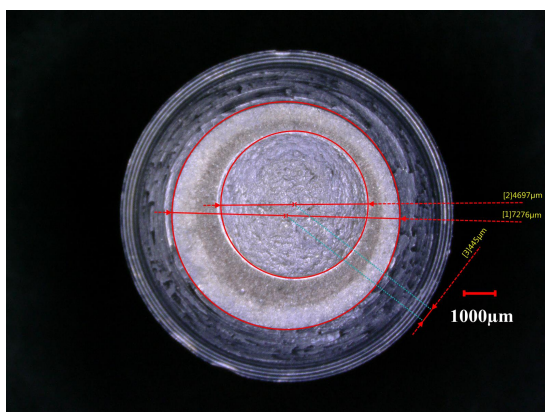


Figure C.49: C17: fracture surface

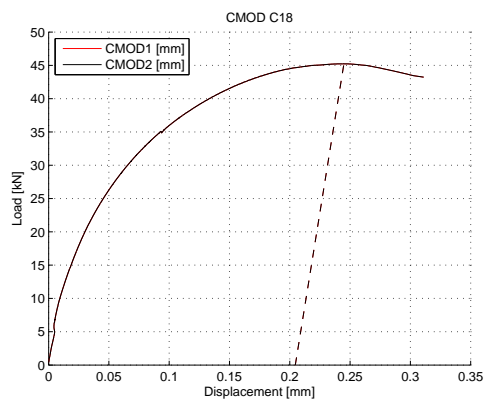


Figure C.50: C18: load-displacement curve

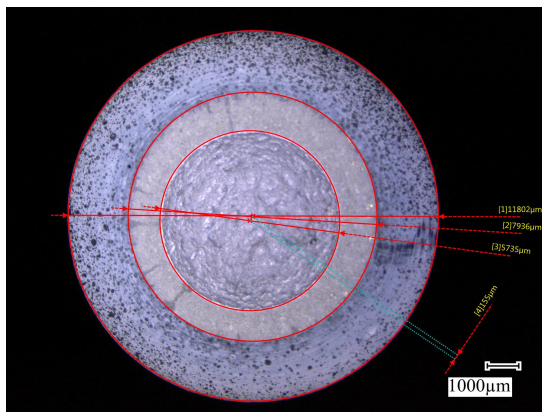


Figure C.51: C19: fracture surface

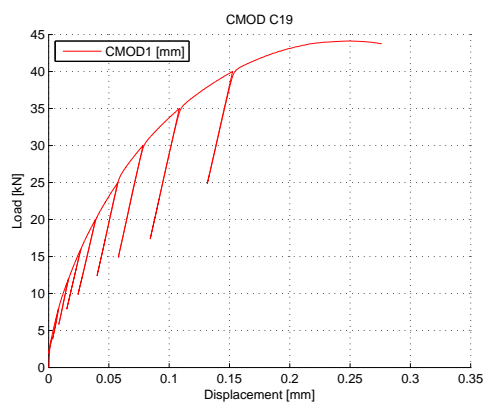


Figure C.52: C19: load-displacement curve

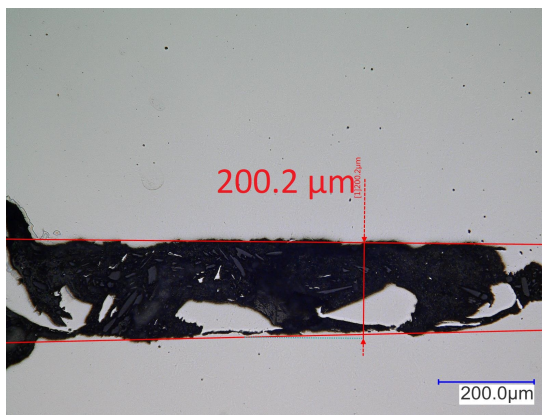


Figure C.53: C19: fracture surface

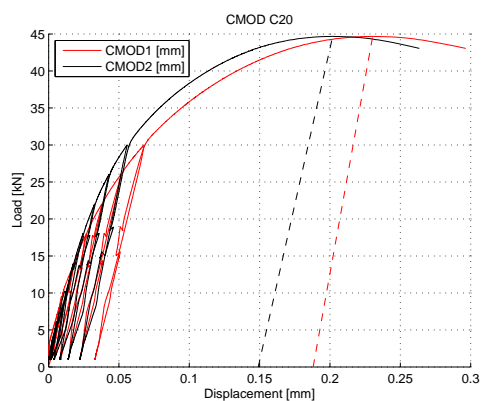


Figure C.54: C20: load-displacement curve

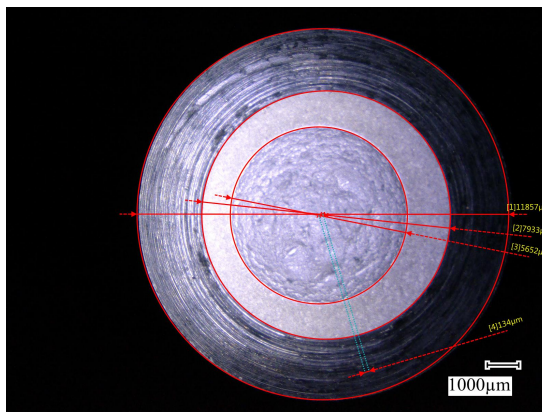


Figure C.55: C20: fracture surface

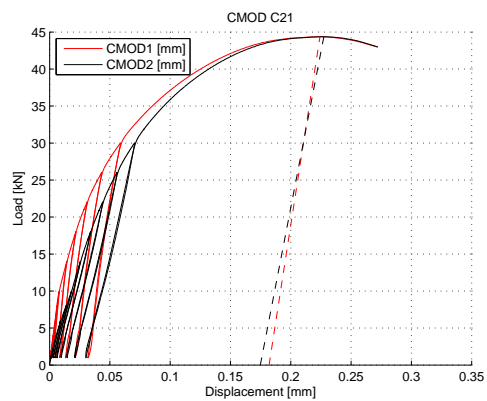


Figure C.56: C21: load-displacement curve

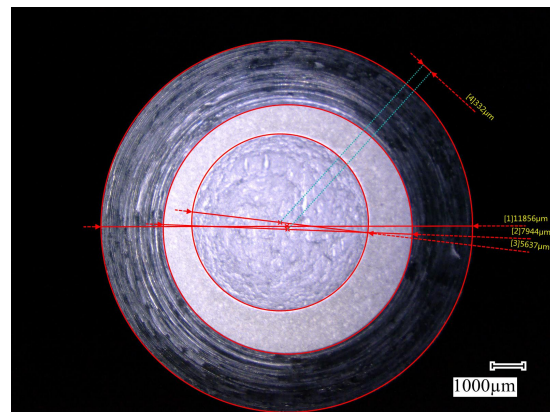


Figure C.57: C21: fracture surface

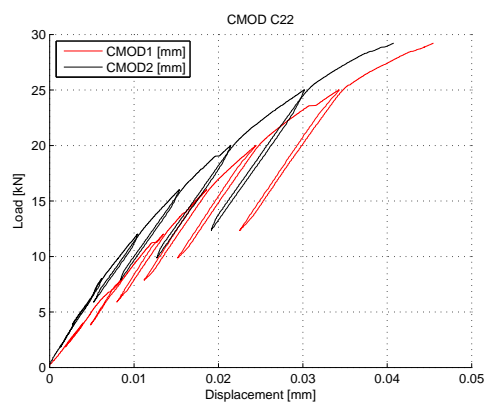


Figure C.58: C22: load-displacement curve

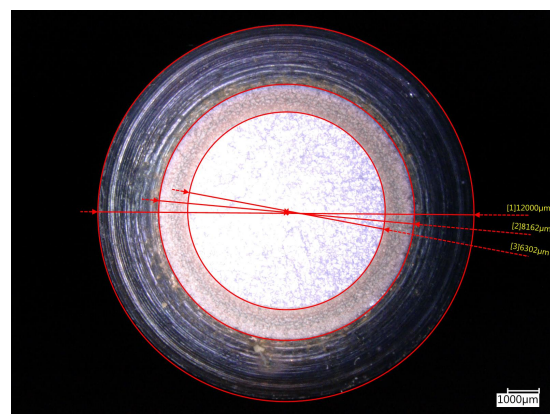


Figure C.59: C22: fracture surface

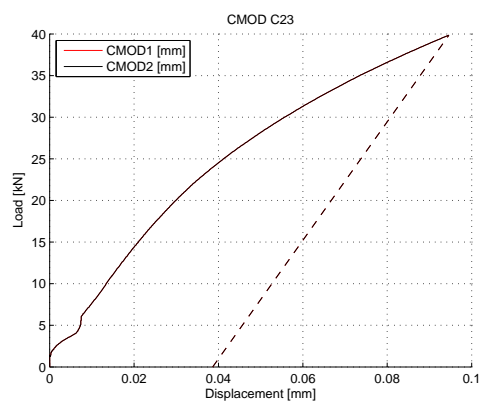


Figure C.60: C23: load-displacement curve

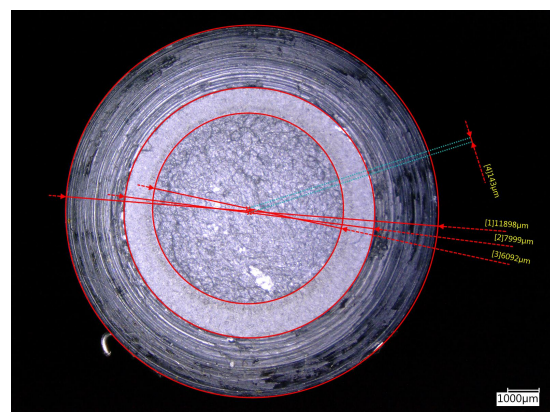


Figure C.61: C23: fracture surface

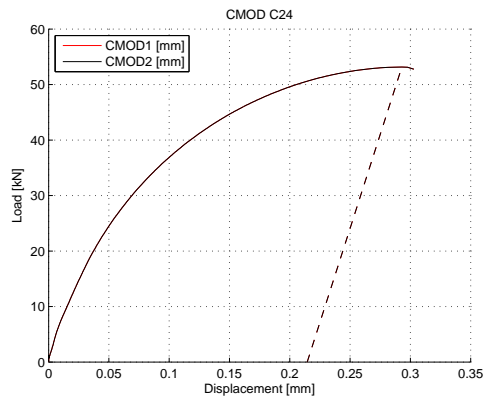


Figure C.62: C24: load-displacement curve

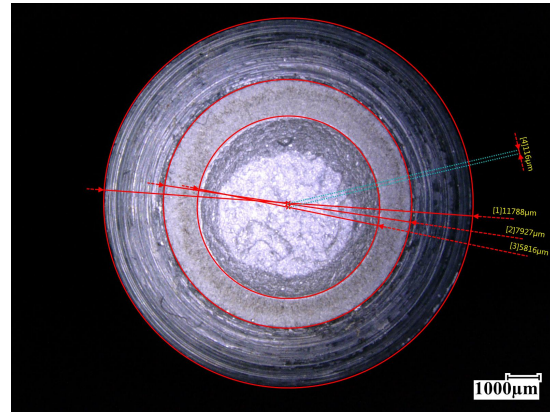


Figure C.63: C24: fracture surface

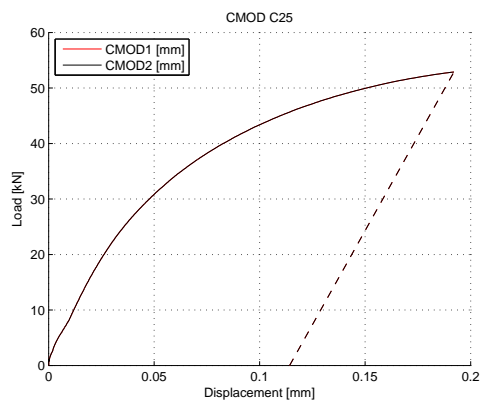


Figure C.64: C25: load-displacement curve

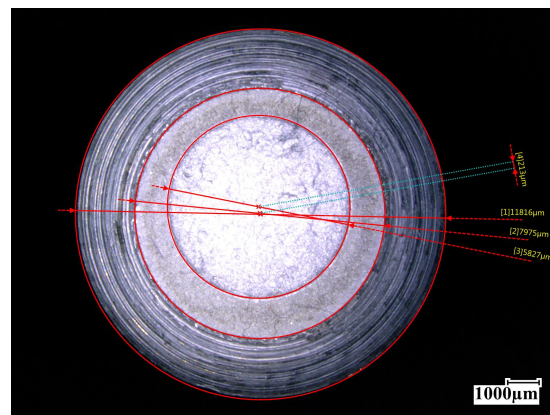


Figure C.65: C25: fracture surface

C.4.2 RB1 - RB12

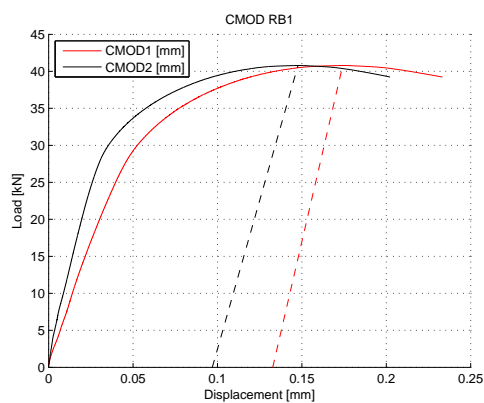


Figure C.66: RB1: load-displacement curve

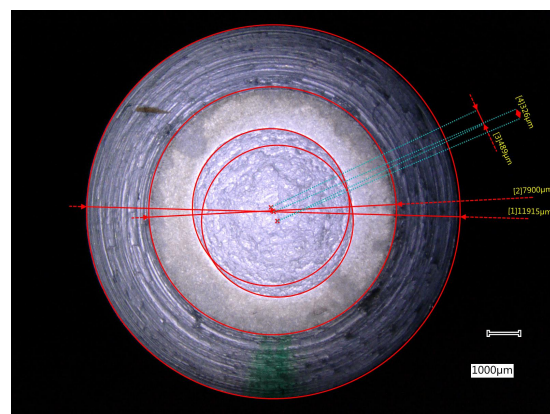


Figure C.67: RB1: fracture surface

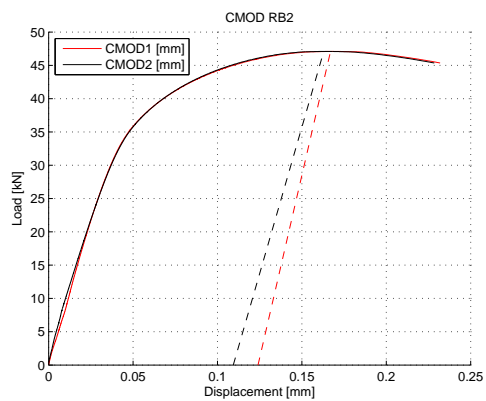


Figure C.68: RB2: load-displacement curve

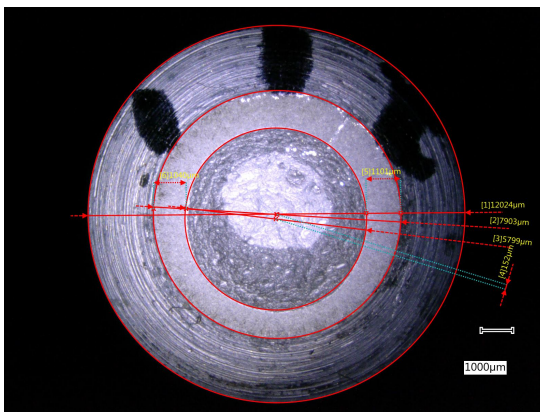


Figure C.69: RB2: fracture surface

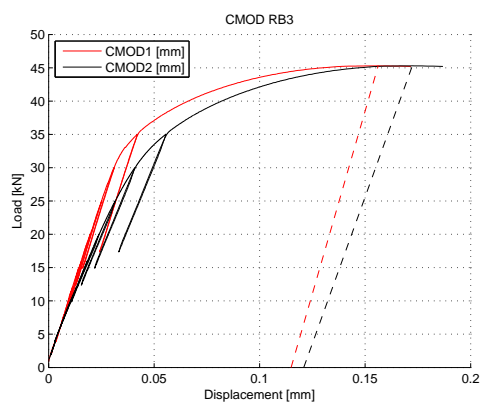


Figure C.70: RB3: load-displacement curve

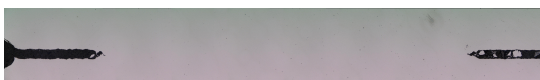


Figure C.71: RB3: fracture surface

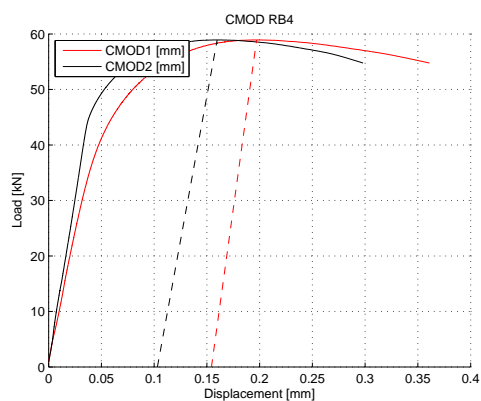


Figure C.72: RB4: load-displacement curve

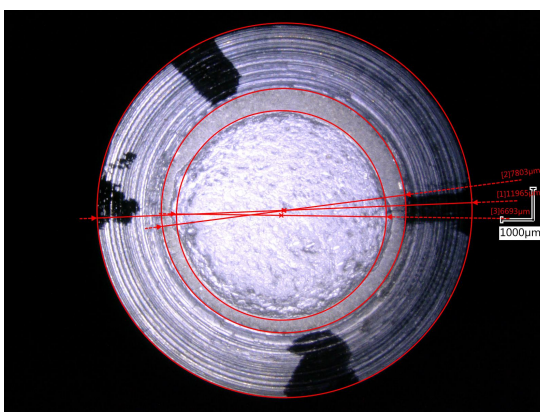


Figure C.73: RB4: fracture surface

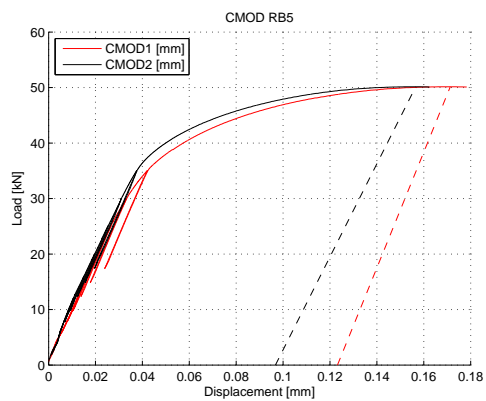


Figure C.74: RB5: load-displacement curve

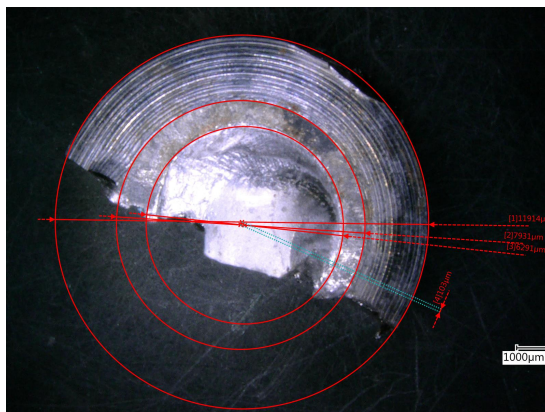


Figure C.75: RB5: fracture surface

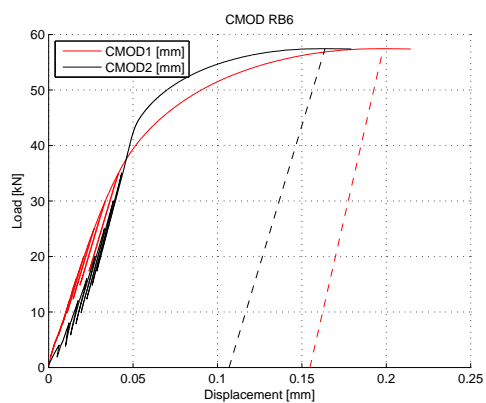


Figure C.76: RB6: load-displacement curve

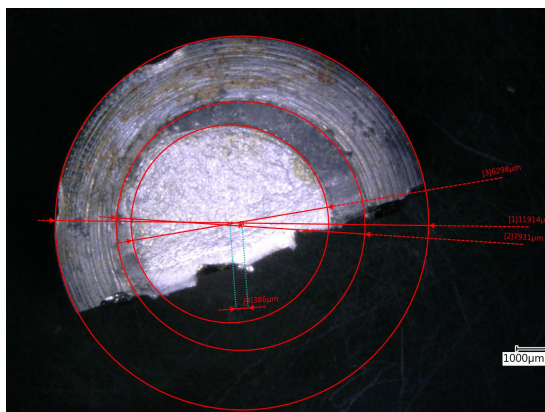


Figure C.77: RB6: fracture surface

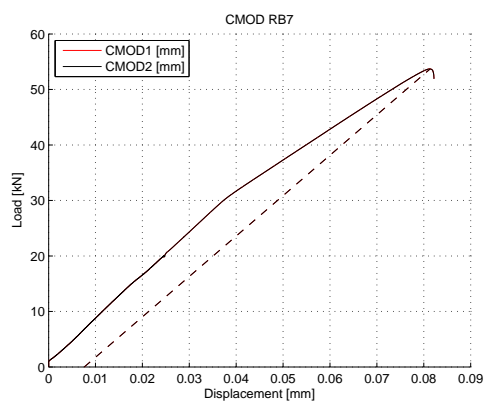


Figure C.78: RB7: load-displacement curve

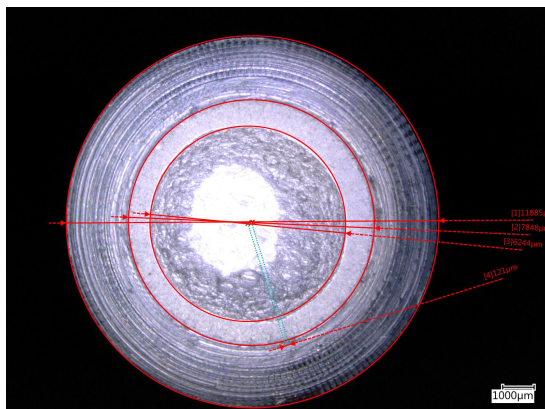


Figure C.79: RB7: fracture surface

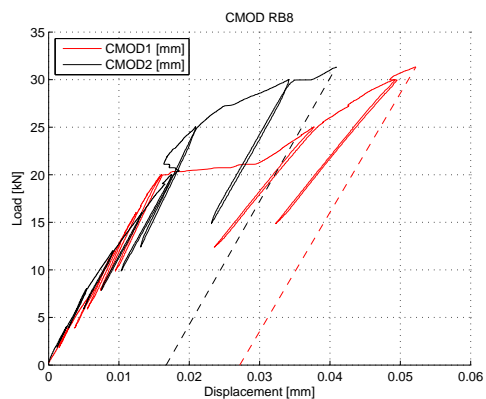


Figure C.80: RB8: load-displacement curve

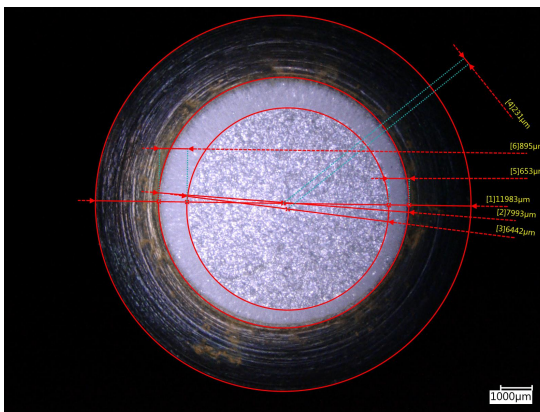


Figure C.81: RB8: fracture surface

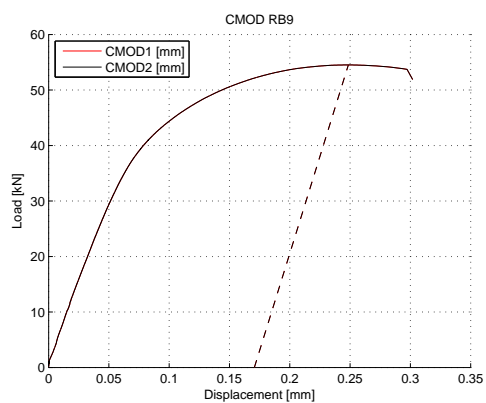


Figure C.82: RB9: load-displacement curve

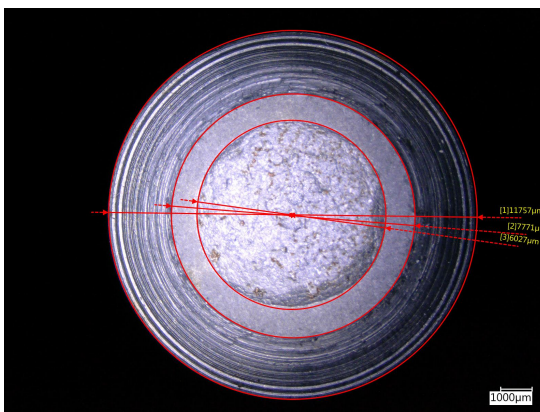


Figure C.83: RB9: fracture surface

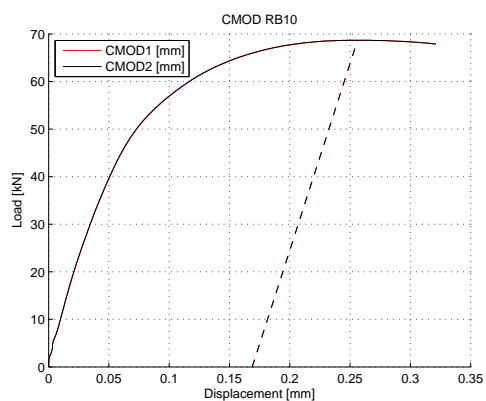


Figure C.84: RB10: load-displacement curve

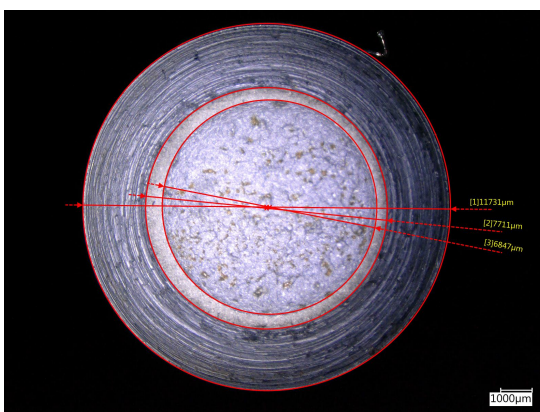


Figure C.85: RB10: fracture surface

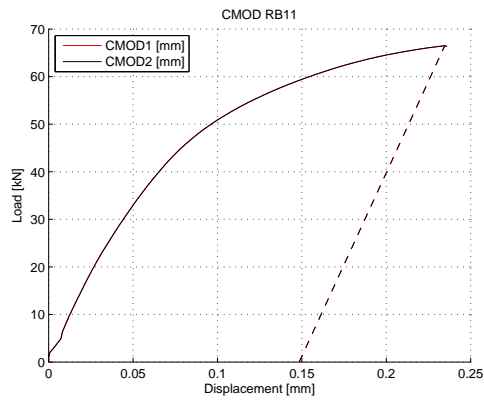


Figure C.86: RB11: load-displacement curve

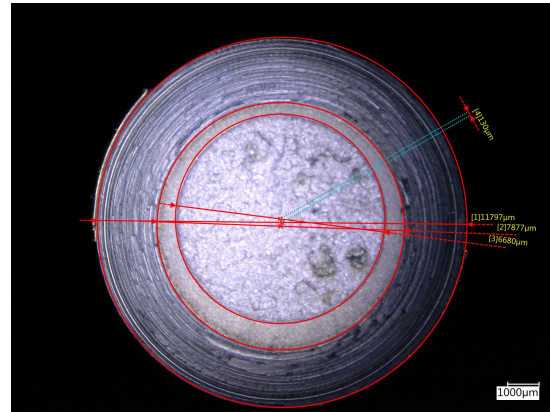


Figure C.87: RB11: fracture surface

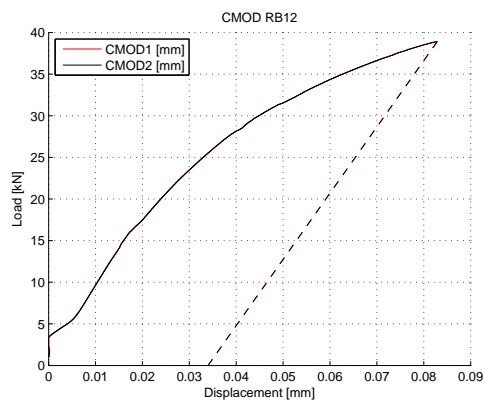


Figure C.88: RB12: load-displacement curve

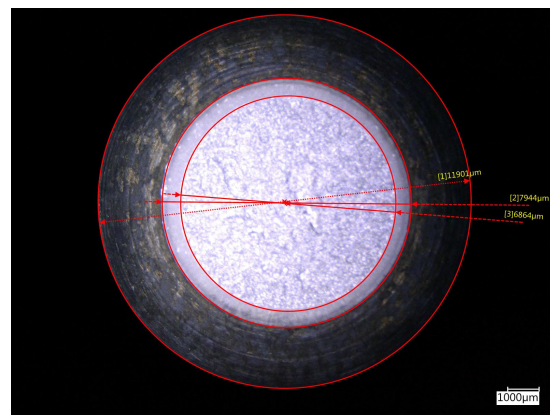


Figure C.89: RB12: fracture surface

C.4.3 S7 - S9

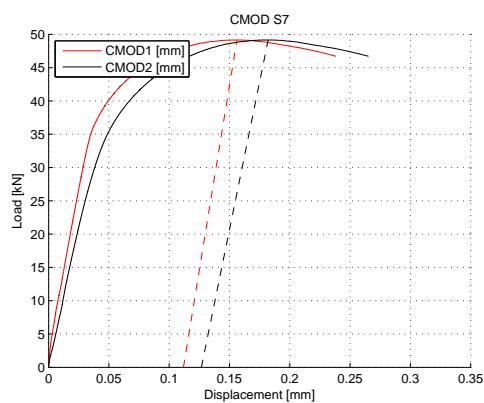


Figure C.90: S7: load-displacement curve

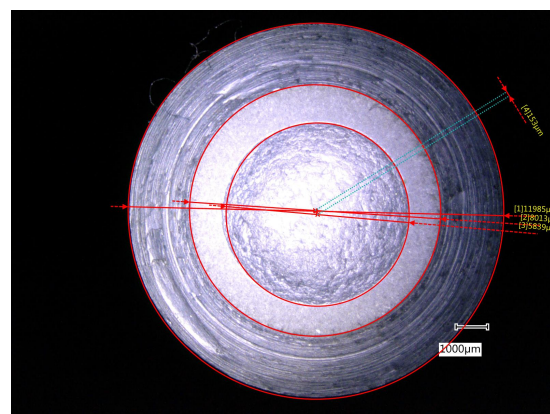


Figure C.91: S7: fracture surface

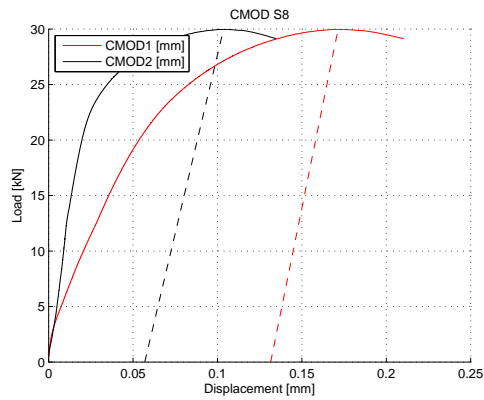


Figure C.92: S8: load-displacement curve

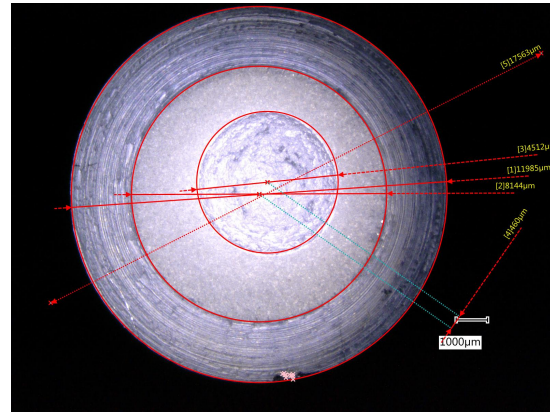


Figure C.93: S8: fracture surface

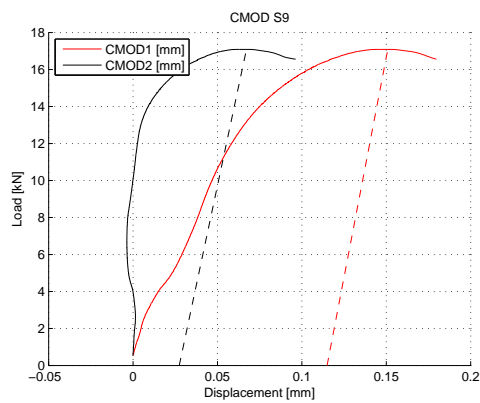


Figure C.94: S9: load-displacement curve

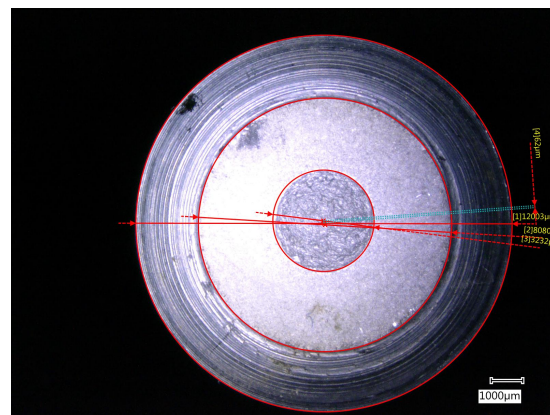


Figure C.95: S9: fracture surface

C.4.4 LTRB1 - LTRB5

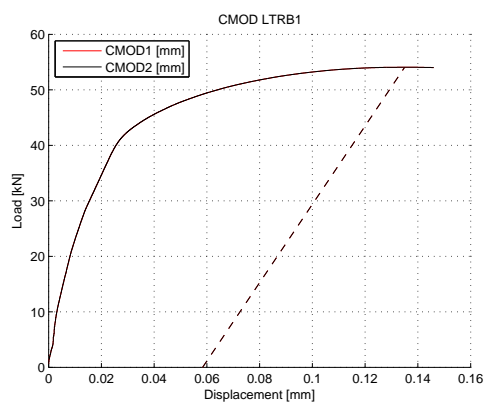


Figure C.96: LTRB1: load-displacement curve

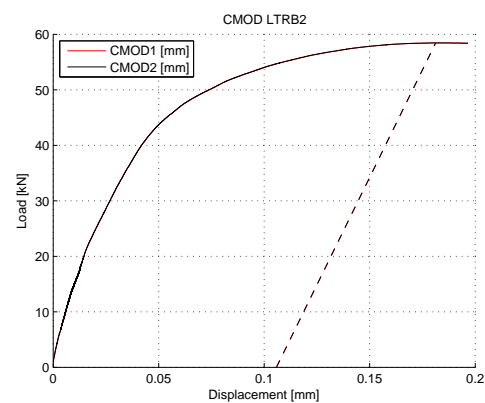


Figure C.97: LTRB2: load-displacement curve

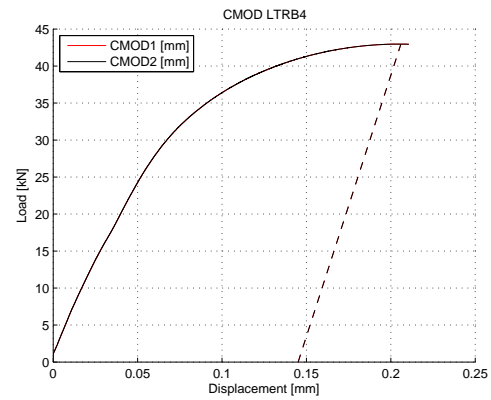
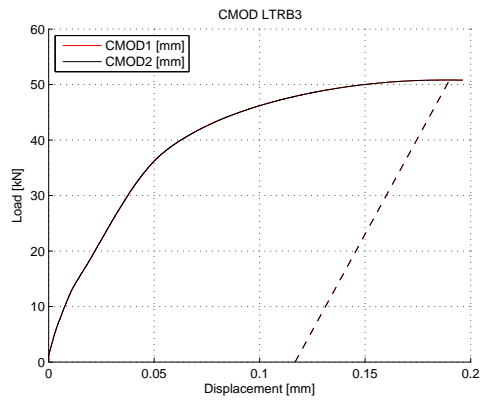


Figure C.98: LTRB3: load-displacement curve Figure C.99: LTRB4: load-displacement curve

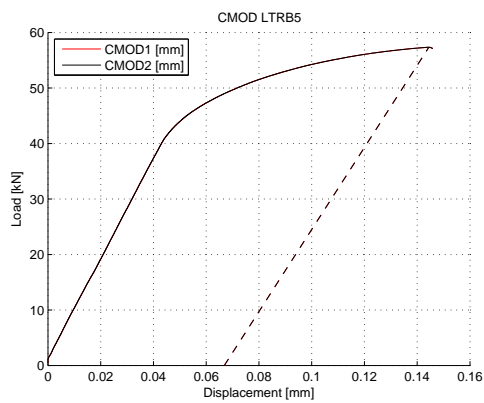


Figure C.100: LTRB5: load-displacement curve

C.4.5 GRT1 - GRT 3

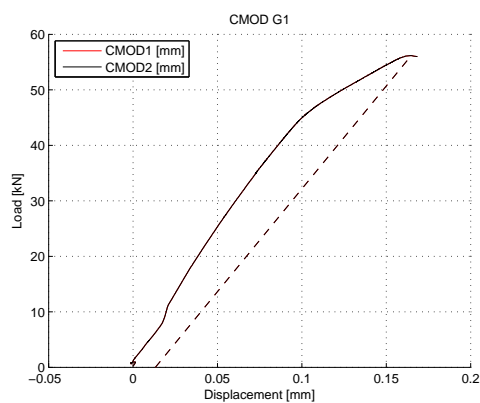


Figure C.101: GRT1: load-displacement curve

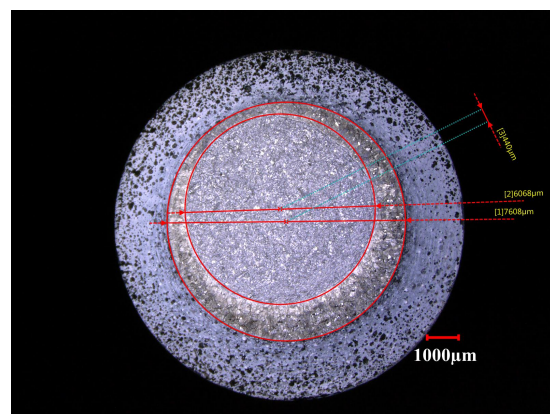


Figure C.102: GRT1: fracture surface

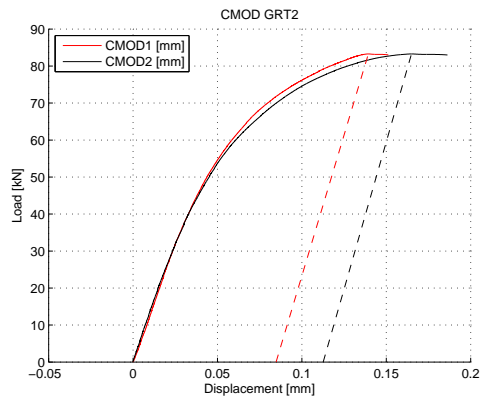


Figure C.103: GRT2: load-displacement curve

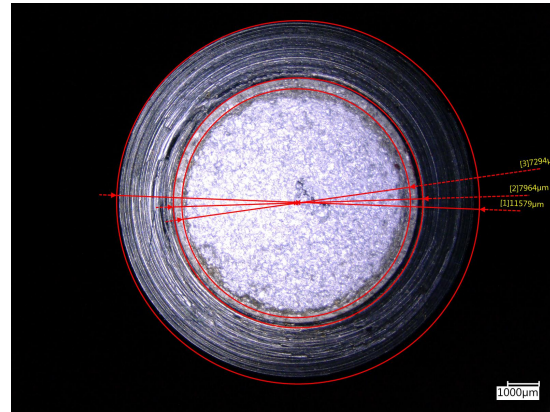


Figure C.104: GRT2: fracture surface

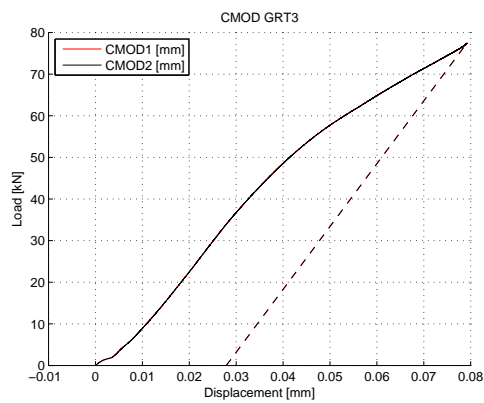


Figure C.105: GRT3: load-displacement curve

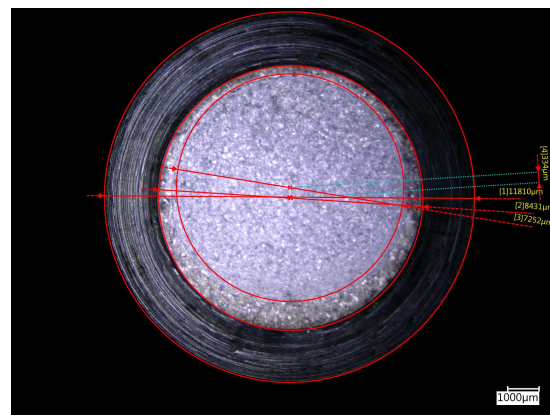


Figure C.106: GRT3: fracture surface

C.4.6 GLT 1 - GLT 3

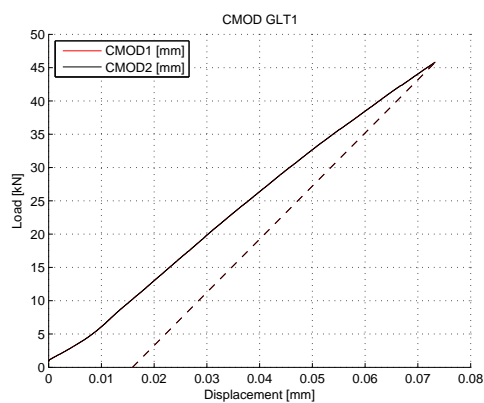


Figure C.107: GLT1: load-displacement curve

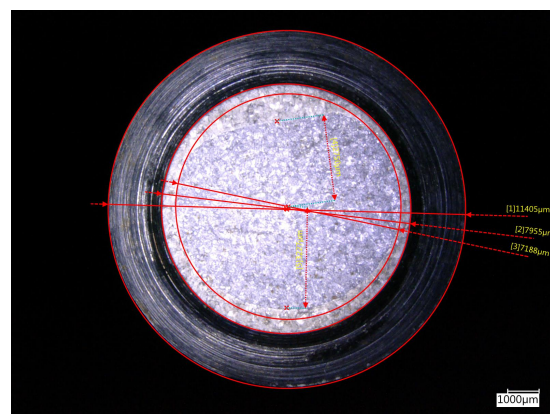


Figure C.108: GLT1: fracture surface

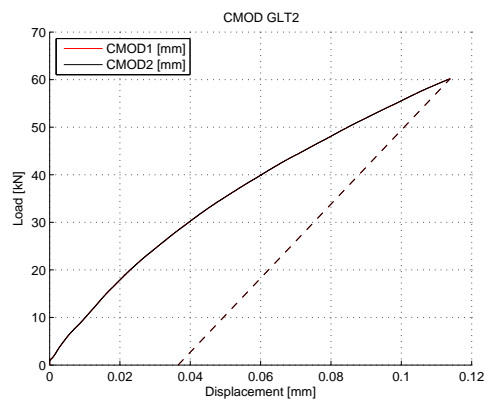


Figure C.109: GLT2: load-displacement curve

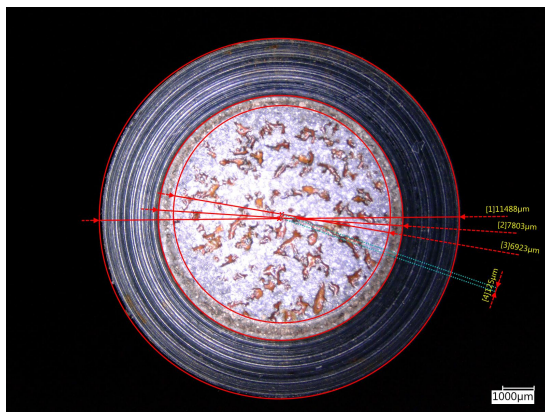


Figure C.110: GLT2: fracture surface

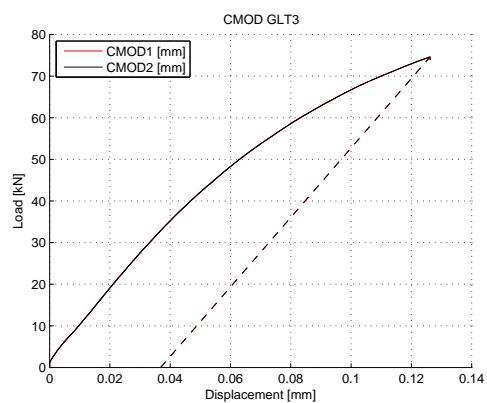


Figure C.111: GLT3: load-displacement curve

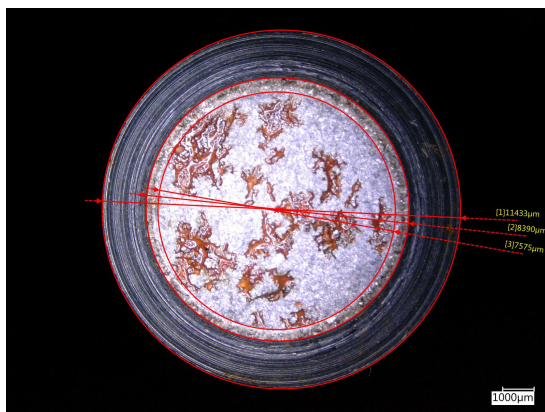


Figure C.112: GLT3: fracture surface

Bibliography

- [1] M. Janssen, J. Zuidema, and R. Wanhill, *Fracture Mechanics*. 2002.
- [2] T. L. Anderson, *Fracture Mechanics: Fundamentals and Applications*, vol. 58. 2012.
- [3] J. R. Rice, “A path independent integral and the approximate analysis of strain concentration by notches and Cracks,” 1967.
- [4] A. A. Wells, “Unstable crack propagation in metals: cleavage and fast fracture,” *Proceedings of the crack propagation symposium*, vol. 1, no. 84, 1961.
- [5] S. Hengeveld, L. Nordin, F. Reijnders, and V. Olijslager, “Research Report,” 2014.
- [6] K. Wallin, “K_{Ic} - a Non-Measure of Plane Strain Fracture Toughness,” *ICF10, Honolulu, Hawaii - 2001*, 2001.
- [7] L. Afferrante, M. Ciavarella, and E. Valenza, “Is Weibull’s modulus really a material constant ? Example case with interacting collinear cracks,” vol. 43, pp. 5147–5157, 2006.
- [8] W. Weibull, “A statistical distribution of wide applicability,” *J. Appl. Mech.*, vol. 18, pp. 293–297, 1951.
- [9] A. H. Cottrell, “Theory of brittle fracture in steel and similar metals,” *Transactions of the Metallurgical society of AIME*, vol. 212, 1958.
- [10] ASTM E1820-15A, “Standard Test Method for Measurement of Fracture Toughness,” pp. 1–54, 2015.
- [11] S. K. Nath and U. K. Das, “Effect of Microstructure and Notches on the Fracture Toughness of Medium Carbon Steel,” *Journal of Naval Architecture and Marine Engineering*, vol. 72, no. D, 2006.
- [12] Z. Śloderbach and J. Pająk, “Determination of Ranges of Components of Heat Affected Zone Including Changes of Structure / Określenie Zakresów Składowych Strefy Wpływu Ciepła Uwzględniając Zmiany Struktury,” *Archives of Metallurgy and Materials*, vol. 60, jan 2015.
- [13] V. A. Popovich, “Project Closure Report,” pp. 1–9, 2016.
- [14] D. A. Porter, “Weldable High-Strength Steels : Challenges and Engineering Applications,” *IIW International Conference High-Strength Materials - Challenges and Applications*, no. Portevin session, 2015.
- [15] J. Devaux and G. Rousselier, “An experimental program for the validation of local ductile fracture criteria using axisymmetrically crack bars and compact tension specimens,” vol. 21, no. 2, pp. 273–283, 1985.
- [16] E. Lucon, “Cylindrical specimens for evaluating a service component’s fracture toughness properties,” 1992.

- [17] R. Ibrahim and A. Kotousov, "Eccentricity correction for the evaluation of fracture toughness from cylindrical notched test small specimens," *Engineering Fracture Mechanics*, vol. 64, no. 1, pp. 49–58, 1999.
- [18] B. K. Neale, "The analytical fracture behaviour of a bar in tension containing a circumferential edge crack (, I !," vol. 73, no. 1997, pp. 191–198, 1998.
- [19] M. Scibetta, R. Chaouadi, and E. V. a. N. Walle, "Fracture toughness analysis of circumferentially-cracked round bars," pp. 145–168, 2000.
- [20] E. Slachter, "Assessing the use of Circumferentially Notched Tension specimen for fracture toughness determination of ductile offshore steels," 2016.
- [21] J. P. Benthem and W. T. Koiter, *Asymptotic approximations to crack problems*, pp. 131–178. Dordrecht: Springer Netherlands, 1973.
- [22] Tada, "K solution of CNT," vol. 1985, p. 1985, 1985.
- [23] G. E. Dieter, *Mechanical Metallurgy*. 1988.
- [24] J. H. Giovanola and T. Kobayashi, "Mechanics of deformation and ductile tearing in cracked round bar specimens," vol. 59, no. 2, pp. 117–136, 1998.
- [25] T. Pardoen, M. Scibetta, R. Chaouadi, and F. Delannay, "Analysis of the geometry dependence of fracture toughness at cracking initiation by comparison of circumferentially cracked round bars and SENB tests on Copper," *International Journal of Fracture*, vol. 103, no. 3, pp. 205–225, 2000.
- [26] F. W. Wu, R. N. Ibrahim, R. Das, and R. K. S. Raman, "Fracture toughness for CNT specimens from numerically obtained critical CTOD values," *Theoretical and Applied Fracture Mechanics*, vol. 52, no. 1, pp. 50–54, 2009.
- [27] D. N. Githinji, S. Northover, and P. J. Bouchard, "Electron backscatter diffraction (EBSD) measurement of accumulated strain Conference Item," *3rd International ECCC- Creep & Fracture Conference: Creep & Fracture in High Temperature Components*, 2014.
- [28] R. Unnikrishnan, S. Northover, H. Jazaeri, and P. J. Bouchard, "Investigating plastic deformation around a reheat-crack in a 316H austenitic stainless steel weldment by misorientation mapping," *Procedia Structural Integrity*, 2016.
- [29] H. L. Stark and R. N. Ibrahim, "Estimating fracture toughness from small specimens," *Engineering Fracture Mechanics*, vol. 25, no. 4, pp. 395–401, 1986.
- [30] J. H. Giovanola, H. Homma, M. Lichtenberger, E. C. James, and R. W. Klopp, "Fracture toughness measurements using small cracked round bars," 1995.
- [31] E. Lucon, "Fracture toughness testing using small cylindrical specimens with ring-shaped cracks," 1993.
- [32] M. Yoda, "J-integral of the notch root radius on the fracture toughness under modes," *Engineering Fracture Mechanics*, vol. 26, no. 3, pp. 425 – 431, 1987.
- [33] D. M. Li and A. Bakker, "Fracture Toughness Evaluation using Circumferentially-Cracked Cylindrical Bar Specimens," *Engineering Fracture Mechanics*, vol. 57, no. 1, pp. 1–11, 1997.
- [34] N. V. Londe, "Use of round bar specimen in fracture toughness test of metallic materials," *International Journal of Engineering Science and Technology*, vol. 26, pp. 3–16, sep 2010.
- [35] R. N. Ibrahim and H. L. Stark, "Validity requirements for fracture toughness measurements obtained from small circumferentially notched cylindrical specimens," *Engineering Fracture Mechanics*, vol. 28, no. 4, pp. 455–460, 1987.

- [36] C. L. Walters and G. V. D. Weijde, “Development and Validation of a Low-Cost CTOD Procedure,” *International Offshore and Polar Engineering*, vol. 9, pp. 234–241, 2013.
- [37] J. H. Giovanola, R. W. K. J. E. Crocker, D. J. Alexander, and R. Giovanola, “Using Small Cracked Round Bars to Measure the Fracture Toughness of a Pressure Vessel Steel Weldment : A Feasibility Study,” pp. 328–352, 1998.
- [38] S. Ghodrat, T. Riemsdag, and L. A. I. Kestens, “Measuring Plasticity with Orientation Contrast Microscopy in Aluminium 6061-T4,” pp. 1–8, 2017.